Theoretical Investigation of Traffic Flow: Inhomogeneity Induced Emergence

A dissertation presented in partial fulfillment of the
requirements for the degree of

Doctor of Philosophy
in
Computer Science

at Massey University, Auckland, New Zealand

Mingzhe Liu

2010

Certificate of Regulatory Compliance

This is to certify that the research carried out in the Doctoral Thesis entitled "*Theoretical Investigation of Traffic Flow: Inhomogeneity Induced Emergence*" in the Institute of Information and Mathematical Sciences at Massey University, New Zealand:

1. is the original work of the candidate, except as indicated by appropriate attribution in the text and in the acknowledgements;

2. that the text does not exceed 100,000 words;

3. all the ethical requirements applicable to this study have been complied with as required by Massey University.

Please insert Ethical Authorization code here: not applicable

Candidate: Mingzhe Liu

Signature:

Date:

Supervisor: Prof. Ken Hawick

Signature:

Date:

Candidate's Declaration

This is to certify that the research carried out for my Doctoral Thesis entitled "*Theoretical Investigation of Traffic Flow: Inhomogeneity Induced Emergence*" in the Institute of Information and Mathematical Sciences, Massey University, Albany, Auckland, New Zealand is my own work and that the thesis material has not been used in part or in whole for any other qualification.

Candidate: Mingzhe Liu

Signature:

Date:

Supervisor's Declaration

This is to certify that the research carried out for the Doctoral Thesis entitled "*Theoretical Investigation of Traffic Flow: Inhomogeneity Induced Emergence*" was done by Mingzhe Liu in the Institute of Information and Mathematical Sciences, Massey University, Albany, Auckland, New Zealand. The thesis material has not been used in part or in whole for any other qualification, and I confirm that the candidate has pursued the course of study in accordance with the requirements of the Massey University regulations.

Supervisor: Prof. Ken Hawick

Signature:

Date:

I dedicate this thesis and my love to my wife Ping Wen,
my daughter Xiner Liu and my son Runxi Liu

Abstract

This research work is focused on understanding the effects of inhomogeneity on traffic flow by theoretical analysis and computer simulations. Traffic has been observed at almost all levels of natural and manmade systems (e.g., from microscopic protein motors to macroscopic objects like cars). For these various traffic, basic and emergent phenomena, modelling methods, theoretical analysis and physical meanings are normally concerned.

Inhomogeneity like bottlenecks may cause traffic congestions or motor protein crowding. The crowded protein motors may lead to some human diseases. The congested traffic patterns have not been understood well so far.

The modelling method in this research is based on totally asymmetric simple exclusion process (TASEP). The following TASEP models are developed: TASEP with single inhomogeneity, TASEP with zoned inhomogeneity, TASEP with junction, TASEP with site sharing and different boundary conditions. These models are motivated by vehicular traffic, pedestrian traffic, ant traffic, protein motor traffic and/or Internet traffic.

Theoretical solutions for the proposed models are obtained and verified by Monte Carlo simulations. These theoretical results can be used as a base for further developments. The emergent properties such as phase transitions, phase separations and spontaneous symmetry breaking are observed and discussed. This study has contributed to a deeper understanding of generic traffic dynamics, particularly, in the presence of inhomogeneity, and has important implications for explanation or guidance of future traffic studies.

Acknowledgements

I would like to take this opportunity to acknowledge those people who have guided and supported me to achieve this qualification.

First and foremost, I would like to thank my thesis supervisors Prof. Ken Hawick and Prof. Stephen Marsland for their strong support and guidance. They set a wonderful example of being an excellent scientist: curiosity, enthusiasm, honesty and hard working towards research! Their intellectual rigor and enthusiastic attitude kept my research on track and well focused. I also greatly appreciate their help when I was going through my personal difficulties.

Special thanks go to my co-supervisor Prof. Rui Jiang for having numerous fruitful discussions on this research work. Rui made a lot of suggestions for theoretical analysis and simulations. Rui has always been prepared to talk about any issues, even in times he was very busy.

I would also like to thank my previous supervisor, Dr. Ruili Wang, who has supervised my first two and half years of my PhD study. He led me to the topic of traffic modelling and simulations. I have learnt a great deal from him.

A special thank-you to Prof. Ray Kemp for always being supportive and patient.

I would further like to acknowledge many academic and supporting staff at Massey University for providing the comfortable and well-equipped environment in which to study, especially, Prof. Hans W. Guesgen, Prof. Martin Hazelton, Prof. Elizabeth Kemp and Dr. Patrick Rynhart.

I thank Prof. Paul Merrick, Dr. Ian Bond and Dr. Marcus Frean for accepting to serve on my thesis committee.

Contents

List of Figures

List of Tables

Chapter 1

Introduction

1.1 Research description

Traffic is a ubiquitous phenomenon and has been observed at almost all levels of natural and manmade systems, covering macroscopic objects like cars, pedestrians, and ants, to microscopic molecular motors [1, 2]. These motile objects are self-driven by converting chemical energy into mechanical works like directed movement. Self-driven systems often exhibit emergent properties (e.g., phase transitions, phase separations) that result from interactions among these motile objects, rather than being imposed by a central controller. In this sense, such systems are regarded as complex systems [3] and characterised by non-zero traffic currents.

A common modelling strategy for such complex systems is to abstract motile objects into particles by neglecting their size and underlying structure, and then looking at traffic as a non-equilibrium system of interacting particles. It is proposed that there has not been a well-established general theoretical framework which can be used to analyse all non-equilibrium systems [4, 5, 6]. As a result the non-equilibrium systems are less understood, compared to the equilibrium systems. In the equilibrium case, the Gibbs measure provides such a theoretical framework [5, 6]. Therefore, seeking for similar stationary properties and general behaviour of non-equilibrium

systems by investigating individually a large variety of mathematical models based on a paradigm has attracted much attention in recent decades.

Such a paradigmatic model for non-equilibrium systems is known as an asymmetric simple exclusion process (ASEP). An ASEP is a one-dimensional lattice model in which particles hop to the nearest-neighbour sites in a preferred direction and interact through hard-core exclusion (i.e., each site can be occupied by no more than one particle at any given time). It was introduced originally in 1968 as a theoretical model for describing ribosome motion along mRNA [7]. The simplest form of the ASEP is that particles can move along only one direction, which is called the totally ASEP (TASEP). The TASEP and its variants have shown to be suitable for modelling traffic flow. The reasons for this can be as follows:

1. TASEP models can describe both single- and multiple-channel traffic easily, which is particularly important in modelling traffic flow.

2. TASEP models can be computationally advantageous and are easy to be implemented in large-scale simulations since traffic variables such as position, speed and time are treated as discrete. Obviously, such models can be easily computed using random and parallel computing paradigms.

3. Random speed fluctuations caused by driver behaviour or external conditions (e.g., night visibility or weather) can be described by different hopping probabilities.

4. Different driver types can be represented as different species of particles.

5. Macroscopic traffic flow variables, such as average flux, average speed and density profiles can be obtained by averaging individual particle or site data.

A better understanding of non-equilibrium steady states in self-driven systems has been a central research topic in recent years. Various models and solutions along

this line have found their natural applications in biology, physics, and chemistry [8, 9] such as gel electrophoresis [10], protein synthesis [11, 12], mRNA translation [13], motion of molecular motors along the cytoskeletal filaments [14], and the de-polymerization of microtubules by special enzymes [15] as well as vehicular traffic [16, 17]. Meanwhile, problems from these systems have motivated many mathematical models. For more details, see Chapter 2 where various TASEP models have been reviewed.

This thesis studies the emergent properties induced by various inhomogeneities on TASEP in single- and multiple-channel systems. In particular, the focus of this study is on theoretically investigating the effects of:

1. A *single* inhomogeneity and a *zoned* inhomogeneity on TASEP in a single-channel system.

2. TASEP with a multiple-input multiple-output junction. The junction point can be viewed as an inhomogeneity.

3. *Random* inhomogeneities on two-species TASEP with site sharing and re-laxed/constrained boundaries in a single-channel system.

This research is expected to:

1. Contribute to a deeper understanding of non-equilibrium systems, especially in the case of inhomogeneity.

2. Advance the theoretical understanding of general behaviour of various systems including vehicular traffic and biological transport by investigating dynamical traffic properties (e.g., phase diagrams, current and density profiles).

3. Provide a theoretical basis for further investigation of non-equilibrium systems. Furthermore, the research findings may have implications for the guidance or explanation of future experiments on vehicular traffic or biological transport.

1.2   Research motivation

As mentioned above, there is no general theoretical framework that can be used to describe general non-equilibrium systems [4, 5, 6]. Alternatively, a large variety of models and solutions need to be further developed, so as to enhance understanding of non-equilibrium systems. Having been extensively studied for decades, TASEP still possess many fascinating, yet non-trivial, phenomena observed in computer simulations that are worth further exploring theoretically.

A broader understanding of transport systems is still required, in particular, a great need for deeper understanding of traffic jams in those systems. It is known that vehicular traffic congestions can pollute the environment and increase fuel consumption. Intracellular traffic jams have been proposed to involve in a variety of diseases such as cardiovascular problems and neuronal diseases (e.g., Alzheimer's, sclerosis, retinitis pigmentosa, see Refs. [18, 19, 20] for more details). One possible explanation for intracellular traffic jams is defective molecular motors or tracks. Thus, a better understanding of traffic jam patterns may help shed light on possible disease treatments.

The experimental observations reveal many interesting motion fashions of molecular motors such as molecular motors moving along cytoskeletal filaments [21], random motors (e.g., kinesins) attaching to and detaching from cytoskeletal filaments [22], freely changing to the adjacent filaments [23], bidirectional transport [24], cooperative many-motor transport [25] and so on.

Studies of the traffic dynamics of non-equilibrium systems, motivated by molecular motor traffic, could have many potential applications in bionanotechnology, for example, alleviating traffic jams in intracellular transport systems, controlling positions and directions of molecular motors, delivering drugs targeted to control or even cure some diseases [26].

Although this research is motivated by vehicular traffic, pedestrian traffic and biological transport, the proposed models are still simplified and far from reality due to the lack of empirical data. Nevertheless it has inspired various TASEP models which revealed many interesting phenomena and gained the attention from interdisciplinary researchers.

1.3 Main contributions

1.3.1 Research contributions

This research is focused on investigating traffic dynamics of TASEP with various inhomogeneities. The main contributions of this research are as follows:

1. Theoretical solutions for the following research issues (except for (e)) have been obtained via mean-field methods as well as domain-wall theory in some cases. The theoretical predictions are well supported by Monte Carlo simulations.

    (a) TASEP with single inhomogeneity in a single-channel system

    (b) TASEP with a zoned inhomogeneity in a single-channel system

    (c) TASEP with multiple-input multiple-output junction

    (d) Two-species TASEP with site sharing and relaxed boundaries in a single-channel system

    (e) Two-species TASEP with site sharing and constrained boundaries in a single-channel system

2. Theoretical results gained in points (a), (b), (c) and (d) can be viewed as *fundamental* results for further developments.

3. In point (c), a generic theoretical solution for TASEP with a m-input n-output junction is presented. Junctions with the same λ ($\lambda = m/n$) are demonstrated

to possess the same phase diagram, stationary current, and density profiles. Furthermore, the areas of the low-density and high-density phases can be calculated directly.

4. In points (d) and (e), the site-sharing model is firstly proposed. The site-sharing mechanism is different from the widely used site-exchanging mechanism in previous two-species TASEP models. The new models allow double occupation of sites, rather than excluding each other. This kind of site-sharing model has been little studied before.

5. In point (e), the model exhibits spontaneous symmetry breaking in two asymmetric phases: low-density-low-density phase and low-density-high-density phase. The flipping processes of particles in these phases have been observed.

1.3.2   Author's contributions

Chapters 3-7, corresponding to research issues (a-e), of this thesis have been published or submitted for review in a variety of academic journals, as listed in Appendix Publications [1-5]. All of these papers have multiple co-authors as well as the author of this thesis, Mingzhe Liu. The input of the co-authors of each paper in all stages of the research development is gratefully acknowledged, as are the suggestions made by the anonymous peer reviewers of the journals.

All of the computational work and theoretical analysis involved in the research described in this thesis is the primary work of the thesis author. While the initial ideas for the papers arose from useful discussions with the co-authors, and their input was useful in all cases, the author of this thesis initiated the research lines leading to the publications in Chapters 3-7. As the primary author for the publications based on Chapters 3-7, he is responsible for their

written materials, and the production of all graphs and figures. The supervision panel of the student changed to reflect the circumstances of the PhD project late in the project.

1.4 Thesis outline

The outline of this thesis is as follows:

Chapter 2: The TASEP model and its variants are comprehensively reviewed. The known results of TASEP with random update and parallel update are briefly summarized, then the review on TASEP models in terms of particle properties (e.g., large particles, multiple-speed particles and Langmuir kinetics) and lattice geometries (e.g., one channel and multiple channels, local inhomogeneity) is made.

Chapter 3: A one-dimensional TASEP with a single inhomogeneity in parallel update is studied. An inhomogeneity is characterized by the reduced hopping probability. The results obtained from the mean-field approach and Monte Carlo simulations are discussed. The phase diagram is shifted with the strength of local inhomogeneity, but topologically unchanged, compared to that of the normal TASEP. The phenomenon of phase separation is observed.

Chapter 4: The effect of a zoned inhomogeneity on a one-dimensional TASEP in parallel update is investigated. By using a simple mean-field approximation, the phase diagram, stationary current and density profiles are predicted and supported by Monte Carlo simulations.

Chapter 5: The traffic dynamics of TASEP with a multiple-input single-output junction in parallel update is investigated, then the model is extended to a general case: m-input n-output junction.

Chapter 6: A two-species TASEP with site sharing and relaxed boundaries in a single-channel system is presented. The model is motivated by multiple-channel traffic and pedestrian traffic. The new aspect of this investigation, compared to previous two-species TASEP models, is that the particles moving in opposite directions do not pass each other by an exchanging mechanism, but by sharing a site.

Chapter 7: Based on Chapter 6, further investigation of a two-species TASEP with site sharing and constrained boundaries is conducted. The spontaneous symmetry breaking is observed and exhibits two asymmetric phases: low-density-low-density phase and low-density-high-density phase. The flipping processes of particles in these phases have been observed.

Chapter 8: A summary is given by revisiting the main findings of the thesis and commenting on possible future work.

Chapter 2

Review on TASEP Models

In this Chapter, the main features of totally asymmetric simple exclusion process (TASEP) in random and parallel updating procedures are reviewed. An overview of some generalizations and extensions of the TASEP is given, and several popular mean-field techniques used to analyze TASEP models are summarized. TASEP variants have been successfully used to model real complex systems in Biology, Physics and Chemistry. However, it is not the purpose of this Chapter to review such applications in any detail. There is much literature on TASEP-related applications; I refer to review articles [1, 31] and the references therein for biological transport, and review articles [16, 17] and the references therein for vehicular traffic.

2.1 Totally asymmetric simple exclusion process

2.1.1 Introduction

The exclusion process in a one-dimensional system has been well studied with extensive computer simulations and some theoretical solutions in the stationary state. Totally asymmetric simple exclusion process (TASEP), a basic model for non-equilibrium systems, describes a single-species particle moving unidirectionally along a homogeneous lattice. Particles can hop to the nearest-neighbor site with

probability 1 provided the target site is empty.

There are normally two kinds of boundary conditions: periodic boundary conditions and open boundary conditions [16]. The former describes closed systems, while the latter simulates open systems. In periodic boundary conditions, the system size N and number of particles M are known. Thus, the system density ρ is given by $\rho = M/N$. Periodic boundary conditions are normally used to calculate the fundamental diagram (i.e., the current-density relationship) in the study of vehicular traffic [16]. The fundamental diagram can describe the dynamic properties of vehicular traffic flow, e.g., free flow and congested flow. Alternatively, systems require input and output parameters under open boundary conditions . Open boundary conditions provide a more realistic description of traffic flow in the real world and will be used in this research.

2.1.2 Updating procedures

In open boundary conditions, the TASEP is defined in a one-dimensional lattice of N sites (see Figure 2.1). Sites 1 and N define the left and right boundaries, respectively, while a set of sites 2, ..., N-1 is referred to as the *bulk*. For the purpose of description, an occupation variable τ_i is used to represent the state of the ith site. $\tau_i = 1$ (0) corresponds to the site being occupied (empty). The following update rules are applied to each *individual* site.

- Site 1. (i) If $\tau_1 = 0$, a particle enters the system with rate α. (ii) If $\tau_1 = 1$ and $\tau_2 = 0$, a particle in site 1 moves into site 2 with probability 1. (iii) If $\tau_1 = 1$ and $\tau_2 = 1$, the particle stays site 1.

- Site N. If $\tau_N = 1$, a particle leaves the system with rate β.

- Site $1 < i < N$. If $\tau_i = 1$, a particle moves into site $i + 1$ with probability 1 if $\tau_{i+1} = 0$. Otherwise, the particle stays there.
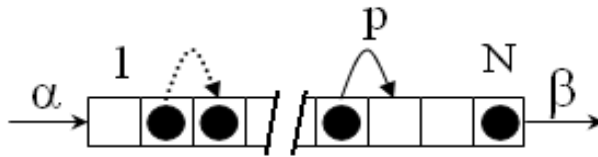
Figure 2.1: Schematic representation of TASEP with open boundary conditions. Particles move from the left to the right with hard-core exclusion (i.e., each site cannot be occupied by more than one particle at a time). The solid arrow indicates an allowable hopping, while the dashed arrow corresponds to a prohibited movement.

To study the TASEP, it is necessary to specify the update order of particles. Basically, there are four types of updating procedures: random, ordered-sequential, sublattice-parallel, and fully parallel [30]. Obviously, the dynamics of particles in the TASEP is different according to different updating procedures. The following updating procedures determine how an individual site is chosen.

1. Random. A site i ($1 \leq i \leq N$) is randomly chosen at each time step.

2. Ordered-sequential. A particle at site $i = N$ is first removed with probability β, then the state of site $N - 1$ is followed. If there is a particle at site $N - 1$, it can move into site N provided site N is empty. The states of sites $N - 2, N - 3, ..., 3, 2, 1$ are updated in order, until the left boundary is reached.

3. Sublattice-parallel. Sites are divided into groups, e.g., the first group is odd number sites, and the second is even number sites, then the system updates those groups in some predefined order. Within the individual group, the sites are updated in parallel.

4. Fully parallel. All sites are updated at the same time.

Most of TASEP variants in the literature are implemented with random update, which shows the weakest interactions between particles [30] and is widely used in

describing biological transport [1, 31]. Parallel update shows the strongest interactions between particles [32, 33] and is more suitable for vehicular, pedestrian, and ant traffic [16] since parallel update can describe better continuous movement of motile objects in a system, compared to other updating procedures. It has been shown that parallel traffic simulations can reproduce observed traffic phenomena more realistically. In addition, TASEP is a simplified version of cellular automata. Parallel cellular automata models have been successfully used in road traffic simulations. Other updating procedures, such as ordered-sequential and sublattice-parallel, can be considered as intermediate versions. Thus, studying TASEP and its extensions with random and parallel updates suffices to understand qualitatively and quantitatively the dynamics of the TASEP and its extensions. Note that the TASEP with ordered-sequential and sublattice-parallel updates have been investigated recently. For instance, [34] studies bi-directional particle transport with ordered-sequential update. Two-species TASEP in ordered-sequential and sublattice parallel updates is investigated in [35]. Jafarpour et al. [36] examined shock profiles for the TASEP with sublattice-parallel update. The exact results of the TASEP with these four updating procedures for general p (see Figure 2.1) have been reported in [30]. Here I briefly summarise the results of the TASEP for $p = 1$ with random and parallel updates.

2.1.3   Random update

The TASEP with random update on a one-dimensional lattice has been analyzed theoretically in [8]. The corresponding equation for the evolution of particle densities $\langle \tau_i \rangle$ in a bulk can be written as follows:

$$\frac{d\langle \tau_i \rangle}{dt} = \langle \tau_{i-1}(1 - \tau_i) \rangle - \langle \tau_i(1 - \tau_{i+1}) \rangle, \tag{2.1}$$

Table 2.1: Relation between current and bulk density of different phases in the normal TASEP with random update. α is the entrance rate, and β is the exit rate. LD (HD) is for low (high) density, and MC for maximal current

phase	conditions	current (J)	bulk density (ρ)
LD	$\alpha < \beta$, $\alpha < 0.5$	$\alpha(1-\alpha)$	α
HD	$\alpha > \beta$, $\beta < 0.5$	$\beta(1-\beta)$	$1-\beta$
MC	$\alpha \geq 0.5$, $\beta \geq 0.5$	0.25	0.5

while at the left and right boundaries one obtains:

$$\frac{d\langle \tau_1 \rangle}{dt} = \alpha\langle(1-\tau_1)\rangle - \langle \tau_1(1-\tau_2)\rangle. \tag{2.2}$$

$$\frac{d\langle \tau_N \rangle}{dt} = \langle \tau_{N-1}(1-\tau_N)\rangle - \beta\langle \tau_N \rangle. \tag{2.3}$$

where $\langle \cdots \rangle$ denotes a statistical average. The first term corresponds to a particle entering into site i, and the second term corresponds to a particle leaving site i. Depending on the values of α and β, the normal TASEP exhibits three stationary phases [8]: low-density (LD), high-density (HD) and maximal-current (MC) (see Figure 2.2(a)). The phase transition from the LD phase to the HD phase is first-order, while the LD phase to the MC phase and the HD phase to the MC phase are continuous. In the LD phase, the system current is independent of β. In the HD phase, the system current is independent of α. In the MC phase, the system current is independent of both α and β. Table 2.1 summarizes the relationship between current and bulk density for different phases in the normal TASEP with random update.
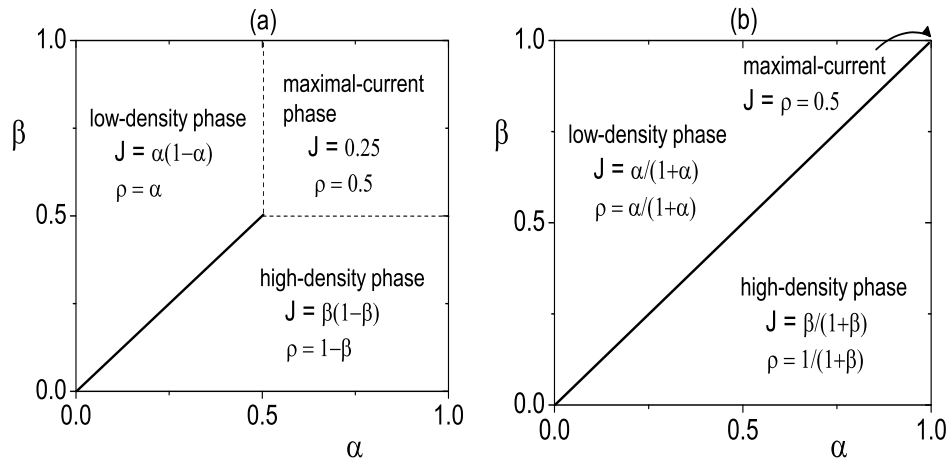
Figure 2.2: Phase diagrams of TASEP under open boundary conditions. The solid lines mean transitions between LD phase and HD phase are the first order, while the dashed lines correspond to continuous transitions between LD phase and HD phase. J is the system current and ρ is the bulk density. (a): random update; (b): parallel update.

2.1.4   Parallel update

The dynamic rules of the TASEP in parallel update can be described by the micro-dynamic equation [32]:

$$\tau_i(t+1) - \tau_i(t) = \hat{J}_{i-1}(t) - \hat{J}_i(t), \tag{2.4}$$

where $\hat{J}_i(t)$ denotes the number of particles passing through the link $(i, i+1)$ at time t, i.e., the current. As the current in the system is conserved, one obtains [32]:

$$J = J_i, \qquad J_i = \langle \hat{J}_i \rangle \qquad i = 1, 2, ..., L, \tag{2.5}$$

where J is the system current and $\langle \hat{J}_i \rangle = \langle \tau_i(1 - \tau_{i+1}) \rangle$ is the average current through the link $(i, i+1)$. Exact solutions for the TASEP in parallel update have been presented in [32, 33] and there are still three stationary phases: low-density (LD), high-density (HD) and maximal-current (MC) phases (see Figure 2.2(b)). Table 2.2

Table 2.2: Relation between current and bulk density of different phases in the normal TASEP with parallel update. α is the entrance rate. β is the exit rate.

phase	conditions	current (J)	bulk density (ρ)
LD	$\alpha < \beta < 1$	$\alpha/(1+\alpha)$	$\alpha/(1+\alpha)$
HD	$\beta < \alpha < 1$	$\beta/(1+\beta)$	$1/(1+\beta)$
MC	$\alpha = \beta = 1$	0.5	0.5

summarizes the relationship between current and bulk density of different phases in the normal TASEP with parallel update.

The differences between the phase diagrams for the TASEP with random and parallel updates are obvious. For instance, the MC phase in random update is specified by $0.5 \leq \alpha \leq 1$ and $0.5 \leq \beta \leq 1$ (see Figure 2.2), while it reduces to a point at $\alpha = \beta = 1$ in parallel update (see Figure 2.2(b)). These differences indicate that different updating procedures can lead to different phase structures even in the simplest case.

The parallel update has been typically adopted for modelling vehicular and pedestrian traffic [16, 37]. It is argued that this might be adopted for modelling motor traffic within cells as well since (i) the number of such motors within cells is huge; (ii) these motors move along cytoskeletal filaments simultaneously; and (iii) normally these motors can make about 100 successive steps in the absence of loads [38].

The TASEP model can be seen as the minimal particle-hopping model for non-equilibrium systems in the sense that all four components (i.g., particles, lattice, boundary conditions and updating procedures) are necessary. Any further simplification of the model will leads to an incomplete description of the system. Thus, a change of particle properties, lattice structures, boundary conditions, and/or updating procedures may lead to a variation of the TASEP. Figure 2.3 shows some
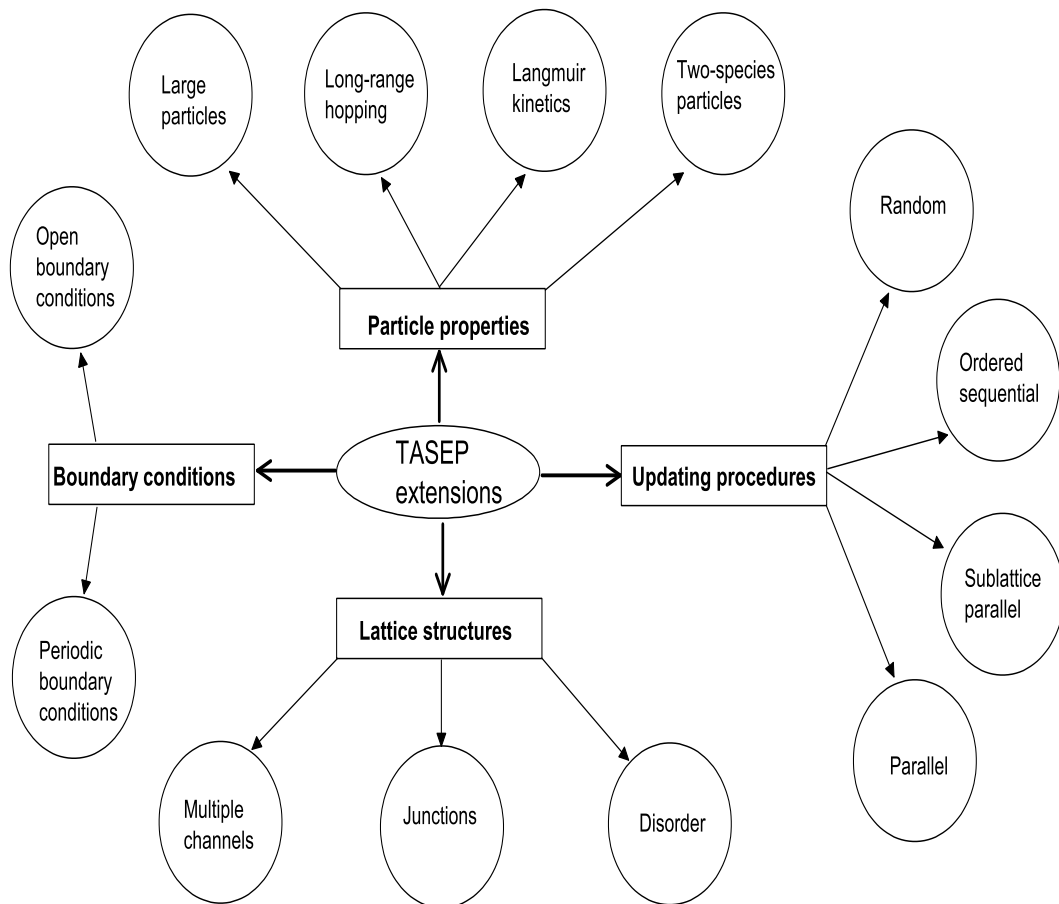
Figure 2.3: Illustration of some possible TASEP extensions. These extensions can be made with particle properties, lattice structures, boundary conditions, or updating procedures to suit various issues.

possible variations derived from these four aspects. Since open boundary conditions, random update and parallel update are normally used in TASEP models, the focus of this review is mainly on particle properties and lattice structures. In other words, this review follows along two lines: TASEP with different particle properties and TASEP with different lattice structures. Particle properties may include: large particles (some researchers also call them extended objects), long-range hopping (or multiple-speed hopping), Langmuir kinetics (LK)[1], and two species of particles. Lattice structures can be multiple parallel channels, multiple-input multiple-output junctions, intersections, roundabouts, and local inhomogeneities (also called *defects* or *bottlenecks* in some cases).

2.2 TASEP with particle properties

2.2.1 TASEP with large particles

Large particles are also referred to as extended objects in the literature. Each of them can occupy several sites (i.e., particle size $\ell > 1$). The counterparts of large particles in nature can be long-size vehicles, ribosomes, dimers, multiple-motor cooperative motion, large molecules or vesicles and so on.

Lakatos and Chou [39] studied the TASEP on a one-dimensional lattice with large particles and *random* update. Their theoretical analysis predicts that there are still three stationary phases: the LD, HD and MC phases similar to the normal TASEP [8]. However, the phase boundaries, current, and bulk density are affected by particle size ℓ. Table 2.3 briefly recalls the theoretical results of possible phases, corresponding conditions, current and density profiles of the TASEP with large par-

---

[1]Irving Langmuir (1881-1957) was an American physicist and chemist. He recieved 1932 Nobel Prize in chemistry for his contributions in surface chemistry. Langmuir kinetics is widely used to describe absorption-desorption process in surface chemistry. In biophysics, it is used to describe particles randomly attachment to and detachment from a lattice, LK for short.

Table 2.3: Relation between current and bulk density of different phases in the normal TASEP with large particles and random update. α is the entrance rate, β is the exit rate, and ℓ is the particle size.

phase	conditions	current (J)	bulk density (ρ)
LD	$\alpha < \beta,\ \alpha < 1/(1+\sqrt{\ell})$	$\alpha(1-\alpha)/[1+\alpha(\ell-1)]$	$\ell\alpha/[1+\alpha(\ell-1)]$
HD	$\alpha > \beta,\ \beta < 1/(1+\sqrt{\ell})$	$\beta(1-\beta)/[1+\beta(\ell-1)]$	$1-\beta$
MC	$\alpha \geq 1/(1+\sqrt{\ell}),\ \beta \geq 1/(1+\sqrt{\ell})$	$1/(1+\sqrt{\ell})^2$	$\sqrt{\ell}/(1+\sqrt{\ell})$

ticles. Note that for $\ell > 1$, no exact solutions exist and results are obtained from mean-field approximations. In what follows, much attention has been devoted to investigating joint effects of large particles and Langmuir kinetics (particles randomly attachment to and detachment from a lattice) on TASEP [40, 41] and joint effects of large particles and local inhomogeneity on TASEP [12, 42, 43]. These articles are reviewed in Sections 2.2.3 and 2.3.3.

Note that these papers considered homogenous traffic (i.e., consisting of particles with the same size) of large particles. The mixed traffic (consisting of particles with different sizes) has not been well understood theoretically although it has been extensively simulated in vehicular traffic. Moreover, the theoretical investigation of the effect of large particles on TASEP in a single-channel system with parallel update has not been conducted so far. The following comparisons of theoretical results should be addressed: (i) TASEP with large particles in random update and in parallel update; (ii) TASEP with large particles in parallel update and the normal TASEP in parallel update.

2.2.2   TASEP with long-range hopping

Long-range hopping means that a particle can hop more than one site at one time step. The effects of long-range hopping in the TASEP with parallel update have been

investigated in [44]. However, the long-range hopping in [44] implies that a particle can jump several successive sites ahead provided all of these sites are empty. The model, essentially, a *multiple-speed* TASEP, can be characterized by the maximal hopping distance, v_{max}. The theoretical calculations indicate that the current is determined by injection or ejection rate, independent of v_{max}. The influence of v_{max} on the bulk density is only in the low-density phase, that is, the increase of v_{max} will lead to a decrease in bulk density.

Recently, Kunwar et al. [45] developed a mathematical model for intracellular traffic of dynein motor proteins. Their model is also a multiple-speed TASEP, but in random update. Furthermore, the kinetics of attachment and detachment of motors on the lattice is incorporated in their model. The model exhibits an unusual feature where low and high density phases can coexist over a range of parameter values.

The TASEP with long-range hopping in random update was investigated in [46] as well. In that model, particles are allowed to pass over each other by jumping l sites with probability $p_l = 1/l^{\sigma+1}$ (σ is a control parameter). This long-range hopping only checks whether the target site is empty, rather than checking whether all successive sites between the current site and the target site are available. This is the main difference from the above-mentioned multiple-speed models. It was found that when $\sigma > 1$,the phase diagram remains the same as the standard one [8]. When $1 < \sigma < 2$, density profiles depend on values of σ. In the MC phase, current decreases with a σ-dependent exponent. One possible application of the model, as the authors suggested [46], is to describe attachment and detachment processes of molecular motors moving along a filament.

2.2.3   TASEP with Langmuir kinetics

Motivated by attachment-detachment kinetics of molecular motors on cytoskeletal filaments [22], [47] studied a one-dimensional TASEP coupled with Langmuir kinet-

ics (LK for short). This model can be regarded as a minimal model for intracellular transport, and is also referred to as the PFF model. In [47], an unexpected phenomenon, a phase coexistence between low-density and high-density phases, is observed and a mean-field theory is developed. The mean field approximation derived for density profiles has been shown to agree with Monte Carlo simulations.

Popkov et al. [49] argued that the mean-field method developed in the PFF model cannot be used in general. They believe that the coincidence with the Monte Carlo simulations in [47] is due to a lack of correlations in the steady state of the TASEP. Furthermore, they claim that stationary density profiles can be derived, in general, using a hydrodynamic equation [49], which can take correlations into account. They have also demonstrated that the equation can correctly describe density profiles on a quantitative level of the Katz-Lebowitz-Spohn (KLS) model [50, 51], which a mean field approach has failed to reproduce, e.g., phase separation into three distinct density regimes.

The PFF model can be used to describe the traffic dynamics of monomers. The authors in [41] extended the PFF model by considering large particle properties, specifically dimers (e.g., two-headed molecular motors). Dimers advance by a single site at each time step. Thus, their model can be viewed as a combination of the TASEP with large particles and LK. Unsurprisingly, the models exhibits the LD/HD phase coexistence, and the phase diagram alters quantitatively, compared to the phase diagram in the PFF model. The reason for that is, probably, due to the fact that the phase diagram of the TASEP with large particles is qualitatively identical with that of the normal TASEP.

A model, incorporating a single-channel TASEP, LK and Brownian ratchet mechanism[2], is proposed by Nishinari et al. [53] to mimic the movement of the

---

[2]Brownian ratchet is a mechanism that can rectify the random Brownian motion of particles to generate a directed steady-state flow. An illustration of Brownian ratchet can be found in

single-headed kinesin motor, KIF1A. A novel feature in their model is that there are *three* states (strong attachment, weak attachment and no attachment) of a KIF1A, compared with *two* states (attachment or detachment) in previous models. Their model can capture explicitly thee effects of adenosine triphosphate (ATP) hydrolysis as well as the ratchet mechanism. In the low-density phase, the experimentally observed single molecular properties are reproduced and a phase diagram is presented.

Recently, the influence of inhomogeneity on TASEP coupled with LK has attracted attention from several research groups [54, 55]. These papers will be reviewed in Subsection 2.3.3.

2.2.4 TASEP with two species of particles

Studies on TASEP with two species of particles under open boundary conditions mainly aim at observing the phenomenon of spontaneous symmetry breaking (SSB). The SSB has been observed in both single- and multiple-channel systems [56, 57, 58, 59, 60, 61, 62, 63, 64, 65].

The SSB means that a system in symmetry (e.g., structures, updating procedures) can be affected by some factors. At this point, the system no longer keeps in a symmetric manner, that is, the symmetry of the system is spontaneously broken [66]. In other words, one can observe two different densities of two species of particles in the SSB. More recently, the SSB is used to describe how one X chromosome is randomly chosen and the other X chromosome stays silent in female cells [67].

Evans et al. [56, 57] firstly observed the phenomenon of the SSB in one-dimensional two species TASEP with open boundary conditions. The first species move from the left to the right while the second species particles move in the opposite direction. The two kinds of particles may exchange each other with a certain

---

http://www.elmer.unibas.ch/bm/index.html, latest access on 14th Sept. 2009.

probability. At the left boundary, the first species may enter the system with rate α if the first site is empty, while the second species may leave the system with rate β. Similarly, at the right boundary, the second species may enter the system with rate α if the last site is empty, while the first species may leave the system with rate β.

As the shape of the model in [56, 57] looks like a bridge (see Figure 2.4), the model is known as the "Bridge model". In the Bridge model, it was shown that a high-density-low-density (HD/LD) phase and an asymmetric LD/LD phase could exist and both of them exhibit broken symmetry. Mean-field analysis shows that the asymmetric LD/LD phase exists in a very small region. However, Monte Carlo simulations suggest that the asymmetric LD/LD phase does not exist in the thermodynamic limit (i.e., as the number of the lattice sites $N \to \infty$) [58, 59, 61, 62].
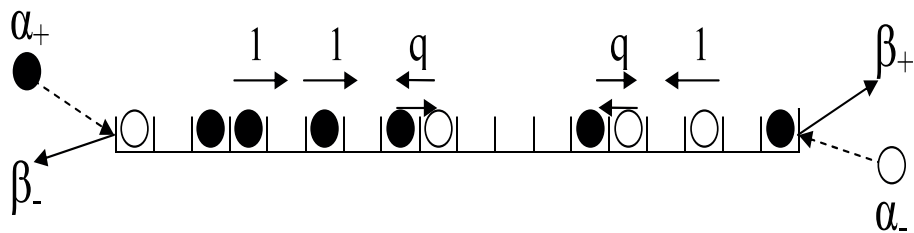
Figure 2.4: Sketch of the Bridge model. First species of particles move from the left to the right, represented by filled circles. Second species of particles move with opposite directions, denoted by open circles. Numbers over the arrows correspond to hopping rates.

Levine and Willmann [60] extended the Bridge model by considering LK on a lattice. The LK dynamics was assumed to be symmetric for two species of particles, that is, two species with the same attachment rate and detachment rate. They found that the SSB could exist and the localized shocks appear in some conditions. The Bridge model with sublattice-parallel update is also investigated in [62]. The symmetry breaking phenomenon, as [62] indicated, can be explained as a result of

an amplification mechanism of fluctuations.

The SSB has been observed in a two-channel system as well. Popkov and Peschel [59] investigated a two-channel system where two species of particles move in the same direction. There is no exchange of particles between two channels. Interactions between two channels are considered via the *hopping rates*. The hopping rates in one channel (denoted as A) are assumed to depend on the local configuration of the other channel (denoted as B). Local configuration can be understood in the following way: in normal conditions, $(1\ 0) \longrightarrow (0\ 1)$ on channel A with rate 1. If the local configuration on the corresponding sites of channel B is $(0\ 1)$, the hopping rate on channel A is ϵ ($\epsilon < 1$). Here $(1\ 0)$ means that site i is occupied, while site $i + 1$ is empty. It is also shown that the symmetry breaking phenomenon could weaken with the increase in values of ϵ.

Recently, the SSB has been investigated using two-species two-channel TASEP with *narrow entrances* and random update under open boundary conditions [63]. Narrow entrances mean that particles cannot enter a channel if the exit site in the other channel is occupied (see Figure 2.5). Two species of particles move along different channels and opposite directions. Interactions between two species of particles are assumed to take place only on left and right boundaries. Four steady phases (LD/HD, LD/LD, LD and MC) are obtained and two of them (LD/HD and LD/LD) exhibit the SSB phenomenon. It is found that the effective boundary defects (e.g., narrow entrances) can lead to the SSB. Moreover, the MC phase can exist in two-channel two species TASEP, while it does not exist in the single-channel two species TASEP [56, 57, 58, 61]. The theoretical calculations qualitatively agree with Monte Carlo simulations. However, as the authors in [63] indicated, the exact solutions using TASEP to describe the SSB have not been obtained so far. The model in [63] is motivated by kinesins and dyneins moving along microtubules in opposite directions [63].
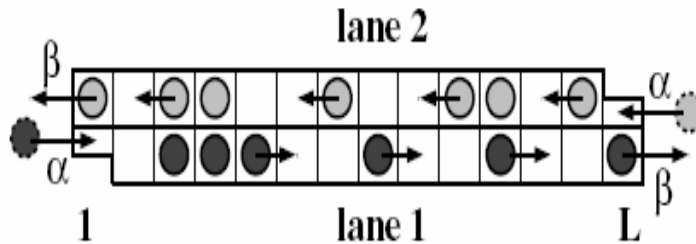
Figure 2.5: Sketch of two-channel TASEP with narrow entrances [63]. Narrow entrances mean that a particle cannot enter a channel if the exit site in the other channel is occupied. First species particle moves from the left to the right, represented by black circles. Second species particle moves oppositely, denoted by grey circles.

Jiang et al. [64] further investigated the SSB in a two-channel system with parallel update. The entrance rules of particles are the same as that in [63]. Two symmetric breaking phases (HD/LD and LD/LD) are obtained and the LD/LD phase just occupies a line in the phase diagram. Their investigations confirm that for the same system, different updating procedures (e.g., random and parallel) can lead to different dynamic properties.
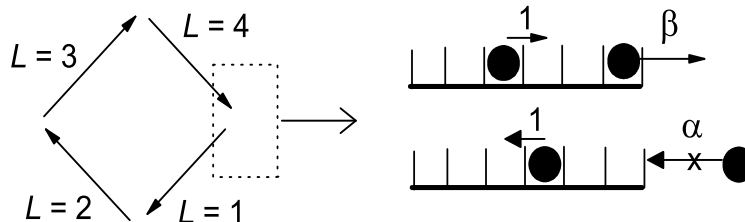
Figure 2.6: Sketch of a four-channel TASEP model with narrow entrances [65]. Narrow entrances mean that particles cannot enter a channel if the nearest-neighbor exit site in another channel is occupied.

More recently, Jiang et al. extended their work in [64] to a n-channel loop system ($n > 2$) [65] (see Figure 2.6). The n-channel system is configured like a loop:

the tail of channel 1 is next to the head of channel 2; the tail of channel 2 is next to the head of channel 3, and so on. The system exhibits more complicated properties. If n is an even number, the results revert to their two-channel system [64], i.e., the HD/LD and LD/LD phases are two symmetric breaking phases. In this case, the SSB is observed. When n is an odd number, a periodic structure is observed and the period is related to n, the system size L, injection rate α and ejection rate β.

2.3 TASEP with different lattice structures

2.3.1 TASEP with multiple parallel channels
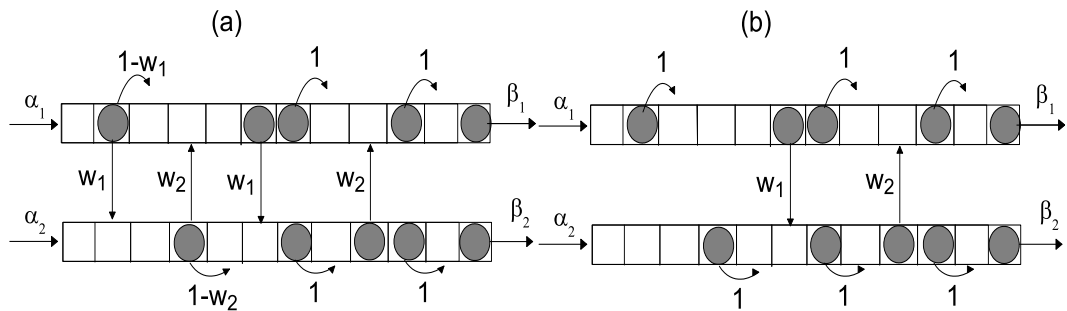
Figure 2.7: General two-channel TASEP models. (a) Positive coupling models. Particles may freely change to the corresponding site on the other channel with probability ω_1 (ω_2) provided the corresponding site on the other channel is empty. (b) Negative coupling models. Particles can change to the corresponding site on the other channel with probability $\omega_1(\omega_2)$ only when the immediately preceding site is occupied and the corresponding site on the other channel is empty.

Most previous work on modelling particle traffic deals with single-channel systems. Obviously, the description of particle traffic would be more realistic if two- or multiple-channel systems can be considered. Two- or multiple-channel vehicular traffic are common in our everyday life. In biological transport, experimental observations have found that molecular motors (e.g., kinesins) can move along parallel protofilaments of microtubules and they can jump between these protofilaments

without restraint [23].

With regard to multiple-channel systems, inter-channel coupling rules have a strong effect on system properties (e.g., phase diagrams, currents, and bulk densities) and thus attract much attention. In general, there are two kinds of basic inter-channel changing models: (a) positive channel-changing (PCC) model; and (b) negative channel-changing (NCC) model (see Figure 2.7). For the purpose of description, I introduce an occupation variable $\tau_{\ell,i}$ denoting the state of the ith $(1 < i < N)$ site in the ℓth channel $(\ell = 1, 2)$. $\tau_{\ell,i} = 1$ (0) corresponds to whether the site is occupied or not. The PCC model corresponds to the following channel-changing rules:

- If $\tau_{\ell,i} = 1$, $\tau_{3-\ell,i} = 1$, and $\tau_{\ell,i+1} = 0$, a particle can move into site $(\ell, i+1)$ with probability 1.

- If $\tau_{\ell,i} = 1$, $\tau_{3-\ell,i} = 0$, and $\tau_{\ell,i+1} = 0$, a particle can move into site $(\ell, i+1)$ with probability $1 - w_\ell$ or move into site $(3 - \ell, i)$ with probability w_ℓ.

In other words, particles in the PCC model may freely change to the corresponding site on the other channel with probability w_1(or w_2) if the corresponding site on the other channel is empty. However, particles in the NCC model can change to the corresponding site on the other channel with probability w_1(or w_2) only when the immediately preceding site is occupied and the corresponding site on the other channel is empty.

A simple symmetric PCC model where $\alpha_1 = \alpha_2 = \alpha$, $\beta_1 = \beta_2 = \beta$, and $w_1 = w_2 = w$ is investigated in [68]. Computational results suggest that values of the coupling rate w have a strong effect on the steady-state properties of the system. In particular, with the increase of w, the particle current of each channel decreases and particle density increases. Following this line, Pronina and Kolomeisky then extended their work in [68] to a general case where the asymmetric coupling rules

are applied (i.e., $w_1 \neq w_2$) [69]. It is found that the asymmetric coupling rules lead to a very complex phase diagram, quite different from symmetric coupling. There are seven phases in the TASEP with asymmetric coupling rules, in contrast to three phases found in the system with symmetric coupling rules [68].

In [68, 69], inter-channel coupling rules are applicable to all sites. Recently, TASEP with two parallel channels and symmetric/asymmetric coupling between them are investigated by Tsekouras and Kolomeisky [70]. Symmetric/asymmetric coupling between two parallel channels is allowed only at one specific site far from the boundaries. In the case of the symmetric coupling there are three stationary phases, similarly to the case of single-channel TASEP with local inhomogeneity [71]. However, the asymmetric coupling lead to a very complex phase diagram with ten stationary-state regimes. Both authors then investigated the symmetric and asymmetric exclusion processes with asymmetric couplings in a two-channel system [72]. Particles in one channel follow the rules of the TASEP, while they move as in symmetric simple exclusion process (SSEP) along the other channel. In the SSEP particles can jump forward and backward with equal probabilities. Their theoretical calculations and computer simulations show that there are three stationary phases (LD, HD, and MC) in the system. The phase boundaries are shifted according to different coupling rates.

A generic solution for positive coupling models is so-called vertical cluster mean-field approximation. In this method, there are four possible states for a cluster of two vertical sites [68, 69, 70]. These states are: (i) Both vertical sites are occupied, denoted as P_{11}; (2) Vertical site on channel 1 is occupied, while the corresponding site on channel 2 is empty, denoted as P_{10}; (3) Vertical site on channel 1 is empty, while the corresponding site on channel 2 is occupied, represented as P_{01}; (4) Both vertical sites are empty, represented as P_{00}. Since these four states can be found in any vertical sites on both channel, the corresponding probabilities for these four

states can be normalized to 1, that is

$$P_{11} + P_{10} + P_{01} + P_{00} = 1. \qquad (2.6)$$

Thus, the bulk density in channel 1 can be written as: $\rho_1 = P_{11} + P_{10}$. Similarly, $\rho_2 = P_{11} + P_{01}$. Combining boundary conditions and coupling rules, the phase diagram, currents, and density profiles are obtained.

With regard to the NCC models, Mitsudo and Hayakawa investigated two-channel TASEP with asymmetric coupling rules [73]. Different injection and ejection rates of particles at the boundaries of two channels are considered. The positions of kinks (i.e., shocks) are reported to be synchronized although the number of particles may be different on two channels.

Jiang et al. [74] introduced LK into one channel of a two-channel system with symmetric coupling rules. It is shown that synchronization of shocks on both channels occurs when the coupling rate exceeds a threshold. A boundary layer is also observed at the left boundary as a finite-size effect. Two-channel TASEP both coupled with LK are investigated in [75]. The model is inspired by the dynamics of molecular motors, for instance, random motor (e.g., kinesin) attachments and detachments on filaments [22], random changing to the adjacent filaments [23], unidirectional motion of molecular motors along filaments [21], and local inhomogeneity in a filament [76]. The shock is found to move left first and then move towards the right with the increase of the channel-changing rates. This phenomenon is called the *jumping effect* [75]. Shocks or kinks are also called domain walls (see Section 3.4 for details of the domain wall theory). It is also shown that increasing attachment and detachment rates will weaken the jumping effect.

Effects of local inhomogeneity in one of the two TASEP channels on its neighbor channel are also investigated in [77]. The system mainly demonstrates following complex behavior on two channels: the local inhomogeneity has strong effects on

both channels when the hopping rate at the local inhomogeneity, p, is small and channel changing rate Ω is not so small. With the increase of p or Ω, the local inhomogeneity effects are weakened.

Jiang et al. investigated a two-channel TASEP with asymmetric weak and strong inter-channel couplings [78]. The weak couplings mean that the coupling rates are inversely proportional to the system size, while in strong coupling conditions, the coupling rates are independent of the system size. In the weak coupling case, localized shock appears on one channel and the discontinuous phase transition is reproduced. For strong coupling, the shock disappears. When $\omega_2 = 0$, the phase diagram consists of six regions. When $\omega_2 \neq 0$, the authors report that the current could be larger than 0.5 due to the correlation effect between neighbour vertical clusters. Note that the NCC models are normally constructed in the hydro-dynamic limit. The phase diagram, currents, and density profiles can be obtained by numerically solving the steady state equations.

2.3.2   TASEP with multiple-input multiple-output junction

Junctions can be seen as an extension of the multiple channels connected by junction points, which are one of the common used traffic facilities in nature. At junction points, several traffic flow are merged into one, which may lead to traffic congestion. In this sense, traffic points can be viewed as local inhomogeneities.

TASEP on lattices with a Y-junction (e.g., two-input-single-out junction) in *random update* have been investigated in [79]. In their model, three stationary phases (LD/LD, HD/HD and HD/MC) are obtained and two phase boundaries (LD/HD and LD/MC) are presented. A domain wall approach is proposed to predict density profiles on phase boundaries in [79, 80]. A similar approach has been used to calculate density profiles on phase boundaries in synchronous TASEP [28]. The basic idea of the domain wall is that, before a stationary state is reached, the left

part and the right part of the system will form different domains of densities in the bulk due to the particles entrance and exit. The coexistence of both domains causes the appearance of a shock (or domain wall). The domain wall will move forward and backward along the channel according to the values of entrance rate α and exit rate β. For the normal TASEP in a stationary state, the domain wall will eventually move to the right (left) end for the LD (HD) phase. For the Y-junction described in [79], the domain wall finally locates at the junction points in a stationary state.

Wang et al. [28] investigated the dynamics of synchronous TASEP on lattices with a multiple-input single-output (MISO) junction. They further extended the MISO junction [28] to a general case, a m-input n-output (MINO) junction, in parallel update by mean-field analysis and computer simulations [29]. This generation shows an integrated picture of the dynamics of TASEP with junctions. Furthermore, the MINO junctions can be classified by a parameter $\lambda = m/n$. Junctions with the same λ possess the same traffic properties (e.g., phase diagrams, stationary currents, and density profiles). This research issue has been completed and reported in Chapter 6.

Recently, Cai et al. [81] introduced LK into the system with a Y-junction described in [79]. Their model exhibit richer stationary phases, depending on the ratio of ω_A and ω_D, the attachment and detachment rates, respectively. Setting $K = \omega_A/\omega_D$, the authors studied three cases: $K > 1$, $K = 1$, and $K < 1$. In the case of $K > 1$, there are four stationary phases. For $K \leq 1$, more phases can be observed. For a fixed K, the phase diagram structure changes with the increase of ω_D.

TASEP with two consecutive junctions connected by a single channel in the middle are studied by Popkov et al. [82]. Particles on junctions are governed by TASEP, while they follow the rules of the Bridge model on the single channel. Two species of particles are involved in the system and move along opposite directions.

The model can be seen as a combination of TASEP with junctions and the Bridge model. The model exhibits SSB, i.e., the low-density-high-density phase. Moreover, there is a coexistence region of the SSB phase and a low-density symmetric phase.

The starting point for analysing TASEP with various junctions is the rule of current conservation through the junction points [81] and through the system [79, 28, 29, 82]. The junction geometry can be divided into two or more sections in terms of junction points. Each section can be treated as a TASEP or its extension. The overall phase diagram is thus a combination of possible phases in all sections. The weakness of this approach is that the correlation near the junction points has not been considered, which leads to deviations of theoretical calculations from computer simulations.

2.3.3   TASEP with local inhomogeneity

Studies on local inhomogeneity in TASEP have received much attention in recent years [27, 43, 54, 71, 77, 83, 84, 85, 87, 88, 89, 90]. Local inhomogeneity is also referred to as site-wise inhomogeneity. It may include (i) a single inhomogeneous site; (ii) a group of consecutive inhomogeneous sites; and (iii) randomly distributed inhomogeneous sites. An inhomogeneous site is normally characterized by a different hopping probability[3] from the homogeneous ones. In other words, if the hopping probability is denoted by p, $p = 1$ represents normal sites, while $p < 1$ corresponds to inhomogeneous sites. In reality, local inhomogeneity may be involved in many biological transport processes [76, 91, 92, 93] as well as in vehicular and pedestrian traffic [94, 95]. For instance, the local inhomogeneity of immunoreactivity may lead to a high susceptibility to respiratory infection [93], while high-density (e.g.,

---

[3]Note that some scholars like to use the word "probability" such as in [30, 32, 33, 56, 57, 71, 85], while others prefer "rate", e.g., in [43, 89, 90]. The word "probability" is adopted in this research work.

Table 2.4: Relation between current and bulk density of different phases in the TASEP with local inhomogeneity and random update [71].

phase	conditions	current (J)	bulk density (ρ)
LD	$\alpha < \beta$, $\alpha < q/(1+q)$	$\alpha(1-\alpha)$	$\rho_L = \rho_R = \alpha$
HD	$\alpha > \beta$, $\beta < q/(1+q)$	$\beta(1-\beta)$	$\rho_L = \rho_R = 1 - \beta$
MC	$\alpha \geq q/(1+q)$, $\beta \geq q/(1+q)$	$q/(1+q)^2$	$\rho_L = 1/(1+q), \rho_R = q/(1+q)$

congested) vehicular traffic may be attributed to some local inhomogeneity, e.g., on-ramps, lane reductions or temporary road works [94, 96]. Moreover, it has been proposed that the crowding of molecular motors may be a source of some human diseases such as neurodegenerative diseases, kidney diseases, and other human diseases [18, 19, 20].

TASEP with a local inhomogeneity in a one-dimensional lattice under open boundary conditions were studied in [71]. Table 2.4 lists the stationary phases, conditions for the existence of the phases, and the corresponding current and bulk density. Such a system can be decomposed to two steps: (i) one system with inhomogeneity can be divided into two homogeneous subsystems. Each of them is treated as a normal TASEP; (ii) two subsystems are connected by this inhomogeneous site. This approach may be called as "Segmented Mean Field Approximation" (SMFA) and has been followed by many researchers [27, 43, 54, 71, 77, 83, 84, 85, 87, 88, 89, 90].

Theoretical analysis of the model in [71] indicates that the phase diagram is similar to the normal TASEP (i.e., the LD, HD and MC phases) [8] with shifts of phase boundaries. Table 2.4 lists the relationship between current and bulk density of different phases in the TASEP with local inhomogeneity and random update.

Based on the research in [39, 71], TASEP with local inhomogeneity and large particles were investigated in [83]. As expected, the phase diagrams are still quali-

tatively the same as the standard TASEP with different phase boundaries.

The effects of clustered slow codons (local inhomogeneities) in mRNA transla-
tion and protein synthesis are investigated using TASEP in [84]. The results show
that the clustered defects can affect the current of ribosomes (particles). However,
when the number of slow codons in a cluster is more than 3 or 4, the current of
ribosomes does not significantly reduce.

TASEP with local inhomogeneity coupled with LK on one-dimensional lattices
has been investigated in [54] and [87] at nearly the same time. In [54], a novel phase,
bottleneck phase, is introduced to describe the current independently of boundary
conditions. Due to the bottleneck phase (BP), several rich bottleneck-induced mixed
phases (e.g., LD-BP, LD-MC-BP, MC-BP-MC) are reported.

Qiu et al. [87] indicated that the system behavior exhibited in their model is
more complex than that in the PFF model [47]. Eight stationary-state phases are
found, and theoretical analysis approximately agrees with computer simulations.

When several inhomogeneities exist, the system becomes more complex. [86]
investigated dynamic properties of a TASEP with two different hopping rates, p_a
and p_b, on a one-dimensional lattice. In their model, sites at rate p_b are arranged
with a period of T. Their theoretical analysis suggests that the dual-rate TASEP
still retains the three stationary phases (e.g., LD, HD and MC).

Dong *et al.* [43] investigated the effects of having inhomogeneities in different
positions on a lattice. For instance, having a slow site near the system boundaries
leads to a higher current than when the inhomogeneity is in the bulk of the lattice.
Foulaadvand *et al.* [88] studied a TASEP with variable hopping probability. The
hopping probability is assumed to follow a binary or uniform distribution. It is
found that the impact of disorder greatly depends upon the boundary conditions.

In [90], the effects of inhomogeneities on a one-dimensional TASEP with open
boundaries are reported. Inhomogeneous sites are randomly distributed with re-

duced hopping rate. [77] studied the effects of local inhomogeneity in two-lane TASEP coupled with LK. A single inhomogeneity is assumed to be located at one of two lanes. It is found that the local inhomogeneity effect can be observed in both lanes due to particles changing to the other channel when the hopping probability of the inhomogeneous site is small. This effect can be reduced by increasing the hopping probability or channel-changing rate.

Most TASEP models are implemented in random update, which shows the weakest spatial correlation, as indicated in [30]. Conversely, the synchronous/parallel update [28, 30, 33, 97, 98, 99] exhibits the strongest interaction between particles, which has been typically adopted in modelling vehicular and pedestrian traffic [16, 37]. TASEP in parallel update have been used to describe traffic flow in a single-lane highway with ramps [100]. For a single ramp (either on-ramp or off-ramp), in their model, the bottleneck phenomenon does not exist. Traffic jams before the ramp and free flow after the ramp are not observed. For two consecutive ramps, in particular, when the on-ramp is placed before the off-ramp, the bottleneck effect occurs and the flow between two ramps saturates. These predictions are obtained from their model. No real traffic experiments have been reported to either confirm or reject these predictions.

2.4   Research methods

There are, in general, three types of research method (theoretical, experimental, and computer simulations) involved in scientific study. In this research, the focus is on theoretical methods (e.g, mean-field approximation and domain-wall theory) and computer simulations, e.g., Monte Carlo method.

This section briefly introduces the Monte Carlo method. To verify theoretical calculations of TASEP models, Monte Carlo simulations are carried out, in which

various dynamical properties of the system: phase diagrams, density profiles, and currents etc. are computed.

The Monte Carlo method is defined as "a method of approximately solving mathematical and physical problems by the simulation of random quantities" [101]. The Monte Carlo method was systematically proposed by Metropolis and Ulam in 1949 [102]. The name "Monte Carlo" originates from the city of Monte Carlo Monaco, famous for its casino.

With the great improvements of computing power and generalization of of vector and parallel computers, the Monte Carlo method has been used in the simulation of many mathematical and physical problems influenced by random factors (see [6,7,9,10,11] for example). Also its variants have been used in signal processing (e.g., stochastic approximation algorithm) and in optimization (e.g., simulated annealing) [103]. On the other hand, the limitations of the Monte Carlo method are obvious as well. For instance, the mathematical justification of the method is not always clear [103].

I briefly explain how to use Monte Carlo method to simulate the normal TASEP with open boundary conditions and random update. The TASEP variants can then be simulated based on the standard Monte Carlo method. The Monte Carlo method includes two parts: pre-processing and sampling. In the pre-processing part, it normally runs 10^8 time steps without sampling dynamical properties of the system in order to let the system reach the steady state. When the overall number of particles entering the system is equal to that of particles exiting the system, one can confirm that the system has reached steady state. For most TASEP systems 10^5 time steps per site is sufficient to obtain good simulation results. In the sampling part, bulk density, boundary currents and other quantities are computed with statistical average. To avoid correlations, one normally performs a sample every 10L (L is the system size). In general, the simulation scheme for particle-hopping process

normally consists of the following steps:

1. Initialize the system (e.g., $T = 1 \times 10^7$, $L = 1000$)

2. Do T Monte Carlo time steps:

   (a) Randomly choose a site index from 1 to L (1 corresponds to the first site, L to the last site and all other indices are for hopping to the neighbour site along the lattice)

   (b) In case of the first site. If the first site is vacant, a particle can enter the system with rate α; If the first site is not empty but the second site is empty, the particle in the first site can hops to the second site

   (c) In case of the last site. If the last site is not empty, the particle can leave the system with rate β

   (d) In case of another site. If the site is occupied and the next right site is empty, the particle can hop to the next one with rate 1

   (e) update the state of the chosen site

3. Repeat Step 2 with 10T time steps and compute average site densities and boundary currents over the running times of 10T

A flow chart of Monte Carlo simulations for this normal TASEP is shown in Figure 2.8.

2.5   Summary

In this Chapter, the totally asymmetric simple exclusion process (TASEP) and its recent developments have been comprehensively reviewed. Several popular theoretical methods are summarized. The Monte Carlo method used to verify theoretical analysis is also introduced. This review provides a basic picture for a better understanding
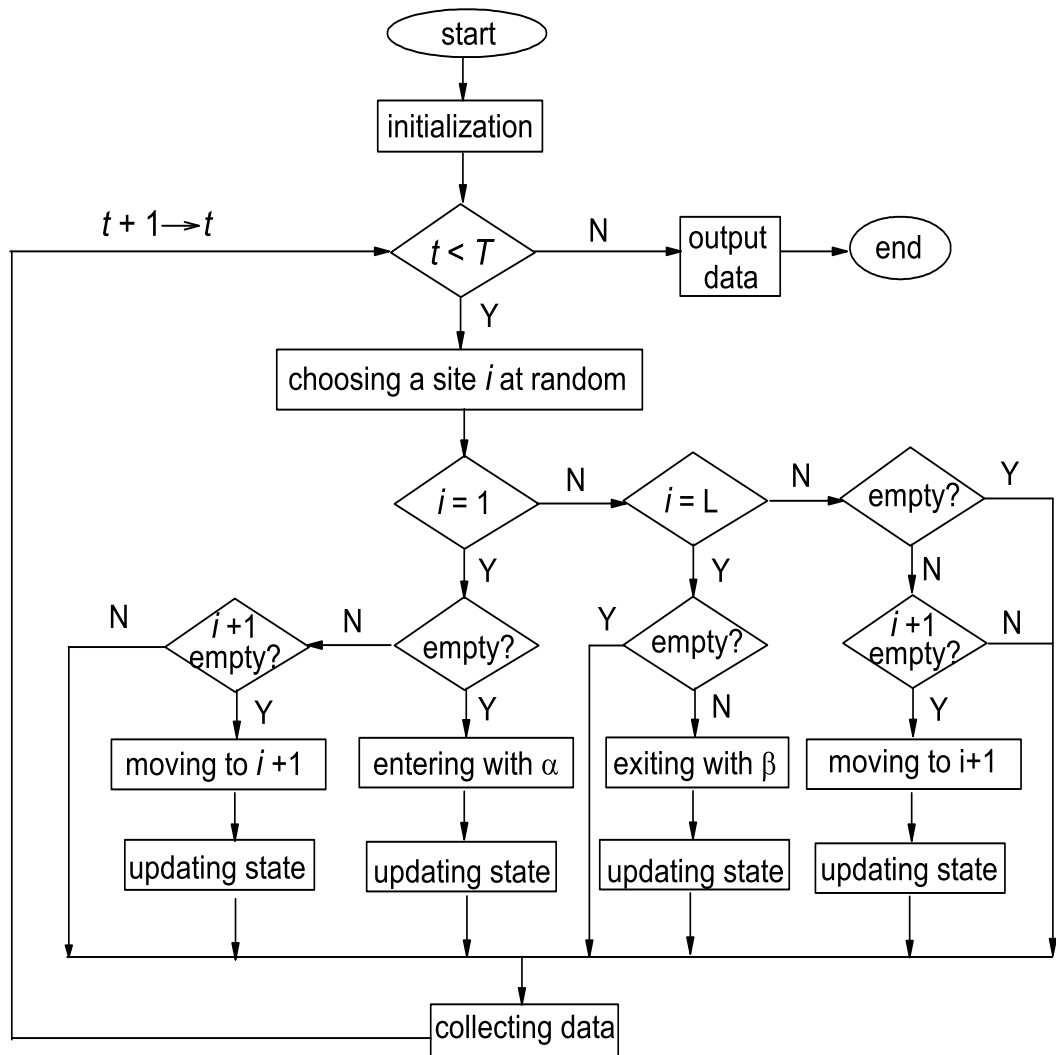
Figure 2.8: Flow chart of Monte Carlo simulations for the normal TASEP with random update.

of non-equilibrium processes in complex systems, such as biological transport and vehicular traffic. These models constitute the fundamental building blocks for this research.

Chapter 3

Local Inhomogeneity in a Single-channel System

3.1 Introduction

Traffic phenomena (e.g., intracellular transport and vehicular traffic) have received much attention since the early 1970s [7]. One important issue in understanding such traffic is to characterise stationary phases and transitions between them, using theoretical analysis. There are also a great number of efforts to integrate traffic theory with empirical observations in order to describe traffic more realistically [16, 104, 120, 121]. These achievements deepen understanding of the collective dynamics of self-driven interacting particles such as cars and molecular motors (e.g., kinesins, dyneins and myosins).

Totally asymmetric simple exclusion process (TASEP) has been widely accepted as a powerful tool in studying traffic, which is far from equilibrium, and has been successfully applied to describing stochastic dynamics of multi-particle interactions in chemistry, physics and biology [9, 105, 106] such as protein synthesis [11, 12, 43, 84], mRNA translation phenomena [13], and motion of molecular motors along the cytoskeletal filaments [14].

As a matter of fact, local inhomogeneity may be involved in many biological

transport processes [76, 91, 92, 93] as well as in vehicular and pedestrian traffic flow [94, 95]. The effects of local inhomogeneity on traffic properties have been extensively investigated in recent years [43, 54, 71, 77, 83, 84, 85, 87, 88, 89, 90] within the framework of non-equilibrium processes (see Section 2.3.3 for details). Most of these TASEP models are based on random update. The focus of this Chapter is on developing the theoretical and computational descriptions of the TASEP with a single inhomogeneity in parallel update. The phase diagram is obtained using a simple approximate theory, which gives an integrated picture of the traffic dynamics of the system and covers the full parameter space. Extensive computer simulations are carried out to verify the theoretical analysis. The parallel update has been typically adopted in modeling vehicular, ant and pedestrian traffic [16, 37]. Obviously, the proposed model may be more suitable for car, ant and pedestrian traffic, but less suitable for molecular motors or other biological transport.

This Chapter is organised as follows. In Section 3.2, A description of a one-dimensional TASEP model with a local inhomogeneity in parallel update is given. In Section 3.3, a mean-field approximation is developed, followed by a phenomenological domain wall approach in Section 3.4. In Section 3.5, the results of theoretical analysis and computer simulations are presented and discussed. Finally, conclusions are given in Section 3.6.

3.2   Model description

The model is defined in a one-dimensional lattice of N sites (N is an even number). Particles are assumed to go through the system from the left to the right. Site 1 (N) defines the left (right) boundary, while a set of sites 2, ..., N-1 is referred to as the bulk (see Figure 3.1(a)). It is assumed that the link between site k and site ($k + 1$) is inhomogeneous and other links are homogeneous. In other words, the

hopping probability at the inhomogeneous link is p, while the hopping probability of other normal links is 1. The inhomogeneous link can be in any position of the lattice; however, it is expected that the phase diagram and density profiles will be qualitatively the same, provided the inhomogeneous link is far away from the boundaries. For simplicity, $k = N/2$ is assumed in this Chapter. The following rules are applied to all sites *in parallel*.

- Entrance: A particle can enter the system from site 1 with rate α if the site is empty.

- Exit: A particle can leave the system from site N with rate β.

- Movement: A particle can move from site i into site $(i+1)$ with probability 1, provided $i \neq k$. If $i = k$, it moves to site $(i+1)$ with probability p; or if site $(i+1)$ is occupied by another particle, the particle stays at site i.
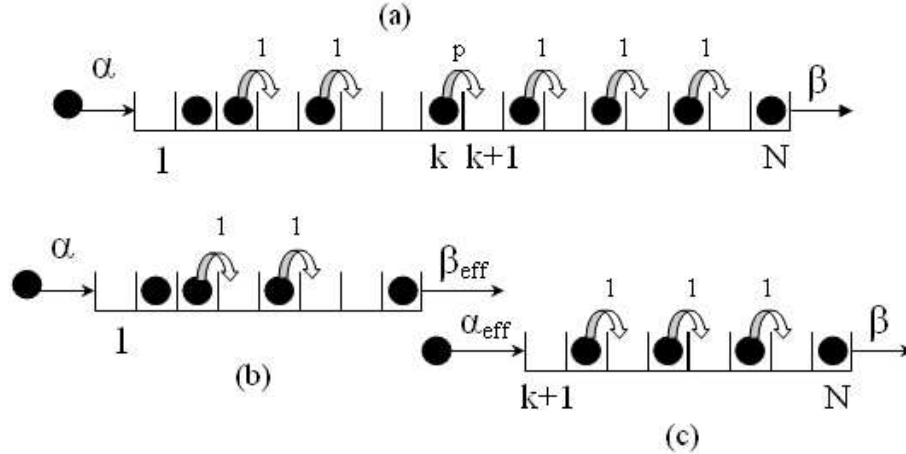
Figure 3.1: (a) Illustration of TASEP with a local inhomogeneity, which can be seen as two subsystems: (b) the left subsystem, and (c) the right subsystem. Arrows mean that the movements are allowed. Numbers over arrows are hopping rates.

A one-dimensional synchronous TASEP with a local inhomogeneity can be seen
as two homogeneous one-dimensional subsystems connected by an inhomogeneous
link between sites k and $(k+1)$ (see Figures 3.1(b) and (c)). The left subsystem
is a homogeneous TASEP with entrance rate α at site 1 and exit rate β_{eff} at site
k. Similarly, the right subsystem is also a homogeneous TASEP with entrance rate
α_{eff} at site $(k+1)$ and exit rate β at site N.

In this Chapter, only $0 \le p < 1$ is considered since the dynamics of such system
can be analyzed and simulated in parallel update. Obviously, when $p = 1$, the
system is the TASEP without local inhomogeneity. The exact solutions for this case
have been obtained in Refs. [32, 33].

3.3   Mean-field approximation

Here the results of a synchronous TASEP without local inhomogeneity is briefly
presented [32, 33]. There are three phases (low density, high density and maximal
current) in that system. The maximum current (MC), $J = 0.5$, can only be reached
at $\alpha = \beta = 1$. When $\alpha < \beta$, a low-density (LD) phase is obtained with

$$J = \rho, \quad \rho = \rho_1, \quad \rho_1 = \frac{\alpha}{1+\alpha}, \quad \rho_N = \frac{\alpha}{\beta(1+\alpha)}, \tag{3.1}$$

where J is the system current; ρ is the bulk density; ρ_1 (ρ_N) is the particle density
at the first (last) site of the system. The condition, $\alpha > \beta$, corresponds to a high-
density (HD) phase, where

$$J = 1 - \rho, \quad \rho = \frac{1}{1+\beta}, \quad \rho_1 = 1 - \frac{\beta}{\alpha(1+\beta)}, \quad \rho_N = \rho. \tag{3.2}$$

The currents in the left subsystem (J_L), the right subsystem (J_R) and the local
inhomogeneity (J_{local}) should be equal in a stationary state, that is

$$J_L = J_R = J_{local}. \tag{3.3}$$

J_{local} can be written as follows [33]

$$J_{local} = \frac{1}{2}(1 - \sqrt{1 - 4p\rho_k(1 - \rho_{k+1})}). \tag{3.4}$$

The overall phases in the system can be obtained from the combinations of phases in the two subsystems. The possible stationary phases of the system are the (LD, LD), (LD, HD), (HD, LD), (HD, HD), (LD, MC), (HD, MC), (MC, LD), (MC, HD) and (MC, MC) phases as there are three possible phases (LD, HD and MC) in each subsystem. As $p < 1$, it cannot guarantee β_{eff} equal to 1, thus, it is impossible for the MC phase to exist in the left subsystem. As a consequence, α_{eff} is less than 1. In this condition, the MC phase would not exist in the right subsystem either. That is, the last five phases could not exist in the system.

For the (LD, LD) phase, the following conditions should be satisfied

$$\alpha < \beta_{eff}, \quad \alpha_{eff} < \beta. \tag{3.5}$$

According to Eqs. (3.1), (3.3) and (3.4), one obtains

$$\frac{\alpha}{1+\alpha} = \frac{\alpha_{eff}}{1+\alpha_{eff}} = \frac{1}{2}(1 - \sqrt{1 - \frac{4p\alpha}{\beta_{eff}(1+\alpha)}(1 - \frac{\alpha_{eff}}{1+\alpha_{eff}})}). \tag{3.6}$$

Then, one gets $\alpha_{eff} = \alpha$ and $\beta_{eff} = p$. Thus, the system is in the (LD, LD) phase when

$$\alpha < \beta, \quad \alpha < p. \tag{3.7}$$

The corresponding current and density profiles in this phase are

$$J = \rho, \quad \rho = \rho_1, \quad \rho_1 = \frac{\alpha}{1+\alpha}, \quad \rho_k = \frac{\alpha}{p(1+\alpha)}, \quad \rho_{k+1} = \frac{\alpha}{1+\alpha}, \quad \rho_N = \frac{\alpha}{\beta(1+\alpha)}. \tag{3.8}$$

The (LD, HD) phase corresponds to

$$\alpha < \beta_{eff}, \quad \alpha_{eff} > \beta. \tag{3.9}$$

As the current is conserved in the system, that is,

$$\frac{\alpha}{1+\alpha} = \frac{\beta}{1+\beta} = \frac{1}{2}(1 - \sqrt{1 - \frac{4p\alpha}{\beta_{eff}(1+\alpha)}\frac{\beta}{\alpha_{eff}(1+\beta)}}), \qquad (3.10)$$

One obtains $\alpha = \beta$ and $\alpha_{eff}\beta_{eff} = p\alpha$. As $\alpha_{eff} > \beta$ and $\beta_{eff} > \alpha$, $\alpha = \beta < p$. This phase corresponds to a transition line between the (LD, LD) and (HD, HD) phases in the system. The density profiles of this phase will be studied using the domain wall theory as shown in the following section.

The (HD, LD) phase corresponds to the following conditions

$$\alpha > \beta_{eff}, \quad \alpha_{eff} < \beta. \qquad (3.11)$$

According to Eqs. (3.1-3.4), one has

$$\frac{\beta_{eff}}{1+\beta_{eff}} = \frac{\alpha_{eff}}{1+\alpha_{eff}} = \frac{1}{2}(1 - \sqrt{1 - \frac{4p}{1+\beta_{eff}}(1 - \frac{\alpha_{eff}}{1+\alpha_{eff}})}), \qquad (3.12)$$

where $\alpha_{eff} = \beta_{eff} = p$ is obtained. Thus, the system is in the (HD, LD) phase when

$$\alpha > p, \quad \beta > p. \qquad (3.13)$$

The current and density profiles in this phase are given by

$$J = \frac{p}{1+p}, \quad \rho_L = \frac{1}{1+p}, \quad \rho_1 = 1 - \frac{p}{\alpha(1+p)}, \quad \rho_k = \frac{1}{1+p},$$

$$\rho_R = \frac{p}{1+p}, \quad \rho_{k+1} = \frac{p}{1+p}, \quad \rho_N = \frac{p}{\beta(1+p)}. \qquad (3.14)$$

The (HD, HD) phase should be satisfied with

$$\alpha > \beta_{eff}, \quad \alpha_{eff} > \beta. \qquad (3.15)$$

Similarly, one reads

$$\frac{\beta_{eff}}{1+\beta_{eff}} = \frac{\beta}{1+\beta} = \frac{1}{2}(1 - \sqrt{1 - \frac{4p}{(1+\beta_{eff})}\frac{\beta}{\alpha_{eff}(1+\beta)}}), \qquad (3.16)$$

which is equivalent to $\beta_{eff} = \beta$ and $\alpha_{eff} = p$. According to Eq. (3.15), the system is in the (HD, HD) phase when

$$\alpha > \beta, \quad \beta < p. \tag{3.17}$$

Thus, the current and density profiles in this phase correspond to

$$J = 1 - \rho, \quad \rho = \frac{1}{1+\beta}, \quad \rho_1 = 1 - \frac{\beta}{\alpha(1+\beta)},$$

$$\rho_k = \frac{1}{1+\beta}, \quad \rho_{k+1} = 1 - \frac{\beta}{p(1+\beta)}, \quad \rho_N = \frac{\beta}{1+\beta}. \tag{3.18}$$
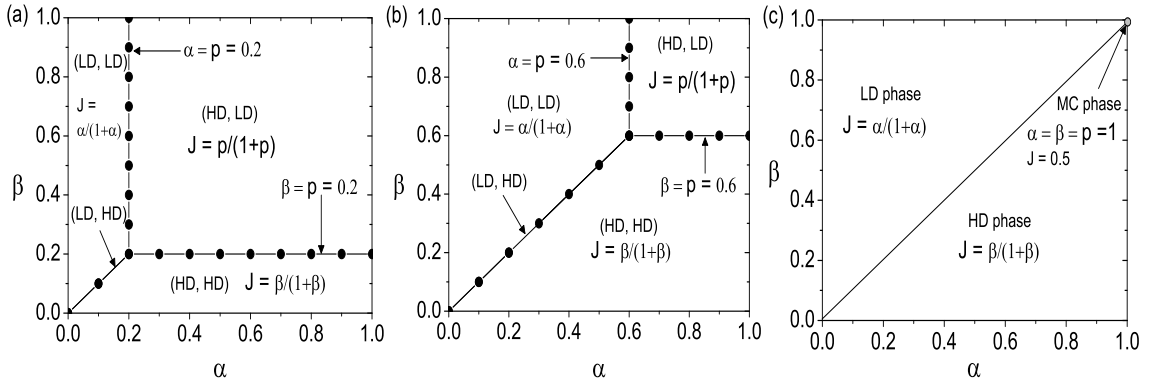
Figure 3.2: Phase diagrams of the TASEP with a local inhomogeneity in parallel update. Filled circles correspond to simulation results, while lines are obtained from the mean-field approximation of Sec. III. (a) $p = 0.2$, (b) $p = 0.6$, and (c) $p = 1.0$.

The above analysis suggests that there are four possible steady-state phases ((LD, LD), (LD, HD), (HD, LD) and (HD, HD)) existing in this system (see Figure 3.2). Theoretical predictions of phase boundaries are almost the same as computer simulations. The (LD, HD) phase is a coexistence line of the first-order phase transition between the (LD, LD) and (HD, HD) phases. The current in the (LD, LD) and (HD, HD) phases is determined by the values of α or β (see Figure 3.2). In other words, the current depends on the boundary conditions. In contrast, the (HD, LD) phase is similar to a maximal current phase. The current through this phase

is $J = p/(1 + p)$. One can see that this current is constant and has the maximal possible value compared to the (LD, LD) and (HD, HD) phases. Also, the current in the (HD, LD) phase is boundary conditions-independent. In Ref. [54], this kind of phase is called as the bottleneck phase.

The (HD, LD) phase region is specified by $p \leq \alpha \leq 1$ and $p \leq \beta \leq 1$. When $p = 0$, $J = 0$. This is obviously correct as $p = 0$ means that no particles can pass the inhomogeneous link. Thus, the current of the system $J = 0$. When $0 < p < 1$, one can see that the (LD, LD) phase region and the (HD, HD) phase region expand with the increase of p, while the (HD, LD) phase region shrinks (see Figures 3.2(a) and (b)). Finally, in the case of $p = 1$, the system reduces to the normal synchronous TASEP without local inhomogeneity (see Figure 3.2(c)).

Note that the phase diagram (see Figure 3.2) of the synchronous TASEP with a local inhomogeneity is related to understanding the general properties of traffic flow. Local inhomogeneities in a system can be blocks (e.g., road reductions or road works) on roads. Although these blocks just cover very short road segments, they can cause congested traffic. In the (LD, LD) and (HD, HD) phases, only local deviations of density profiles can be observed when p changes. However, when the system changes from the (LD, LD) phase to the (HD, LD) phase, a phase separation between high and low densities occurs at the local inhomogeneity. Experimental data collected on a German highway near Cologne (see Fig. 2 in Ref. [94]) exhibit such a separation in the presence of an on-ramp where the transition from free flow to congested flow is characterized by a sudden fall of the local velocity. This allows us to separate the data set into free-flow and congested regimes.

I also compare theoretical results (e.g., stationary currents and bulk densities) of TASEP with a single inhomogeneity in parallel update (present model) and random update (in [71]) in Table 3.1. It has shown that different updating procedures produce different dynamical properties even for the same system.

Table 3.1: Comparisons of stationary currents and bulk densities of TASEP with local inhomogeneity in parallel update (present model) and in random update [71].

update	$\rho_{LD}^L = \rho_{LD}^R$	J_{LD}	$\rho_{HD}^L = \rho_{HD}^R$	J_{HD}	$\rho_{MC}^L \neq \rho_{MC}^R$	J_{MC}
parallel	$\frac{\alpha}{1+\alpha}$	$\frac{\alpha}{1+\alpha}$	$\frac{1}{1+\beta}$	$\frac{\beta}{1+\beta}$	$\frac{1}{1+p}$, $\frac{p}{1+p}$	$\frac{p}{1+p}$
random	α	$\alpha(1-\alpha)$	$1-\beta$	$\beta(1-\beta)$	$\frac{1}{1+p}$, $\frac{p}{1+p}$	$\frac{p}{(1+p)^2}$

3.4 Domain wall theory
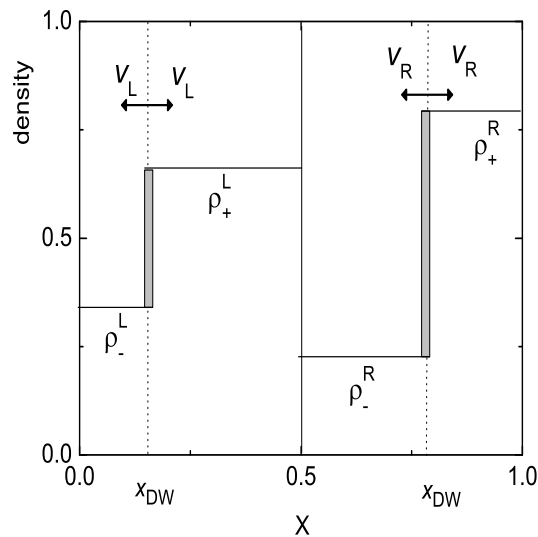
Figure 3.3: Schematic diagram of the domain wall dynamics in the (LD, HD) phase, i.e., the phase coexistence line. The domain wall moves in the left and right subsystems at rates v_L and v_R, respectively.

Although the mean-field method introduced in the above section predicts the existence of four phases, it fails for the prediction of bulk densities in the (LD, HD) phase. This gives a direct justification to apply domain wall (shock) theory instead. The domain wall theory has been employed successfully to explain the phase behavior of the TASEP with a junction in *random* update in Ref. [79]. The

domain wall theory is a phenomenological approach of the system dynamics [80]. That is, two different domains (of constant density) will appear in the bulk staring from the left and right boundaries, respectively before the steady state of the system reaches. When the system is in the steady state, two domains meet. The coexistence of two domains in the bulk means the existence of a wall (shock). It is believed that this approach could be applied to the TASEP with a local inhomogeneity in *parallel* update. In this Chapter, the domain wall approach is used to calculate the density profiles of the line $\alpha = \beta < p$, i.e., the (LD, HD) phase. To determine a position of the domain wall in the system, I define x as $x = i/N$, where i is the site index and N is the length of the system size. The case of $0 < x \le 0.5$, thus, corresponds to the domain wall moving at rate v_L in the left subsystem, and $0.5 < x \le 1$ for the domain wall moving at rate v_R in the right subsystem (see Figure 3.3). v_L and v_R can be given by

$$v_L = \frac{J_L}{\rho_+^L - \rho_-^L}, \quad v_R = \frac{J_R}{\rho_+^R - \rho_-^R}. \tag{3.19}$$

where

$$J_L = \frac{\alpha}{1+\alpha}, \quad \rho_+^L = \frac{1}{1+\alpha}, \quad \rho_-^L = \frac{\alpha}{1+\alpha}, \tag{3.20}$$

and

$$J_R = \frac{\beta}{1+\beta}, \quad \rho_+^R = \frac{1}{1+\beta}, \quad \rho_-^R = \frac{\beta}{1+\beta}. \tag{3.21}$$

As a result, v_L and v_R are rewritten as:

$$v_L = \frac{\alpha}{1-\alpha}, \quad v_R = \frac{\beta}{1-\beta}. \tag{3.22}$$

Similarly to Ref. [79], q_L (q_R) is denoted as a probability to find the domain wall at any position in the left (right) subsystem. For a special site i in the left (right) subsystem, the probability is obviously equal to $2q_L/N$ ($2q_R/N$). Then, at the local inhomogeneity, one reads

$$\frac{2v_L q_L}{N} = \frac{2v_R q_R}{N}. \tag{3.23}$$

In addition, normalized q_L and q_R are satisfied with:

$$q_L + q_R = 1. \tag{3.24}$$

Instituting Eq. (3.24) into Eq. (3.23), one obtains

$$q_L = \frac{v_R}{v_L + v_R}, \quad q_R = \frac{v_L}{v_L + v_R}. \tag{3.25}$$

As $\alpha = \beta < p$ corresponds to the transition line, one has $v_L = v_R$ and $q_L = q_R = 1/2$. These expressions reflect the fact that the domain wall can travel the left and right subsystems within the same probability.

Accordingly, the probability of the domain wall falling in a certain zone in the left subsystem is given by

$$Prob(x_{DW} < x) = 2q_L x, \quad 0 < x \le 0.5, \tag{3.26}$$

and in the right subsystem

$$Prob(x_{DW} < x) = q_L + 2q_R(x - 0.5), \quad 0.5 < x \le 1. \tag{3.27}$$

Thus, the density at any position in the system becomes

$$\rho(x)_m = \rho_-^m Prob(x_{DW} > x) + \rho_+^m Prob(x_{DW} < x), \quad m = L, R \tag{3.28}$$

Finally, from Eqs. (3.22-3.28), one can obtain

$$\rho(x)_L = \frac{\alpha}{1 + \alpha} + \frac{1 - \alpha}{1 + \alpha}x, \quad 0 < x \le 0.5, \tag{3.29}$$

and

$$\rho(x)_R = \frac{1}{2} + \frac{1 - \alpha}{1 + \alpha}(x - 0.5), \quad 0.5 < x \le 1. \tag{3.30}$$

Densities in the boundary conditions can be calculated as $\rho(x = 0)_L = \alpha/(1+\alpha)$ and $\rho(x = 1)_R = 1/(1 + \alpha)$. At the inhomogeneous site k ($k = N/2$), the densities are equal to $\rho(x = 0.5)_L = \rho(x = 0.5)_R = 1/2$. These results are completely identical with the theoretical analysis in Ref. [33] without inhomogeneity.

3.5 Theoretical calculations and computer simulations

In this section, computer simulations are carried out to validate the theoretical analysis. The length of the system size is assumed to be $N = 1000$ sites. For larger size N, simulation results show almost identical results with the ones presented here.

The simulation results for the density profiles are shown in Figure 3.4. In the (LD, LD), (HD, HD) and (HD, LD) phases, density profiles are still quantitatively and qualitatively the same as theoretical calculations (see Figures 3.4(a)-(c)). As mentioned, the (LD, HD) phase corresponds to the phase coexistence line between the (LD, LD) and (HD, HD) phases. Figure 3.4(d) shows the density profiles in this phase obtained from computer simulations and theoretical predictions. It is found that the density profiles derived from mean-field approximation are close to that obtained in computer simulations except around the local inhomogeneity. One possible explanation of these deviations is that the interaction between the particles near the local inhomogeneity is stronger than theoretical predictions.

The effects of hopping probability p on density profiles are examined when $\alpha < \beta$. The influence of p with $\alpha > \beta$ can be obtained using particle-hole symmetry [71] and the phase diagram shown in Figure 3.2. In Figure 3.5(a), $\alpha = 0, 2$, $\beta = 0.6$, and $p = 0.1$ lead to the (HD, LD) phase which is determined by $\alpha_{eff} = \beta_{eff} = 0.1$ (see Eq. (3.11)). When $p > 0.2$, a phase transition from the (HD, LD) phase to the (LD, LD) phase is observed. In the (LD, LD) phase, the bulk density $\rho = \alpha/(1+\alpha)$, which is independent of the value of p. The details of densities near the inhomogeneous site are shown in Figure 3.5(b). It can be seen that the amplitude of density increment near the local inhomogeneity in the left subsystem decreases with the increase of p, while densities remain unchanged in the right subsystem when $p > 0.2$.

Currents with different hopping probabilities are also investigated. For simplicity, it is assumed that exit rate β is constant in each figure, i.e., $\beta = 0.5$ in Fig-
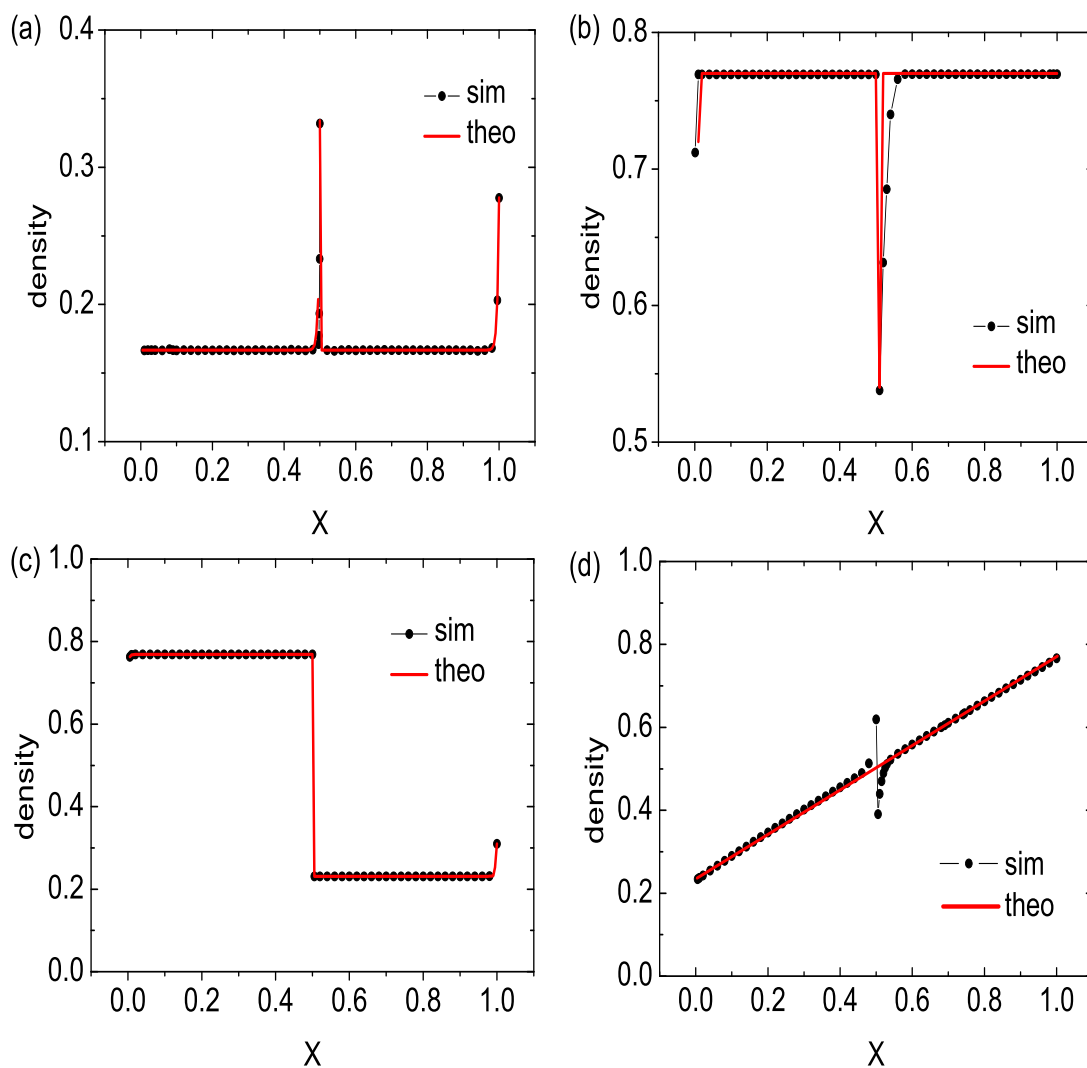
Figure 3.4: Density profiles from simulations and theoretical analysis in the stationary states. (a) the (LD, LD) phase with $\alpha = 0.2, \beta = 0.6$ and $p = 0.5$ (Eq. (3.8) for theoretical calculation); (b) the (HD, HD) phase with $\alpha = 0.8, \beta = 0.3$ and $p = 0.5$ (Eq. (3.18) for theoretical calculation); (c) the (HD, LD) phase with $\alpha = 0.9, \beta = 0.7$ and $p = 0.3$ (Eq. (3.14) for theoretical calculation); and (d) the (LD, HD) phase with $\alpha = 0.3, \beta = 0.3$ and $p = 0.5$ (Eqs. (3.29) and (3.30) for theoretical calculations).
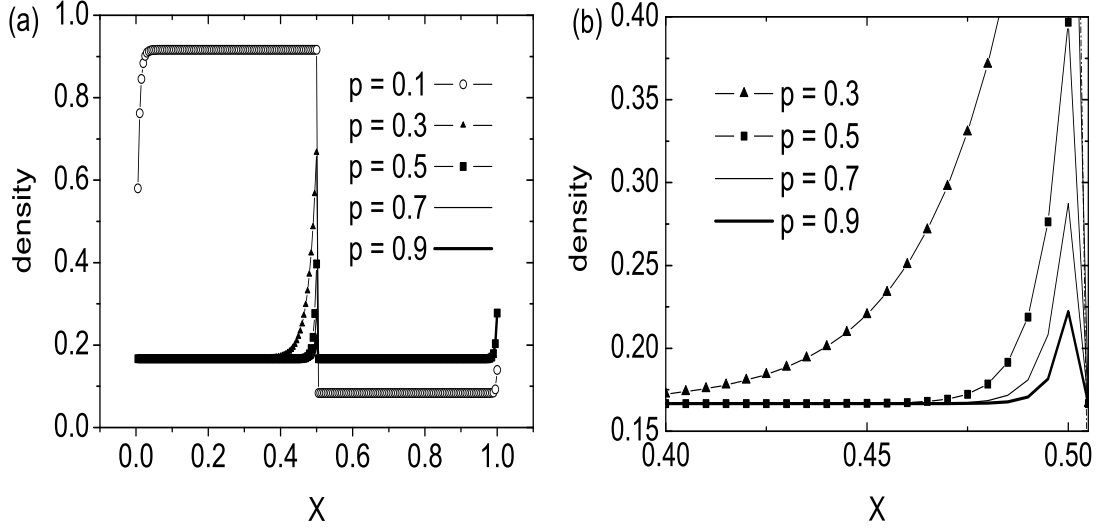
Figure 3.5: Density profiles with $p = 0.1, 0.3, 0.5, 0.7$ and 0.9. (a) and (b) $\alpha = 0.2$ and $\beta = 0.6$. (b) is the detailed density profiles near the inhomogeneous site in the left subsystem.

ure 3.6(a) and $\beta = 1$ in Figure 3.6(b). Entrance rate α changes within $[0, 1]$. From the phase diagram (see Figure 3.2(a)) one observes that the system is in the (LD, LD) phase when $p = 0.2$, $\beta = 0.5$ and $\alpha < 0.2$. In these situations, $J = \alpha/(1 + \alpha)$. Upon increasing α to 0.2, a saturation point S is reached with $S = p = 0.2$ and $J = p/(1 + p) \approx 0.16667$. Further increasing α, the system transfers from the (LD, LD) phase to the (HD, LD) phase, while the current is constant (see Figure 3.6(a)) since p dictates the dynamics of the system, in particularly, the right subsystem. When $p = 0.8$ and $\beta = 0.5$, a phase transition from the (LD, LD) phase to the (HD, HD) phase can be observed with α increasing to 0.5 (see Figure 3.2(b)). Clearly, saturation point S is at $S = \beta = 0.5$ with $J = \beta/(1+\beta) \approx 0.3333$. Similarly, one can obtain theoretically currents with $\beta = 1.0$ and $p = 0.2$ and 0.8 (see Figure 3.6(b)). It can be seen that theoretical calculations are in perfect agreement with computer simulations. In this Chapter, saturation point S and corresponding current J_{sat} can

be expressed as follows (see Eq. (3.31)). However, I note that Eq. (3.31) is not general since this equation gives the saturation point and current only for fixed p, β and upon varying α.

$$S = \min(p, \beta), \quad J_{sat} = \min(\frac{p}{1+p}, \frac{\beta}{1+\beta}). \tag{3.31}$$
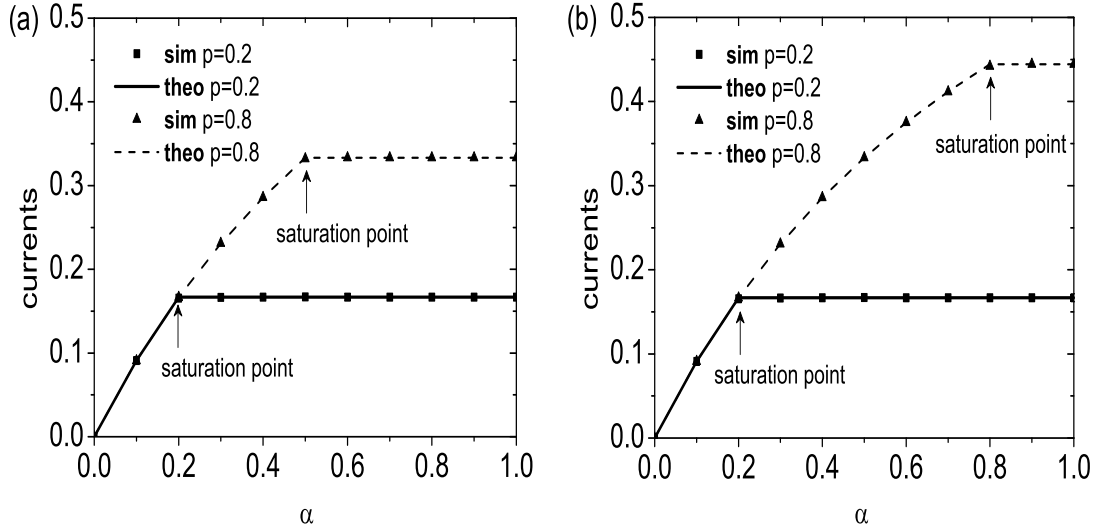
Figure 3.6: Dependence of current on entrance rate α with hopping probability $p = 0.2$ and 0.8. The exit rate is constant with: (a) $\beta = 0.5$ and (b) $\beta = 1$. The lines correspond to theoretical calculations, while symbols are the results of computer simulations.

In order to investigate the system behavior close to the phase boundaries, e.g., in Figure 3.2(a), a verification with Monte Carlo simulations is carried out. Figure 3.7 shows simulated results of density profiles near the theoretical phase boundaries (see Figure 3.2(a)) with hopping probability $p = 0.2$. In Figure 3.7(a), the system is in the (LD, LD) phase when $\alpha = 0.195$ and $\beta = 0.5$. When α increases to 0.2, the phase boundary is reached. In other words, a saturation point (see Figure 3.6) appears. Further increasing the value of α (e.g., $\alpha = 0.205$), the system transfers
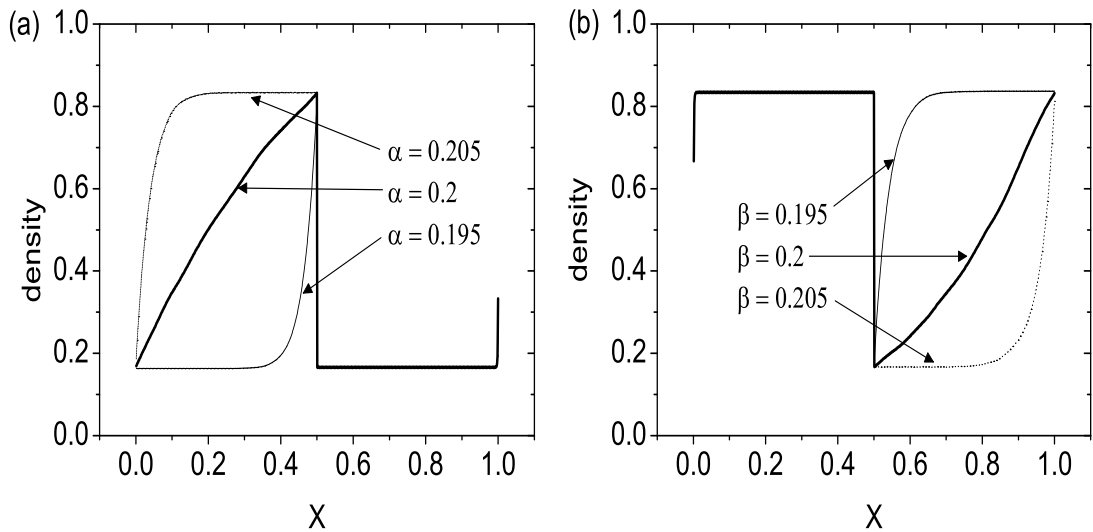
Figure 3.7: Simulation results of density profiles near the predicted phase boundaries (see Figure 3.2(a)) with hopping probability $p = 0.2$. (a) $\beta = 0.5$ and (b) $\alpha = 0.5$.

into the (HD, LD) phase. One can observe that the transition from the (LD, LD) phase to the (HD, LD) phase is discontinuous in the left subsystem, while it is continuous in the right subsystem. Also, the transition from the (HD, HD) phase to the (HD, LD) phase is continuous in the left subsystem, while it is discontinuous in the right subsystem (see Figure 3.7(b)). The simulation results show that there is little deviation of phase boundaries between theoretical calculations and computer simulations, compared to Ref. [71] in which the random update is used. The reasons for this are, probably, the different update procedures as well as different treatment with the local inhomogeneity, e.g., see Eq. (3.4) in the present model and Eqs. (3.6) and (3.7) in Ref. [71].

3.6   Summary and conclusions

A one-dimensional TASEP with a single inhomogeneity in parallel update is studied via mean-field approximation and extensive computer simulations. The approxi-

mate calculation is accomplished by separating the system into two subsystems. Both subsystems are connected at the inhomogeneity. The current through both subsystems is the equal. There are four possible stationary phases ((LD, LD), (LD, HD), (HD, LD) and (HD, HD)) in the system for $p < 1$. The (HD, LD) phase can be seen as a bottleneck phase in which the current is constant and dictated by the local inhomogeneity. With the increase of p, the (HD, LD) phase region shrinks, while the (LD, LD) and (HD, HD) phase regions expand. A phenomenological domain wall approach is developed to predict density profiles of the (LD, HD) phase. Density profiles and currents are simulated, and show very good agreement with theoretical calculations.

This approach can be extended to investigate effects of a local inhomogeneity in synchronous TASEPs with extended objects. It is also interesting to study the dynamics of synchronous TASEPs with an inhomogeneity near one of boundaries or randomly distributed inhomogeneities on the bulk.

This Chapter is based on the paper "Defect-induced transitions in synchronous asymmetric exclusion processes". The paper has been published in Physics Letters A 373 (2009) 195-200.

Chapter 4

Zoned Inhomogeneity on Asymmetric Exclusion Process

4.1 Introduction

Totally asymmetric simple exclusion process (TASEP) on lattices has been widely acknowledged as a paradigm in modelling vehicular traffic [16] and biological transport such as motion of molecular motors on microtubules [1, 31]. The corresponding tracks in these non-equilibrium systems are lanes, protofilaments or actin filaments. It is observed that the existence of local inhomogeneities (or defects) on these tracks can badly affect the dynamics of the systems such as in biological transport and vehicular traffic.

Theoretical investigations of effects of local inhomogeneity on non-equilibrium systems have been conducted intensively in recent years. TASEPs with an inhomogeneity under open boundary conditions attracted more attention from physicist and traffic scientists [27, 43, 54, 71, 77, 83, 84, 85, 87, 88, 89, 90] (see Section 2.3.3 for details). In reality, a segment of a road can be marked as a speed limit zone due to road works or safety reasons. Also in biological transport, molecular motors may experience diffusive processes until they reach filaments and then move along these filaments in a preferred direction [14]. Therefore, it is necessary to investigate

emergent traffic properties induced by a zoned inhomogeneity.

This Chapter studies effects of a zoned inhomogeneity on a one-dimensional TASEP in parallel update. The zoned inhomogeneity is a sequence of consecutive inhomogeneous sites with a reduced hopping probability p ($0 < p < 1$). Two lattice geometries are considered here: Cases *V* and *W* (see Figures 4.1(a) and (b)). In Case *V*, the system consists of a left subsystem (segment I) and right subsystem (segment II). Segment I is a homogeneous lattice with hopping probability 1, while segment II is also a homogeneous one, but with hopping probability p. Case *W* is a natural extension of Case *V*, but has three segements (I, II and III). The three segments correspond to the left, middle and right subsystems, respectively (see Figure 4.1(b)). Segments I and III are the normal TASEPs. Phase diagrams are obtained, and currents and density profiles are calculated. Phase diagrams of Cases *V* and *W* are compared as well as the system with an inhomogeneous site in parallel update [27].

The Chapter is organised as follows. In Section 4.2, the model of Case *V* is described. Theoretical analysis of Case *V* is developed and the phase diagram is obtained. Saturation points are defined. The results of theoretical analysis and computer simulations are presented and discussed. In Section 4.3, solutions for Case *W* are presented. Finally, conclusions are given in Section 4.4.

4.2   Case *V*

4.2.1   Model description

With regard to Case *V*, the model is defined in a one-dimensional lattice of N sites (see Figure 4.1(a)). Particles are assumed to hop to the right end. Site 1 (N) represents the left (right) boundary, while sites 2, ..., N-1 are referred to as the bulk. The following rules are applied to all sites *in parallel*: (i) A particle can enter the system at site 1 with probability α ($0 \leq \alpha \leq 1$), if the site is empty; (ii) A

particle at site N can leave the system with probability β ($0 \leq \beta \leq 1$); (iii) If site $i + 1$ is not occupied, a particle at site i can hop to that site with probability 1 for $i \leq k$ or with probability p for $k + 1 \leq i < N$ (i is an index of the sites). In other words, in the left subsystem, the hopping probability on the bulk is equal to 1, while it is equal to p in the right subsystem (see Figure 4.1(a)).

Both subsystems are linked by sites k and $k + 1$. The left subsystem is a homogeneous TASEP with entrance probability α at site 1 and exit probability β_{eff} at site k (see Figure 4.1(c)). Similarly, the right subsystem is, in fact, also a homogeneous TASEP with entrance probability α_{eff} at site $(k+1)$ and exit probability β ($0 \leq \beta \leq 1$ at site N (see Figure 4.1(c)). For simplicity, $k = N/2$ is asumed in this Chapter. Note that the phase diagram would be qualitatively the same provided site k is far away from the boundaries.

Only $0 < p < 1$ is considered in this Chapter here since the dynamics of the system can be affected under such circumstances. When $p = 0$, particles cannot hop to the right subsystem, thus the current through the system is equal to 0. When $p = 1$, the system becomes a homogeneous one. The theoretical analysis can exactly restore the current for two extreme cases: $p = 0$ and $p = 1$.

4.2.2 Theoretical analysis

The results of a synchronous TASEP for general p ($0 < p \leq 1$) has been presented in Refs. [30, 33]. There are three phases (low density, high density and maximal current) in that system. When $\alpha < \beta$ and $\alpha < 1 - \sqrt{1 - p}$, a low-density (LD) phase is obtained with the current $J = \alpha(p - \alpha)/(p - \alpha^2)$. When $\alpha > \beta$ and $\beta < 1 - \sqrt{1 - p}$, the system is in the high-density (HD) phase with $J = \beta(p - \beta)/(p - \beta^2)$. The conditions, $\alpha > 1 - \sqrt{1 - p}$ and $\beta > 1 - \sqrt{1 - p}$, correspond to the maximal current (MC) phase with $J = (1 - \sqrt{1 - p})/2$. Obviously, when $p = 1$, the currents in LD, HD and MC phases reduce to $J = \alpha/(1 + \alpha)$, $J = \beta/(1 + \beta)$ and $J = 1/2$,
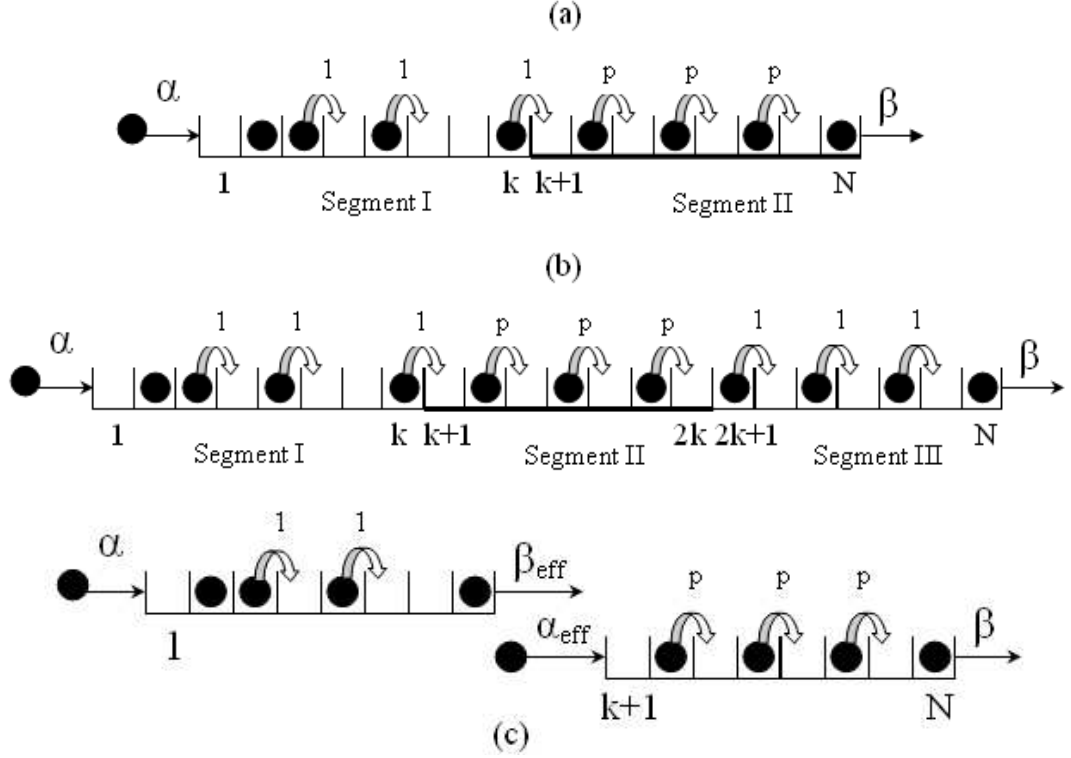
Figure 4.1: Illustration of an inhomogeneous TASEP on a one-dimensional lattice. Arrows mean allowed hoppings. Numbers over arrows represent hopping probabilities. (a) two subsystems in case V: left (segment I) and right (segment II); (b) three subsystems in case W: left (segment I), middle (segment II), and right (segment III); (c) Description of the left and right subsystems in case V in details.

respectively (see Refs. [32, 33]).

The theoretical analysis is based on a solid fact that the stationary current in the left subsystem (J_L) should be equal to that in the right subsystem (J_R), i.e., $J_L = J_R$ in a steady state, which is called the rule of current conservation.

Note that the MC phase cannot exist in the left subsystem for Case V shown in Figure 4.1(a). If the MC phase exists in the left subsystem, the maximal current should be equal to $J_L^{max} = 1/2$. However, in the right subsystem, $J_R^{max} = (1 - \sqrt{1-p})/2 < 1/2$ when $0 < p < 1$ [33]. Thus, according to the rule of current

conservation, the maximal current in the left subsystem cannot exist. Therefore, the possible stationary phases in the system of Case V include the following six phases: LD/LD, LD/HD, LD/MC, HD/LD, HD/HD and HD/MC. The LD/MC phase means that the left subsystem is in the LD phase, while the right subsystem is in the MC phase.

If the system is in the LD/LD phase, based on the rule of current conservation, the current can be written as

$$J_L = \frac{\alpha}{1+\alpha} = J_R = \frac{\alpha_{eff}(p - \alpha_{eff})}{p - \alpha_{eff}^2}. \tag{4.1}$$

Thus,

$$\alpha_{eff} = \frac{1}{2}(p + p\alpha \pm \sqrt{(p + p\alpha)^2 - 4p\alpha}). \tag{4.2}$$

Since the right subsystem is in the LD phase, $\alpha_{eff} < 1 - \sqrt{1-p}$. However, as $\frac{1}{2}(p + p\alpha + \sqrt{(p + p\alpha)^2 - 4p\alpha}) > 1 - \sqrt{1-p}$, one can obtain:

$$\alpha_{eff} = \frac{1}{2}(p + p\alpha - \sqrt{(p + p\alpha)^2 - 4p\alpha}). \tag{4.3}$$

Also, since $\alpha_{eff} < \beta$, one can get:

$$\frac{1}{2}(p + p\alpha - \sqrt{(p + p\alpha)^2 - 4p\alpha}) < \beta. \tag{4.4}$$

The above expression is meaningful only when the term in the square root is not negative, which implies

$$(p + p\alpha)^2 - 4p\alpha \geq 0. \tag{4.5}$$

Accordingly, one has

$$\alpha \leq \frac{2 - p - 2\sqrt{1-p}}{p}, \quad \alpha \geq \frac{2 - p + 2\sqrt{1-p}}{p}. \tag{4.6}$$

As $0 < p < 1$, $\alpha \geq (2 - p + 2\sqrt{1-p})/p > 1$, which violates the condition $0 \leq \alpha \leq 1$. Hence, $\alpha \geq (2 - p + 2\sqrt{1-p})/p$ should be discarded. Moreover, the current in the

system is less than the maximal current, that is, the following inequality should be met

$$J_L = \frac{\alpha}{1 + \alpha} < \frac{1 - \sqrt{1 - p}}{2} = J_{max}, \qquad (4.7)$$

which means

$$\alpha < \frac{2 - p - 2\sqrt{1 - p}}{p}. \qquad (4.8)$$

Thus, the conditions for the system to be in the LD/LD phase are:

$$\alpha < \frac{2 - p - 2\sqrt{1 - p}}{p}, \quad \beta > \frac{1}{2}(p + p\alpha - \sqrt{(p + p\alpha)^2 - 4p\alpha}). \qquad (4.9)$$

For the LD/HD phase one gets

$$\frac{\alpha}{1 + \alpha} = \frac{\beta(p - \beta)}{p - \beta^2}, \qquad (4.10)$$

which is equivalent to

$$\beta = \frac{1}{2}(p + p\alpha \pm \sqrt{(p + p\alpha)^2 - 4p\alpha}). \qquad (4.11)$$

Since the right subsystem is in the HD phase, $\beta < 1 - \sqrt{1 - p}$. However, since $\frac{1}{2}(p + p\alpha + \sqrt{(p + p\alpha)^2 - 4p\alpha}) > 1 - \sqrt{1 - p}$, one obtains:

$$\beta = \frac{1}{2}(p + p\alpha - \sqrt{(p + p\alpha)^2 - 4p\alpha}). \qquad (4.12)$$

Thus, the following conditions can guarantee the LD/HD phase in the system

$$\alpha < \frac{2 - p - 2\sqrt{1 - p}}{p}, \quad \beta = \frac{1}{2}(p + p\alpha - \sqrt{(p + p\alpha)^2 - 4p\alpha}). \qquad (4.13)$$

For the LD/MC phase the current can be written as

$$\frac{\alpha}{1 + \alpha} = \frac{1 - \sqrt{1 - p}}{2}, \qquad (4.14)$$

which means

$$\alpha = \frac{2 - p - 2\sqrt{1 - p}}{p}. \qquad (4.15)$$

Also, when the right subsystem is in the MC phase, the condition $\beta > 1 - \sqrt{1-p}$ should be satisfied. Thus, the LD/MC phase exists in the system when

$$\alpha = \frac{2 - p - 2\sqrt{1-p}}{p}, \quad \beta > 1 - \sqrt{1-p}. \tag{4.16}$$

In the HD/MC phase the current is satisfied with

$$\frac{\beta_{eff}}{1 + \beta_{eff}} = \frac{1 - \sqrt{1-p}}{2}, \tag{4.17}$$

which means

$$\beta_{eff} = \frac{2 - p - 2\sqrt{1-p}}{p}. \tag{4.18}$$

The left subsystem is in the HD phase only when $\alpha > \beta_{eff}$. Thus, the system is in the HD/MC phase when

$$\alpha > \frac{2 - p - 2\sqrt{1-p}}{p}, \quad \beta > 1 - \sqrt{1-p}. \tag{4.19}$$

The HD/HD phase corresponds to the following conditions

$$\frac{\beta_{eff}}{1 + \beta_{eff}} = \frac{\beta(p - \beta)}{p - \beta^2}. \tag{4.20}$$

That is

$$\beta_{eff} = \frac{\beta(p - \beta)}{p(1 - \beta)}. \tag{4.21}$$

Since the left subsystem is in the HD phase (i.e. $\alpha > \beta_{eff}$), The solutions for the HD/HD phase can be obtained similarly to that of the LD/LD phase. They include:

$$\alpha > \frac{\beta(p - \beta)}{p(1 - \beta)}, \quad \beta < 1 - \sqrt{1-p}. \tag{4.22}$$

The HD/LD phase describes the following current relationship

$$\frac{\beta_{eff}}{1 + \beta_{eff}} = \frac{\alpha_{eff}(p - \alpha_{eff})}{p - \alpha_{eff}^2}. \tag{4.23}$$

Thus, α_{eff} and β_{eff} cannot be represented as functions of p, α or β. This suggests that the HD/LD phase would not appear in the $\alpha - \beta$ plane. From the traffic flow

point of view, when the right subsystem is in the LD phase, particles in the right subsystem will hop forward without any block until they approach to the exit. In this condition, the effective exit rate $\beta_{eff} \rightarrow 1$, which leads to the left subsystem in the LD (or MC) phase as $\alpha \leq \beta_{eff}$. Thus, the HD/LD phase does not exist in the system.
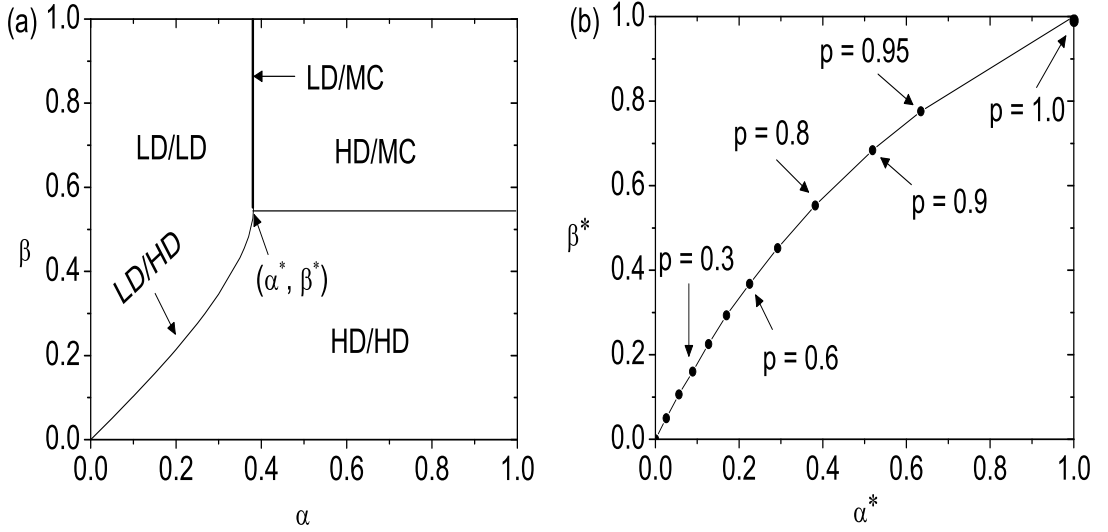
Figure 4.2: (a) Diagram of possible stationary-state phases in the system with $p = 0.8$; and (b) Saturation point pair (α^*, β^*) with different values of p.

Figure 4.2(a) illustrates all possible stationary phases in the system, which include the LD/LD, LD/HD, LD/MC, HD/MC, and HD/HD phases. The LD/HD phase corresponds to a first-order transition line between the LD/LD and HD/HD phases, while the LD/MC phase corresponds to a straight line specified by $\alpha = (2 - p - 2\sqrt{1-p})/p$ and $\beta \geq 1 - \sqrt{1-p}$. The transition from the LD/LD phase to the HD/MC phase is discontinuous in the left subsystem, while it is continuous in the right subsystem. Meanwhile, continuous transitions can be found in both subsystems between the HD/MC and HD/HD phases.

When the value of p is fixed, currents in the LD/LD, LD/HD and HD/HD

phases are determined by the values of α or β. However, currents in the LD/MC and HD/MC phases are only related to p (i.e., $J = (1 - \sqrt{1 - p})/2$). In other words, the currents in both the LD/MC and HD/MC phases are independent of boundary conditions.

For a better understanding the phase diagram, a saturation point pair (α^*, β^*) of the current is introduced, which can be written as

$$\alpha^* = \frac{2 - p - 2\sqrt{1 - p}}{p}, \quad \beta^* = 1 - \sqrt{1 - p}. \tag{4.24}$$

Values of α^* and β^* are plotted in Figure 4.2(b) with different p. With the increase of p, α^* and β^* increase, which corresponds to a decrease of regions in the LD/MC and HD/MC phases and an increase of the currents in both phases.

4.2.3 Results and discussion

This section discusses theoretical and simulation results. The system length is set to be $N = 2,000$ sites for Case *V* and $N = 3,000$ sites for Case *W*. The number of the running time steps in each experiment is 1.1×10^9 in order to obtain the stationary current and density profiles. The first 10^8 time steps are discarded as transients.

Theoretical and simulation results for currents are shown in Figure 4.3. One can see they are in good agreement. The hopping probability p is arbitrarily assumed to be $p = 0.3$, 0.6, and 0.9, respectively. In Figure 4.3(a), one can see that the current increases with the increase of the hopping probability. For instance, the saturated current $J_{sat} \approx 0.082$ for $p = 0.3$, while it increases to $J_{sat} \approx 0.186$ for $p = 0.6$ and $J_{sat} \approx 0.345$ for $p = 0.9$.

When $p = 0.3$, the saturation point, according to Eq. (4.24), corresponds to $\alpha^* = 0.089$ and $\beta^* = 0.163$. Thus, the system is in the HD/MC phase when $\alpha > 0.089$ and $\beta > 0.163$. Similarly, one can calculate $\alpha^* = 0.225$ and $\beta^* = 0.3675$ for $p = 0.6$, and $\alpha^* = 0.52$ and $\beta^* = 0.684$ for $p = 0.9$. As I assume $\beta = 1.0 > \beta^*$,
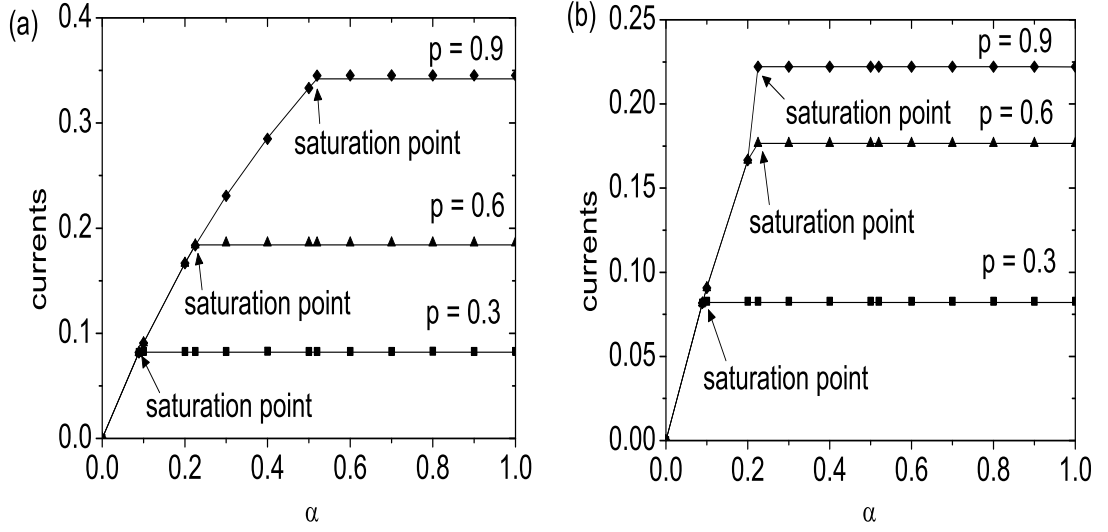
Figure 4.3: Currents with different hopping probabilities $p = 0.3$, 0.6, and 0.9. The lines describe theoretical calculations, while symbols correspond to computer simulations. The exit rate is: (a) $\beta = 1.0$ and (b) $\beta = 0.3$.

the system is only in one of the three phases: LD/LD, LD/MC, and HD/MC (see Figure 4.3). In other words, the HD/HD phase cannot be reached. One then set $\beta = 0.3$ to check the currents in the HD/HD phase (see Figure 4.3(b)). It is found that, when $p = 0.6$ and $p = 0.9$, the system is in the HD/HD phase as $\beta < \beta^*$. The corresponding saturation currents can be obtained using Eq. (4.20), which are $J_{sat} \approx 0.176$ for $p = 0.6$ and $J_{sat} \approx 0.222$ for $p = 0.9$.

The effects of hopping probability p on density profiles are simulated with different α and β (see Figure 4.4). In Figure 4.4(a), the system is in the HD/MC phase. This can be explained as follows. When p is increased from 0.1 to 0.5, $\alpha^*(\beta^*)$ is still less than 0.2(0.8), which is the entrance (exit) rate. One can also observe that the bulk density in the left subsystem decreases with the increase of p. However, when $p \geq 0.6$, the system transfers to the LD/LD phase (see Figure 4.4(b)). The bulk density decreases in the right subsystem upon increasing p to 1.0. One can see that

the bulk density remains unchanged in the *right* subsystem in Figure 4.4(a), while it is constant in the *left* subsystem in Figure 4.4(b). Figure 4.4(c) shows a similar picture when $\alpha = 0.7$ and $\beta = 0.3$, compared to Figure 4.4(a). Density profiles in the HD/HD phase are illustrated in Figure 4.4(d). With the increase of p, density profiles decrease in the left subsystem, while they increase in the right subsystem.

4.3 Case W

In this section, the phase diagram, currents and density profiles in Case W are discussed. As shown in Figure 4.1(b), in Case W, hopping probability p $(0 < p < 1)$ in the middle subsystem is different from that in the left and right subsystems. Both left and right subsystems have the same hopping probability $(p = 1)$ (see Figure 4.1). The phase diagram can be obtained in the same way as discussed above, which is shown in Figure 4.5(a). In other words, the rule of current conservation is still applied in a stationary state, i.e., $J_L = J_M = J_R$. J_M is the current through the middle segment.

Differences between Figure 4.2 and Figure 4.5(a) are compared as follows: (1) saturation point (α^*, β^*) pair for Case V corresponds to $\alpha^* = (2 - p - 2\sqrt{1-p})/p$ and $\beta^* = 1 - \sqrt{1-p}$ in Figure 4.2, while it changes to $\alpha^* = \beta^* = (2-p-2\sqrt{1-p})/p$ for Case W (see Figure 4.5(a)). This is because that segment I and segment III have the same system dynamics; (2) the number of stationary phases is 5 for Case V in Figure 4.2, while it becomes 7 for Case W in Figure 4.5(a). Two new LD/MC/HD and HD/MC/HD phases appear in Case W as shown in Figure 4.5(a). The LD/MC/HD phase corresponds to a point which is described by $\alpha^* = \beta^* = (2 - p - 2\sqrt{1-p})/p$. The HD/MC/HD phase is specified by a line $(\alpha > (2 - p - 2\sqrt{1-p})/p$ and $\beta = 1 - \sqrt{1-p})$. Despite these differences, Figure 4.5(a) is still qualitatively similar to Figure 4.2 since: (1) the phases of segment
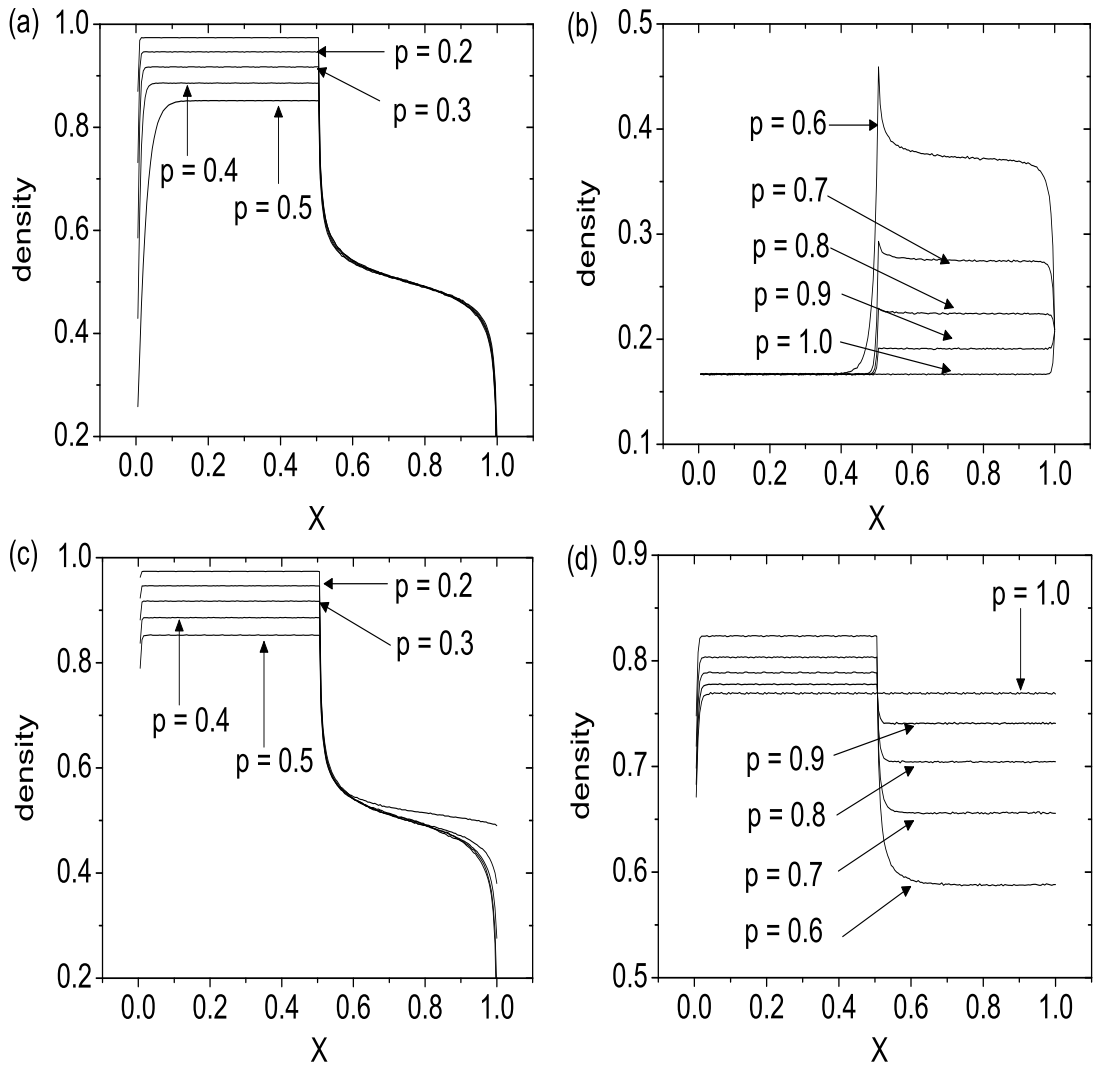
Figure 4.4: Density profiles from simulations in the stationary state with different p. $x = i/N$, i is an index of sites and N is the system length. (a) and (b) $\alpha = 0.2$ and $\beta = 0.8$; (c) and (d) $\alpha = 0.7$ and $\beta = 0.3$.

I and segment II in both cases are the same (see Figures 4.2 and 4.5(a)), that is, the introduction of segment III does not lead to a new phase in either segment I or segment II, and (2) Figure 4.5(a) will reduce to Figure 4.2 if segment III is ignored.

If there is only one inhomogeneous site in the system, the maximal-current (MC) region is specified by $\alpha = \beta \geq p$ and $\alpha = \beta \leq 1$ [27]. The corresponding maximal current is $J = p/(1 + p)$. For Case V, the MC region is described by $\alpha \geq (2 - p - 2\sqrt{1 - p})/p$, $\beta \geq 1 - \sqrt{1 - p}$, and $\alpha = \beta \leq 1$. Finally, for Case W, the MC region is determined by $\alpha = \beta \geq 1 - \sqrt{1 - p}$ and $\alpha = \beta \leq 1$. The different MC regions are illustrated in Figure 4.5(b) and details in Table 1. In other words, Case W has the maximal area of the MC region.

Currents are calculated and plotted in Figure 4.6 when $p = 0.8$ with different values of β, and α ranges from 0 to 1. When $\beta < \beta^* \approx 0.382$, the system changes to the HD/HD/HD phase from the LD/LD/LD phase with the increase of values of α (see Figure 4.5(a)). In the LD/LD/LD phase, the current increase when α increases, while the current becomes constant $(J = \beta/(1 + \beta))$ in the HD/HD/HD phase, independent of α. Similarly, when $\beta > \beta^*$, the system transfers into the HD/MC/LD phase from the LD/LD/LD phase upon increasing α (see Figure 4.5(a)). In the HD/MC/LD phase, the current is determined by p $(J = (1 - \sqrt{1 - p})/2)$, independent of α and β.

Density profiles in Case W are shown in Figure 4.7. In Figure 4.7(a), the system is in the HD/MC/LD phase and the increase of p only affects density profiles in the left and right subsystems. Further increasing p, e.g., $p \geq 0.6$, the system transfers to the LD/LD/LD phase and only density profiles in the middle subsystem are affected (see Figure 4.7(b)). A similar picture is also shown in Figure 4.7(c). However, the phase transition is complex with the change of p (see Figure 4.7(d)). The system first transfers into the HD/MC/HD phase from the HD/MC/LD when $p = 0.7$, and then changes to the HD/HD/HD phase.
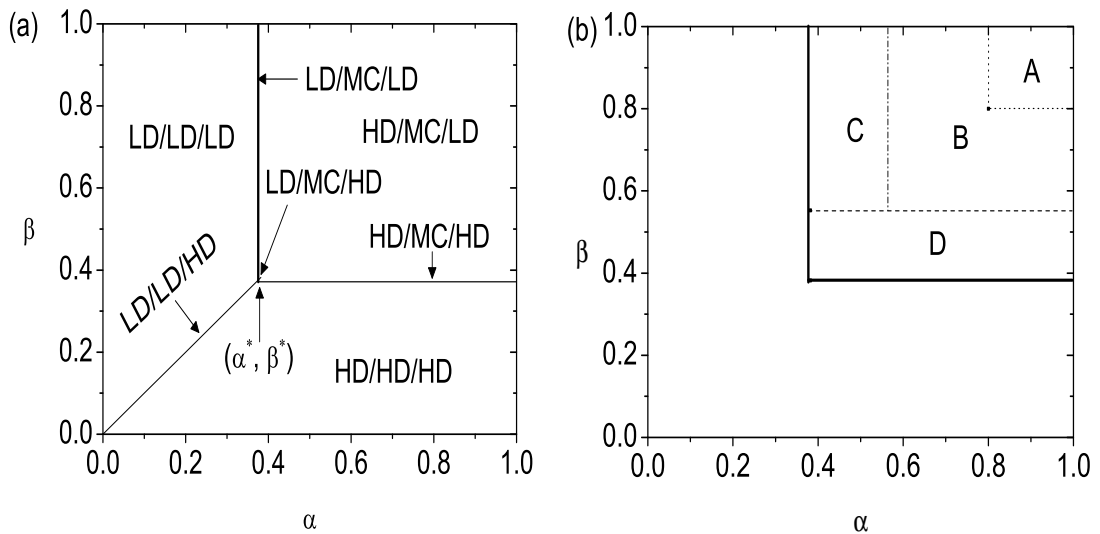
Figure 4.5: (a) Phase diagram of inhomogeneous asymmetric exclusion process with hopping probability p in the middle subsystem when $p = 0.8$; (b) Comparisons of the MC regions with the following relationship: A⊆B, B⊆C, and C⊆D. Details of A, B, C, and D see Table 4.1.

4.4 Summary and conclusions

A one-dimensional TASEP with a zoned inhomogeneity in parallel update is studied theoretically and by extensive computer simulations. A sequence of consecutive sites with hopping probability p $(0 < p < 1)$ is called a zoned inhomogeneity. A zoned inhomogeneity in the real world may correspond to a speed limit zone for vehicular traffic. Two cases of lattice geometries are discussed. In Case V, the system consists of two subsystems. The left subsystem (segment I) is a normal TASEP (i.e., $p = 1$), while the right subsystem (segment II) is the TASEP with hopping probability p. In Case W, the left and right subsystems are normal ones, while the middle subsystem (segment II) is the TASEP with hopping probability p.

The phase diagrams of Cases V and W are qualitatively the same with shifts of the phase boundaries. However, the differences between these two phase diagrams

Table 4.1: Details of Figure 4.5(b)

Region	Number and position of inhomogeneous sites	MC
A	an inhomogeneous site far away from boundaries	p/(1+p)
B	all sites are inhomogeneous	$(1 - \sqrt{1-p})/2$
C	case V	$(1 - \sqrt{1-p})/2$
D	case W	$(1 - \sqrt{1-p})/2$
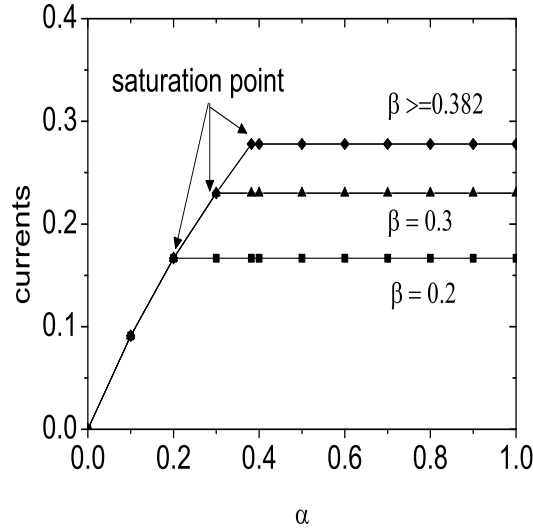
Figure 4.6: Currents with fixed hopping probabilities $p = 0.8$ and flexible exit rate β. The lines describe theoretical calculations, while symbols correspond to computer simulations.

include: (1) the number of the stationary phases in Case V is 5, while it is 7 in Case W, and (2) the saturation point pair (α^*, β^*) is $\alpha^* = (2 - p - 2\sqrt{1-p})/p$ and $\beta^* = 1 - \sqrt{1-p}$ in Case V, while it is $\alpha^* = (2 - p - 2\sqrt{1-p})/p$ and $\beta^* = (2 - p - 2\sqrt{1-p})/p$ in Case W. This indicates that the MC region in Case W is larger than that in Case V. In other words, the introduction of segment III into Case W can enhance the current in some situations. It is also found that the TASEP with an inhomogeneous site has the minimal MC region. The maximal
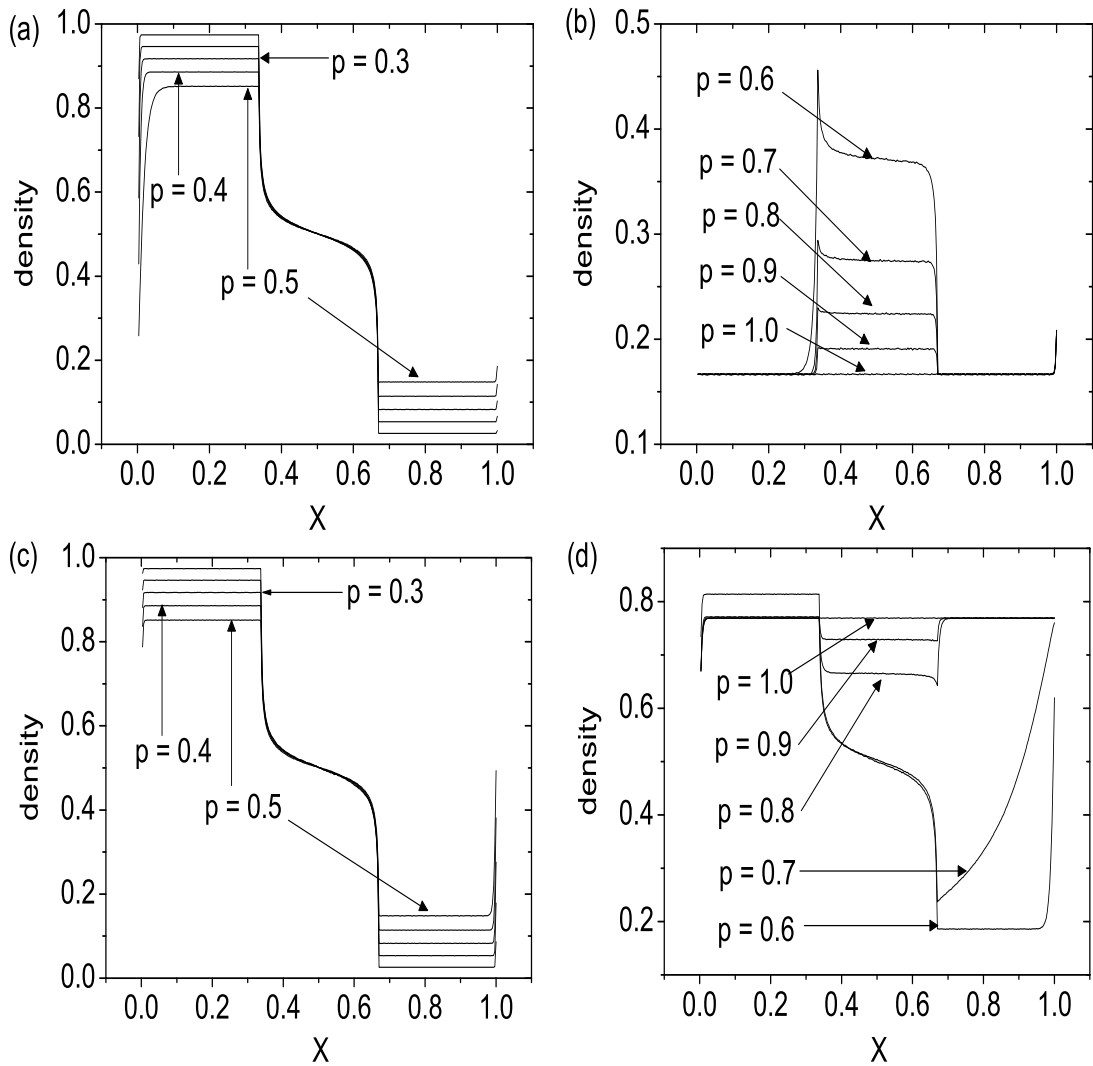
Figure 4.7: Density profiles from simulations in the stationary state with different p. $x = i/N$, i is an index of sites and N is the system length. (a) and (b): $\alpha = 0.2$ and $\beta = 0.8$; (c) and (d): $\alpha = 0.7$ and $\beta = 0.3$.

current in a system with an inhomogeneous site is equal to $p/(1+p)$ which is larger than that in either Cases V or W where the maximal current is $(1 - \sqrt{1-p})/2$. Density profiles and currents are simulated, which shows very good agreement with

theoretical calculations. It is interesting to investigate a zoned inhomogeneity in synchronous TASEPs with large particles or different positions.

The present model and the previous one in Chapter 3 investigated the effects of inhomogeneities on a one-dimensional traffic system. For simplicity, the size of inhomogeneities used in these models is arbitrarily assumed to be 1, $L/2$ and $L/3$, respectively. L is the length of the lattice in the system. In other words, Chapters 3 and 4 just discussed several special cases of inhomogeneity in a one-channel lattice. Further investigation of the effect of inhomogeneity with any size on traffic dynamics would be expected to lead to a general solution for this subject.

This Chapter is based on the paper "Synchronous asymmetric exclusion process with an extended defect". The paper has been published in Physics Letters A 374 (2010) 1407-1413.

Chapter 5

Asymmetric Exclusion Process with Junction

5.1 Introduction

Traffic has been observed at almost all levels of natural and manmade systems (e.g., from microscopic molecular motors to macroscopic objects like vehicles) and proved to be a rewarding research topic in the last few decades [1, 16, 31, 108]. Totally asymmetric simple exclusion processes (TASEPs), as a paradigmatic model for non-equilibrium processes, have been widely applied in the study of traffic phenomena in chemistry, physics and biology [1, 9, 31]. To describe traffic more realistically, it is necessary to study traffic flow on more complex geometries. In particular, some of these geometries are associated with local inhomogeneity [27, 43, 54, 71, 77, 83, 84, 85, 87, 88, 89, 90]. A decrease of stationary current can be seen as a major effect of the presence of local inhomogeneity. Two-channel TASEPs with different inter-channel coupling rules have been studied as well (e.g., in Refs. [68, 69, 70, 73, 74, 75, 78]). More recently, investigations on multiple-channel TASEPs with two species particles [63, 64, 65] have been conducted, which aims at exploring the phenomenon of spontaneous symmetry breaking on multiple-channel systems.

Junctions can be seen as connections of several single-channel systems, which

are one of the commonly used traffic facilities in nature. Such systems with junctions may be used to describe a wide range of possible applications such as: (i) kinesins moving on a microtubule in which the number of protofilaments may vary [109]; (ii) transport of vesicles in a branching axon or dendrite [110]; (iii) vehicular traffic on intersections or roundabouts [111], and (iv) data traffic through hubs (e.g., switches, routers) on local/wide networks [112]. As a junction can also be viewed as a "local inhomogeneity" in a transport system, it is necessary to study the effects of such "local inhomogeneity" on traffic dynamics.

Inspired by this wide range of possible applications, the dynamics of synchronous (i.e., in *parallel update*) TASEP on lattices with a multiple-input single-output (MISO) junction is investigated. The MISO junction is shown in Figure 5.1. In reality, it can be observed that several traffic lanes merge into one lane and multiple protofilaments come together to form one protofilament [109]. However, they have not been understood well from the viewpoint of theoretical analysis.

This work is then extended to a general case, TASEPs with a m-input n-output (MINO) junction in parallel update. The aim of this extension is to give an integrated picture of macroscopic dynamic traffic properties at MINO junctions within the framework of TASEPs. This generalization produced three main results: (1) A general theoretical solution for traffic dynamics of TASEPs with junctions is obtained; (2) m-input n-output junctions can be classified by a parameter, $\lambda = m/n$. The systems with the same λ exhibit the same dynamic properties (e.g., phase diagrams, stationary currents, and density profiles); (3) When the number of input or output channels is increased or decreased, the low-density and high-density regions can be measured qualitatively and quantitatively. Such systematic analysis of the dynamics of TASEPs with junctions has not been studied before.

The Chapter is organized as follows. In Section 5.2, a description of a synchronous TASEP model with a MISO junction is given. The mean-field approx-

imation is developed in section 5.2.1. In Section 5.2.2, the phase boundaries is analyzed using a phenomenological domain wall theory. In Section 5.2.3, the results of theoretical calculations and computer simulations are presented. In Secion 5.3, A *m*-input *n*-output junction is studied, which includes a general theoretical solution of TASEPs with a MINO junction, a simple classification for MINO junctions, and a theoretical solution for areas of low-density and high-density regions. Finally, conclusions are given in Section 5.4.

5.2 *m*-input 1-output junction

5.2.1 Model and Mean-field Approximation

A MISO junction is illustrated in Figure 5.1. The system consists of m subchains for input and one main chain (chain $m+1$) for output connected by junction points– sites N on the subchains and site $N+1$ on the main chain. Each subchain and the main chain includes N sites. Particles are assumed to move from the left to the right.

For simplicity, inter-lane transitions between subchains are not permitted in this Chapter. This assumption is reasonable. In real-world situations, junctions can be seen as connections between inputs (e.g., road lanes, proto-filaments or data lines) from different directions and outputs to different directions. Although sometimes those multiple inputs may come from the same direction, lane-changing may not always be applicable. As a junction can also be seen as a "local inhomogeneity" in a transport system, to study the traffic dynamics at such "inhomogeneity" (i.e., the junction point) is important regardless of whether lane-changing can occur.

An occupation variable, $\tau_{\ell,i}$, denotes the state of the ith site in the ℓth subchain ($\ell = 1, 2, ..., m$) and the main chain ($\ell = m + 1$). $\tau_{\ell,i} = 1$ (or $\tau_{\ell,i} = 0$) means that site $\tau_{\ell,i}$ is occupied (or empty). The system updates all particles *in parallel* by the
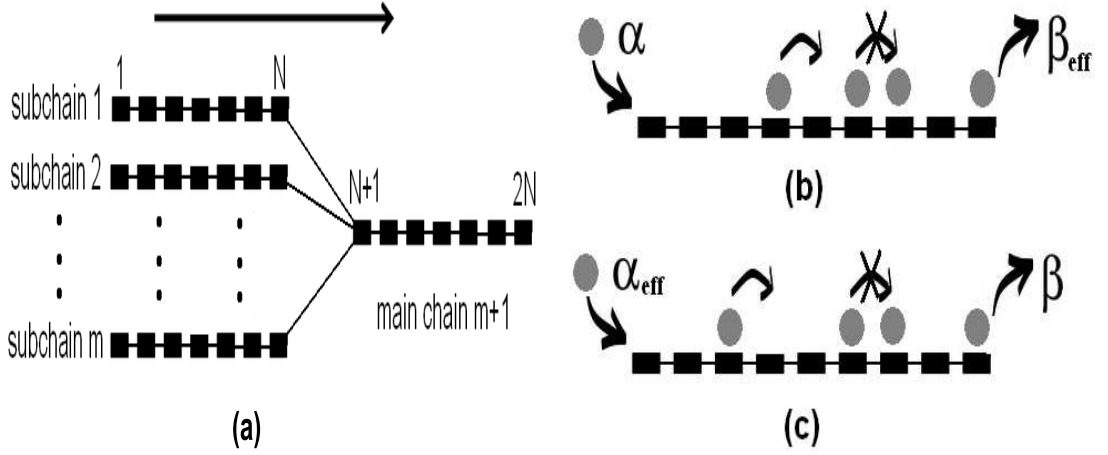
Figure 5.1: (a) Schematic diagram of a synchronous TASEP with a multiple-input single-output junction. Particles move from the left to the right with hard-core exclusion. (b) In a subchain, the injection rate at site 1 and the ejection rate at site N are given by α and β_{eff}, respectively. (c) In the main chain, the injection rate at site $N + 1$ and the ejection rate at site $2N$ are given by α_{eff} and β, respectively.

following rules (see Figure 5.1):

- $i = 1$. (i) If $\tau_{\ell,1} = 0$, a particle enters the system at rate α; or (ii) If $\tau_{\ell,1} = 1$ and $\tau_{\ell,2} = 0$, then the particle at site $(\ell, 1)$ moves into site $(\ell, 2)$; or (iii) If both $\tau_{\ell,1} = 1$ and $\tau_{\ell,2} = 1$, then the particle at site $(\ell, 1)$ does not move.

- $i = N$. (i) If sites N of k subchains ($1 < k \le m$) are occupied by k particles at the same time, particles have the same priority to hop to site $N + 1$. However, only one particle will enter site $N + 1$ at any single time step, providing that site $N + 1$ is empty; or (ii) If only one site N of the subchains is occupied by a particle, the particle can directly hop to site $N + 1$ providing that site $N + 1$ is empty.

- $i = 2N$. If $\tau_{m+1,2N} = 1$, the particle leaves the system with rate β.

- $1 < i < N$ or $N + 1 \le i < 2N$. If $\tau_{\ell,i} = 1$, the particle can move into site

$(\ell, i+1)$ providing $\tau_{\ell, i+1} = 0$. Otherwise, the particle cannot move.

Exactly solvable results of an one-dimensional synchronous TASEP have been obtained in Ref. [32, 33], which are briefly reviewed here since the solution of the proposed model can be derived from them. There are three phases (low density (LD), high density (HD) and maximal current(MC)) and a transition line when $\alpha = \beta$. The MC $J = 0.5$ can only be reached at $\alpha = \beta = 1$ [33].

- When $\alpha < \beta \leq 1$, a low-density (LD) phase is obtained with

$$J = \rho, \quad \rho = \rho_1, \quad \rho_1 = \frac{\alpha}{1+\alpha}, \quad \rho_N = \frac{\alpha}{\beta(1+a)}. \tag{5.1}$$

where J is the system current; ρ is the bulk density; ρ_1 (ρ_N) is the particle density at the first (last) site.

- When $1 \geq \alpha > \beta$, a high-density (HD) phase is obtained with

$$J = 1 - \rho, \quad \rho = \frac{1}{1+\beta}, \quad \rho_1 = 1 - \frac{\beta}{\alpha(1+\beta)}, \quad \rho_N = \rho. \tag{5.2}$$

- When $\alpha = \beta < 1$, a transition line between LD and HD is obtained.

- When $\alpha = \beta = 1$, the maximal current (MC) is obtained and $J = 0.5$.

Based on the above results, exactly solvable results for TASEPs with a MISO junction can be developed. For a MISO junction, as the current is conserved through the system, one has

$$J_1 + J_2 + \cdots + J_m = J_{m+1}, \quad J_1 = J_2 = \cdots = J_m, \quad mJ_\ell = J_{m+1} \leq 0.5 \tag{5.3}$$

where J_ℓ ($\ell = 1, 2, ..., m$) is the current on the ℓth subchain; J_{m+1} is the current of the main chain.

Each of the m subchains of the MISO junction can be seen as a synchronous TASEP with injection rate α and ejection rate β_{eff}, while the main chain can be

seen as a synchronous TASEP with injection rate α_{eff} and ejection rate β. α_{eff} and β_{eff} can be written as

$$\beta_{eff} = 1 - \rho_{N+1}, \quad \alpha_{eff} = m\rho_N. \tag{5.4}$$

These m subchains should have the identical phases when particles on the m subchains merge into the main chain with the same priority. Computer simulations also support this prediction. Thus, the stationary state of the system can be obtained by combining the possible phases that exist in each of these subchains and the main chain. As each single chain may have three possible phases (LD, HD and MC), due to the equivalence of these subchains, the number of possible stationary phases of the system is equal to $3^2 = 9$. In other words, a stationary state can be one of the following nine phases: the (LD, LD), (LD, HD), (LD, MC), (HD, LD), (HD, HD), (HD, MC), (MC, LD), (MC, HD), and (MC, MC) phases.

One can see that three phases cannot exist: (MC, LD), (MC, HD) and (MC, MC). According to Eq. (5.3), it is impossible for the maximal current phase to exist in a subchain since the maximal possible current in the system is no more than 0.5. Therefore, the number of the possible phase combinations reduce to 6, i.e., the (LD, LD), (LD, HD), (LD, MC), (HD, LD), (HD, HD), (HD, MC) phases.

- The (LD, HD) phase. The conditions for this case are as follows

$$\alpha < \beta_{eff}, \quad \alpha_{eff} > \beta. \tag{5.5}$$

From Eqs. (5.1) and (5.2), the stationary properties of this phase are given by

$$J_1 = \frac{\alpha}{1+\alpha}, \quad J_{m+1} = \frac{\beta}{1+\beta}, \quad \rho_1 = \frac{\alpha}{1+\alpha},$$

$$\rho_N = \frac{\alpha}{\beta_{eff}(1+\alpha)}, \quad \rho_{N+1} = 1 - \frac{\beta}{\alpha_{eff}(1+\beta)}, \quad \rho_{2N} = \frac{1}{1+\beta}. \tag{5.6}$$

According to Eq. (5.3), $mJ_1 = J_{m+1}$, one gets

$$\alpha = \frac{\beta}{m + (m-1)\beta} \tag{5.7}$$

However, α_{eff} and β_{eff} are not solvable from above equations. In other words, the bulk density cannot be obtained through above equations. The density will be solved through the domain wall theory in Section III. From Figures 5.2(a) and (b), one can see that $\alpha = \beta/[m + (m-1)\beta]$ (when $\beta < 1$) corresponds to the transition line between the (LD, LD) phase and the (HD, HD) phase.

- The (LD, MC) phase. This phase corresponds to the following conditions

$$\alpha < \beta_{eff}, \quad \alpha_{eff} = \beta = 1. \tag{5.8}$$

According to Eqs. (5.1) and (5.3), one obtains:

$$\alpha = \frac{1}{2m-1}, \quad J_1 = \frac{1}{2m}, \quad J_{m+1} = 0.5. \tag{5.9}$$

When the left subsystem is in the LD phase, particles are in free flow. This leads to $\alpha_{eff} < 1$. According to Eq. (5.8), $\alpha_{eff} = 1$. The two statements contradict each other. So the (LD, MC) phase does not exist in the system. But, when $\beta_{eff} = \alpha$, the coexisted phase (LD/HD) appears in the left subsystem. Therefore, the (LD/HD, MC) phase coexists in the system, which corresponds to a point specified by $\alpha = \beta_{eff}$ and $\alpha_{eff} = \beta = 1$.

Again, the bulk density cannot be calculated through above equations. The density will also be solved through domain wall theory in Section 5.2.2. From Figures 5.2(a) and (b), one can see that the (LD/HD, MC) phase is the transition phase between the (LD, LD), (LD, HD), (HD, HD) and (HD, MC) phases.

- The (LD, LD) phase. The following conditions should be satisfied

$$\alpha < \beta_{eff}, \quad \alpha_{eff} < \beta. \tag{5.10}$$

According to Eq. (5.1), the stationary current and density are given by

$$J_1 = \frac{\alpha}{1+\alpha}, \quad J_{m+1} = \frac{\alpha_{eff}}{1+\alpha_{eff}}, \quad \rho_1 = \frac{\alpha}{1+\alpha},$$

$$\rho_N = \frac{\alpha}{\beta_{eff}(1+\alpha)}, \quad \rho_{N+1} = \frac{\alpha_{eff}}{1+\alpha_{eff}}, \quad \rho_{2N} = \frac{\alpha_{eff}}{\beta(1+\alpha_{eff})}. \tag{5.11}$$

Using Eqs. (5.3) and (5.4), α_{eff} and β_{eff} are expressed as

$$\alpha_{eff} = \frac{m\alpha}{1-(m-1)\alpha}, \quad \beta_{eff} = \frac{1-(m-1)\alpha}{1+\alpha}. \tag{5.12}$$

Since $\alpha_{eff} \leq 1$ and $\alpha_{eff} = m\alpha/[1-(m-1)\alpha]$, $\alpha \leq 1/(2m-1)$. Substituting Eq. (5.13) into Eq. (5.11), one obtains $\alpha < \sqrt{1+m^2/4} - m/2$ for $\alpha < \beta_{eff}$, and $\alpha < \beta/[m+(m-1)\beta]$ for $\alpha_{eff} < \beta$. Since $1/(2m-1) < \sqrt{1+m^2/4} - m/2$ (when $m \geq 2$) and $\beta/[m+(m-1)\beta] \leq 1/(2m-1)$ (as $\beta \leq 1$), the system is in the (LD, LD) phase when

$$\alpha < \frac{\beta}{m+(m-1)\beta}, \quad \beta \leq 1. \tag{5.13}$$

- The (HD, HD) phase. The conditions for this case are given by

$$\alpha > \beta_{eff}, \quad \alpha_{eff} > \beta. \tag{5.14}$$

The current and density of this phase in a stationary state are

$$J_1 = \frac{\beta_{eff}}{1+\beta_{eff}}, \quad J_{m+1} = \frac{\beta}{1+\beta}, \quad \rho_1 = 1 - \frac{\beta_{eff}}{\alpha(1+\beta_{eff})},$$

$$\rho_N = \frac{1}{1 + \beta_{eff}}, \quad \rho_{N+1} = 1 - \frac{\beta}{\alpha_{eff}(1 + \beta)}, \quad \rho_{2N} = \frac{1}{1 + \beta}. \quad (5.15)$$

From Eqs. (5.3) and (5.15), one obtains $\beta_{eff} = \beta/[m + (m-1)\beta]$. Thus, the system is in the (HD, HD) phase when

$$\alpha > \frac{\beta}{m + (m-1)\beta} \quad (5.16)$$

- The (HD, MC) phase. The corresponding conditions for this phase are

$$\alpha > \beta_{eff}, \quad \alpha_{eff} = \beta = 1. \quad (5.17)$$

According to Eqs. (5.2-5.3), one obtains

$$J_1 = \frac{1}{2m}, \quad \rho_N = \frac{1}{m}, \quad \rho_{N+1} = \frac{2m - 2}{2m - 1}, \quad \beta_{eff} = \frac{1}{2m - 1}. \quad (5.18)$$

Thus, the (HD, MC) phase can exist in the system when

$$\alpha > \frac{1}{2m - 1}, \quad \beta = 1. \quad (5.19)$$

- (HD, LD) phase. The conditions of existence for this phase can be written as

$$\alpha > \beta_{eff}, \alpha_{eff} < \beta. \quad (5.20)$$

The corresponding expressions for stationary current and density are

$$J_1 = \frac{\beta_{eff}}{1 + \beta_{eff}}, \quad J_{m+1} = \frac{\alpha_{eff}}{1 + \alpha_{eff}}, \quad \rho_1 = 1 - \frac{\beta_{eff}}{\alpha(1 + \beta_{eff})},$$

$$\rho_N = \frac{1}{1 + \beta_{eff}}, \quad \rho_{N+1} = \frac{\alpha_{eff}}{1 + \alpha_{eff}}, \quad \rho_{2N} = \frac{\alpha_{eff}}{\beta(1 + \alpha_{eff})}. \quad (5.21)$$

According to Eq. (5.3), one reads

$$\alpha_{eff} = \frac{m\beta_{eff}}{1 - (m-1)\beta_{eff}}. \quad (5.22)$$

From Eqs. (5.4) and (5.21), α_{eff} and β_{eff} can be rewritten as follows

$$\alpha_{eff} = \frac{m}{1 + \beta_{eff}}, \quad \beta_{eff} = \frac{1}{1 + \alpha_{eff}}. \tag{5.23}$$

Substituting Eq. (5.23) into Eq. (5.22), one obtains $\alpha_{eff} = \sqrt{1 + m^2/4} + m/2 - 1$ and $\beta_{eff} = \sqrt{1 + m^2/4} - m/2$. It can be seen that values of α_{eff} and β_{eff} are determined by the number of subchains m, independent of α and β. This indicates that the (HD, LD) phase cannot be represented in the $\alpha - \beta$ plane. In other words, the (HD, LD) phase does not exist in the system. In fact, when the subchains are in the high density phase, particles at site N will hop to site $N + 1$ at almost each time step, which leads to $\alpha_{eff} \approx 1$. Thus, it is impossible for the main chain to maintain the low density phase.
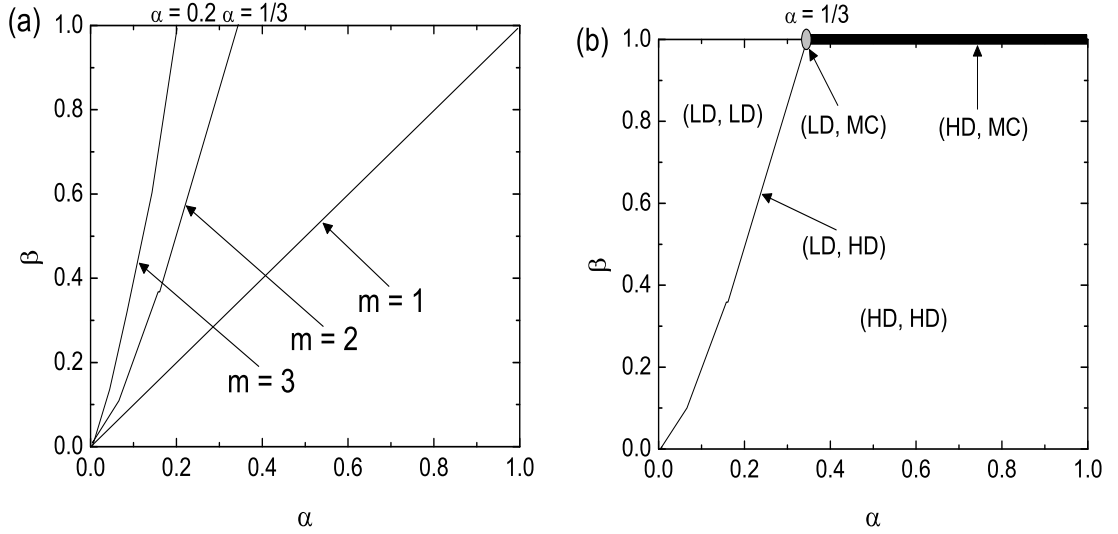
Figure 5.2: (a) Phase boundaries (or transition lines) for $m = 1, 2$ and 3 in the synchronous TASEPs with a MISO junctions. (b) Phase diagram for $m = 2$ in the synchronous TASEPs with a MISO junction. The solid line represents the (LD, HD) phase specified by $\alpha = \beta/[m + (m - 1)\beta]$ and $\beta < 1$; the grey oval corresponds to the (LD/HD, MC) phase specified by $\alpha = 1/(2m - 1)$ and $\beta = 1$; and the black rectangle for the (HD, MC) phase specified by $\alpha > 1/(2m - 1)$ and $\beta = 1$.

From the analysis above, one can see that there are five possible phases ((LD, LD), (LD, HD), (LD/HD, MC), (HD, HD) and (HD, MC)) in this system. Figure 5.2(a) shows the possible phase boundaries ($\alpha = \beta/[m + (m-1)\beta]$) for $m = 1, 2$ and 3. With the increase of m, one can predict that the phase boundary moves toward the left in the phase diagram, which means that the low-density area decreases while the high-density area increases. The phase diagram for $m = 2$ is also shown in Figure 5.2(b). From Figure 5.2(b), one can see that: (i) The (LD, HD) phase corresponds to the transition line between the (LD, LD) phase and the (HD, HD) phase specified by $\alpha = \beta/[m + (m-1)\beta]$ and $0 \leq \beta < 1$. (ii) The (LD/HD, MC) phase is the transition phase between the (LD, LD),(LD, HD), (HD, HD) and (HD, MC) phases specified by $\alpha = 1/(2m-1)$ and $\beta = 1$. Also, note that the transition from the (LD, LD) phase to the (LD, HD) phase, the density change on the subchains is continuous, while the density change on the main chain is discontinuous. Similarly, the transition from the (LD, HD) to the (HD, HD) phases, the density change on the subchains is discontinuous, while the density change of the main chain is continuous. Also, for the transition from the (LD/HD, MC) phase to the (HD, MC) phase, the density change on the subchains is discontinuous, while the density profile on the main chain is unchanged.

5.2.2 Domain Wall Dynamics

A phenomenological domain wall approach is introduced in Section 3.4. In this Chapter, the line specified by $\alpha = \beta/[m + (m-1)\beta]$ corresponds to the coexistence of the (LD, LD) and (HD, HD) phases. Similarly, one can see

$$q_L = \frac{\beta(1-\alpha)}{\alpha + \beta - 2\alpha\beta}, \quad q_R = \frac{\alpha(1-\beta)}{\alpha + \beta - 2\alpha\beta}. \tag{5.24}$$

Accordingly, the probabilities of the domain walls falling in certain zones in the

left and right subsystems are also given by:

$$Prob(x_{DW} < x) = q_L x, \quad 0 < x \leq 1, \tag{5.25}$$

and

$$Prob(x_{DW} < x) = q_L + q_R(x - 1), \quad 1 < x \leq 2. \tag{5.26}$$

Thus, the density at any position in the system becomes:

$$\rho(x)_k = \rho_-^k Prob(x_{DW} > x) + \rho_+^k Prob(x_{DW} < x), \quad k = L, R \tag{5.27}$$

Finally, from Eqs. (5.24)-(5.27), one can obtain:

$$\rho(x)_L = \frac{\alpha}{1 + \alpha} + \frac{\beta(1 - \alpha)^2}{(1 + \alpha)(\alpha + \beta - 2\alpha\beta)} x, \quad 0 < x \leq 1 \tag{5.28}$$

and

$$\rho(x)_R = \frac{\beta}{1 + \beta} + \frac{\beta(1 - \alpha)(1 - \beta)}{(1 + \beta)(\alpha + \beta - 2\alpha\beta)} + \frac{\alpha(1 - \beta)^2}{(1 + \beta)(\alpha + \beta - 2\alpha\beta)}(x - 1), \quad 1 < x \leq 2 \tag{5.29}$$

Densities in the boundary conditions can be calculated as $\rho(x = 0)_L = \alpha/(1+\alpha)$ and $\rho(x = 2)_R = 1/(1 + \beta)$. These results are completely identical with theoretical analysis in Refs. [32, 33]. At the junction point N, the densities are equal to $\rho(x = 1)_L = [\alpha^2(1 - \beta) + \beta(1 - \alpha)]/[(1 + \alpha)(\alpha + \beta - 2\alpha\beta)], \rho(x = 1)_R = \beta(1 - \alpha\beta)/[(1 + \beta)(\alpha + \beta - 2\alpha\beta)]$. Note that in the transition line between the (LD, LD) and (HD, HD) phases, the relationship $\alpha = \beta/[m + (m - 1)\beta]$ can be obtained.

5.2.3   Simulation results and discussions

To validate the theoretical analysis, computer simulations are performed. Here, the results only for a synchronous TASEP with a Y-type junction, that is $m = 2$, are presented. The numbers of sites of the subchains and the main chain are all equal

to 1,000. In simulations, stationary density profiles are obtained by averaging 10^8 sampling at each site. The first $10^5 N$ time steps are discarded to let the transient time out.

The density profiles for the (LD, LD), (HD, HD) and (HD, MC) phases are shown in Figure 5.3. Only the density properties of subchain 1 and the main chain are illustrated since the density properties of the other subchain is essentially the same as subchain 1. It is found that there is a good agreement between Monte Carlo simulations (MCS) and mean field (MF) analysis (see Figures 5.3(a)-(e)), which verifies theoretical investigations.

A phenomenological domain wall (DW) theory developed in Section 3.4 is used to calculate the density profiles of phase boundaries such as the (LD, HD) and (LD/HD, MC) phases (see Figure 5.4). The results obtained from the domain wall theory show an agreement with computer simulations. When α and β both increase and also maintain $\alpha = \beta/[m + (m-1)\beta]$, the system keeps in the (LD, HD) phase until $\beta = 1$; the slope of the density profiles for $x < 1$ decreases until the slope reduces to 0.5, while the slope of the density profiles for $1 < x < 2$ also decrease until the slope decreases to 0. For instance, the slope decreases from 0.588 to 0.542 when α increases from 0.1 to 0.2 (see Figures 5.4(a) and (b)). Finally, the slopes of density profiles of the subchains become 0.5 and the slope of density profile of the main chain becomes 0 when $\alpha = 1/3$ and $\beta = 1$ (see Figure 5.4(c)). Additionally, Monte Carlo simulations, theoretical calculations and domain wall theory all show that, when $\alpha = 1/3$ and $\beta = 1$ (i.e., the transition phase between the other four phases), the main chain is in the maximal current phase.

Density profiles of the systems for $m = 2$ and $m = 3$ with the synchronous update scheme are simulated and compared (see Figure 5.5). According to Eq. (5.7), the phase boundary between the (LD, LD) and (HD, HD) phases can be described as $\alpha = \beta/(2 + \beta)$ for $m = 2$ and $\alpha = \beta/(3 + 2\beta)$ for $m = 3$. Figure 5.5 shows that

both systems are in the (LD, LD) phase when $\alpha = 0.1$ and $\beta = 0.8$. However, when α increases (e.g., $\alpha = 0.2$), the system for $m = 2$ is still in the (LD, LD) phase, while the system for $m = 3$ is in the (HD, HD) phase (see Figure 5.5(b)). This is due to the phase boundary between the (LD, LD) and (HD, HD) phases moving towards the left when m increases (see Figure 5.2(a)). Density profiles in the (HD, HD) phase for both $m = 2$ and $m = 3$ are shown in Figure 5.5(c). Compared with Figure 5.5(a) and (c), it can be seen that the density profiles of the subchains of both systems are the same when both systems in the (LD, LD) phase, while the density profiles of the main chains of both systems are the same when both systems are in the (HD, HD) phase. Figure 5.5(d) illustrates that the system is in the (LD, LD) phase for $m = 2$, while it is in the (HD, MC) phase for $m = 3$.

A comparison of the phase diagrams between the system with the *parallel* update (see Figure 5.2(b)) and that of the *random* update (see Figure 3 in [79]) is also made. One can see that the structures of the phase diagrams are similar. All have five phases in their phase diagrams. Also, increasing the number of subchains (i.e., inputs) only shifts the transition line between the (LD, LD) phase and the (HD, HD) phase that does not fall on the boundaries of the phase diagrams. However, the differences in the phase diagrams include: (i) the (HD, MC) phase region in the phase diagram of the system with the random update scheme reduces to a line in that of the system with the synchronous update scheme; and (ii) the line of the (LD/HD, MC) phase in the phase diagram of the system with the random update scheme reduces to a point in the phase diagram of the system with the synchronous update scheme.

Figure 5.6 shows the differences in the density profiles of the systems with the *synchronous* update scheme and the system with the *random* update scheme when $m = 2$. In Figure 5.6(a), these two systems are in the (LD, LD) phase when $\alpha = 0.1$ and $\beta = 0.8$. When α is increased to 0.2 and β is unchanged, the system with

the synchronous update scheme is still in the (LD, LD) phase, while the phase of the system with the random update scheme becomes the (HD, MC) phase (see Figure 5.6(b)). Figure 5.6(c) shows the system in the (HD, HD) phase in both systems when $\alpha = 0.8$ and $\beta = 0.32$. With the increase of β (e.g., $\beta = 0.8$),the phase of the system with the random update scheme changes to the (HD, MC) phase, while it still keeps in the (HD, HD) phase in the other system. It is found that parallel and random update results differ, especially when the differences are so marked as in Figure 5.6(b). These results are supported by theoretical predictions though only simulation results are presented here (see phase diagrams in Figure 5.2(b) and Figure 3 in [79])). These differences illustrate that different update rules will lead to different results. These differences are quantitative as well as qualitative for special values of α and β.

Note that the system also exhibits a particle-hole symmetry. Since particles moving forward at junction points with the same priority is equivalent to holes moving backward at the same priority. Also, the method can be used to analyze synchronous TASEPs with a single-input multi-output (SIMO) junction. Other inhomogeneous synchronous TASEPs can be investigated in the similar way. For instance, it would be interesting to study a MISO junction where these parallel subchains are dynamically different.

5.3 m-input n-output junctions

5.3.1 Model and Theoretical Analysis

A MINO junction is illustrated in Figure 5.7. The system can be seen as two parts: the left and right subsystems. The former includes m one-dimensional TASEPs, while the latter consists of n one-dimensional TASEPs. Particles are assumed to move from the left to the right with the discrete time step. Each channel includes

N sites. The behavior of the system can be described by applying the following rules to all sites *simultaneously* (see Figure 5.8). At sites 1 (in total, the number of sites 1 is m), particles can enter each site 1 with probability α, provided the site is empty. They can leave the left subsystem from each site N with probability β_{eff} and enter the right subsystem from each site $N+1$ with probability α_{eff}. For the purpose of description of interactions at the junction, the number of particles at sites N is denoted as K_N and the number of empty sites $N+1$ is represented as L_{N+1}. If $K_N \leq L_{N+1}$, all particles at sites N can hop to sites $N+1$ at one time step. If $K_N > L_{N+1}$, not all particles at sites N can enter the right subsystem at the same time. Under such conditions, only L_{N+1} particles are selected from K_N particleswith probability L_{N+1}/K_N to hop to the right, and the rest $(K_N - L_{N+1})$ particles have to stay at sites N. Particles finally leave the system from each site $2N$ with probability β.

This Chapter focuses on $m < n$. The dynamics of the system for $m > n$ can be easily obtained from the condition $m < n$ as the system should exhibit a particle-hole symmetry [71]. The particle-hole symmetry in the system means that particles enter each of the m channels at the left boundary with probability α and exit from each of the n channels at the right boundary with probability β, which is equivalent that holes are injected into each of the n channels at the right boundary with probability β and removed from each of the m channels at the left boundary with probability α. When $m = n$, it is obvious that the dynamics of the system is similar to the normal TASEP.

Since the dynamics of $m(n)$ TASEPs in the left(right) should be identical, and the total current in the steady state is conserved through the system, one has

$$J_1 + \cdots + J_m = J_{m+1} + \cdots + J_{m+n},$$

$$J_1 = \cdots = J_m, \ J_{m+1} = \cdots = J_{m+n}, \ mJ_1 = nJ_{m+1} = J \qquad (5.30)$$

where J_ℓ $(\ell = 1, ..., m, m + 1, ..., m + n)$ is the current on the ℓth channel. Using the similar theoretical analysis as in Ref. [28], five possible stationary phases ((LD, LD), (LD, HD), (HD, HD), (MC, LD), (MC, LD/HD)) are obtained. Among them, the (LD, HD) phase is a phase boundary between the (LD, LD) phase and (HD, HD) phase, defined by

$$\beta = \frac{m\alpha}{n + (n - m)\alpha}. \tag{5.31}$$

Then, let

$$\lambda = \frac{m}{n}, \quad \lambda \in (0, 1], \tag{5.32}$$

where λ is the proportion between m and n. Instituting Eq. (5.3) into Eq. (5.2), one obtains

$$\beta = \frac{\lambda\alpha}{1 + (1 - \lambda)\alpha}. \tag{5.33}$$

It can be seen that Eq. (5.4) is independent of m and n, but dependent of the proportion between m and n. In other words, when λ is fixed, the phase boundaries of TASEPs with a *group* of MINO junctions (not only a given one) are the same. For example, $m = 1, n = 2$ and $m = 2, n = 4$ correspond to the same phase boundaries ($\lambda = 0.5$ in both cases). Table 5.1 lists the five phases and corresponding conditions as well as stationary properties on each channel of the left and right subsystems, respectively. It is shown that the stationary current and bulk densities keep constant for the same λ. Figure 5.9(a) shows the phase boundaries defined by Eq. (5.5) for $\lambda = 1$ ($m = n$), $\lambda = 0.5$ ($m = n/2$), $\lambda = 1/3$ ($m = n/3$), and $\lambda = 2/3$ ($m = 2n/3$). Once the phase boundary is determined, the phase diagram is obtained as well.

On the other hand, the slope of the phase boundaries can be written approximately as $\kappa \approx \lambda/(2 - \lambda) = m/(2n - m)$. With increasing n (m is fixed), the phase boundary curves downward, which means that the (LD, LD) phase region expands while the (HD, HD) phase region shrinks. In the extreme case of $n \to \infty$, $\kappa \to 0$ indicates that almost the whole phase space is covered by the (LD, LD) phase. For

Table 5.1: Possible stationary phases and corresponding conditions. $J_L(J_R)$ represents the stationary current on each channel of the left (right) subsystem. $\rho_L(\rho_R)$ is the corresponding bulk density. $\lambda = m/n$.

Phase	Conditions	J_L	J_R	ρ_L	ρ_R
(LD, LD)	$\beta > \frac{\lambda\alpha}{1+(1-\lambda)\alpha}$	$\frac{\alpha}{1+\alpha}$	$\frac{\lambda\alpha}{1+\alpha}$	$\frac{\alpha}{1+\alpha}$	$\frac{\lambda\alpha}{1+\alpha}$
(HD, HD)	$\beta < \frac{\lambda\alpha}{1+(1-\lambda)\alpha}$	$\frac{\beta}{\lambda(1+\beta)}$	$\frac{\beta}{1+\beta}$	$1 - \frac{\beta}{\lambda(1+\beta)}$	$\frac{1}{1+\beta}$
(LD, HD)	$\beta = \frac{\lambda\alpha}{1+(1-\lambda)\alpha}$	$\frac{\alpha}{1+\alpha}$	$\frac{\beta}{1+\beta}$	Eq. 5.28	Eq. 5.29
(MC, LD)	$\beta > \frac{\lambda}{2-\lambda}$, $\alpha = 1$	$\frac{1}{2}$	$\frac{\lambda}{2}$	$\frac{1}{2}$	$\frac{\lambda}{2}$
(MC, LD/HD)	$\beta = \frac{\lambda}{2-\lambda}$, $\alpha = 1$	$\frac{1}{2}$	$\frac{\lambda}{2}$	$\frac{1}{2}$	Eqs. 5.28-5.29

vehicular traffic, this can explain that increasing the number of outlets can alleviate jammed traffic.

The phase diagram for $m = 2n/3$ is shown in Figure 5.9(b). The (MC, LD/HD) phase corresponds to a point specified by $\alpha = \beta_{eff} = 1$ and $\alpha_{eff} = \beta = m/(2n-m)$. Also, it is a critical phase connected by the (LD, LD), (MC, LD), (LD, HD) and (HD, HD) phases. The (MC, LD) phase is specified by a line ($\alpha = 1$ and $\beta > 1/2$). The (LD, HD) phase is a coexistence line of first-order phase transitions between the (LD, LD) and (HD, HD) phases. The transition of density profiles from the (LD, LD) phase to the (MC, LD) phase is continuous. However, the density change from the (LD, LD) phase to the (MC, LD/HD) phase is discontinuous in the right subsystem. It is found that computer simulations support well theoretical predictions of the phase diagram. Clearly, the phase diagrams for $m < n$ and $m > n$ are symmetric along the line $\alpha = \beta \leq 1$.

The (LD, LD) and (HD, HD) phase regions can be calculated quantitatively based on Eq. (5.4) and $S_{LD} + S_{HD} = 1$. S_{LD} and S_{HD} are areas of the (LD, LD) and (HD, HD) phases, respectively. The solution for S_{HD} is:

$$S_{HD} = \int_0^1 \frac{\lambda\alpha d\alpha}{1 + (1-\lambda)\alpha} = \frac{\lambda}{1-\lambda} + \frac{\lambda}{(1-\lambda)^2} \ln \frac{1}{2-\lambda}$$

$$= \frac{m}{n-m} + \frac{mn}{(n-m)^2} \ln \frac{n}{2n-m}. \qquad (5.34)$$

Using Eq. (5.5), one obtains $S_{HD} = 0.19$ for $m = 1$ and $n = 2$, and $S_{HD} = 0.1175$ for $m = 1$ and $n = 3$. Thus, when n is increased from 2 to 3, the (HD, HD) phase region will decrease by $0.0725(=0.19\text{-}0.1175)$. It is equivalent to say that the (LD, LD) phase region will increase by 0.0725. Also, when $m = 1$ and $n = 1$, one has $S_{HD} = 0.5$ which is reduced to the normal synchronous TASEP. In the same way, it is easily to measure areas of the (LD, LD) and (HD, HD) regions using Eq. (5.5) for any integer values of m and n under $m < n$. Correspondingly, one can directly obtain S_{HD} and S_{LD} for $m > n$ using the expressions as follows. Thus, a general theoretical solution for TASEPs with MINO junctions in parallel update is obtained. The low-density and high-density regions can be measured qualitatively and quantitatively for both $m \le n$ and $m \ge n$.

$$S_{HD}^{m>n} = S_{LD}^{m<n}, \quad S_{LD}^{m>n} = S_{HD}^{m<n}. \qquad (5.35)$$

5.3.2 Simulation Results and Discussions

As mentioned above, the theoretical solution is in general for TASEPs with MINO junctions. To verify the theoretical results, computer simulations are carried out in this section. I arbitrarily set $N = 500$, $m = 2$ and $n = 3, 4$. However, I also checked larger system sizes and found that the results do not deviate from the ones used here. Stationary current and density profiles are obtained by averaging 1×10^9 sampling at each site. The first 1×10^8 time steps are discarded to let the system steady state.

The density profiles for the (LD, LD), (HD, HD), (MC, LD), and (MC, LD/HD) phases are shown in Figure 5.10. It is found that there is a good agreement between computer simulations and theoretical analysis (see Figure 5.10(a-c)). Also, there is no phase transitions when the number of outputs in the right subsystem is increased

from 3 to 4. In Figure 5.10(d) a phase transition from the (HD, HD) phase to the (MC, LD/HD) phase occurs. When $m = 2$, $n = 3$, $\alpha = 1.0$, and $\beta = 1/3$, the system is in the (HD, HD) phase. Upon increasing the number of outputs in the right subsystem (e.g., $n = 4$), the system transfers to the (MC, LD/HD) phase. In the (MC, LD/HD) phase, theoretical calculations deviate from simulation results in the right subsystem. This deviation could partially be related to correlations which are in general strong in parallel updating scheme.

The domain wall approach produces almost identical estimates for density profiles comparable to the results from Monte Carlo simulations in the left subsystem, while it shows deviations from simulations in the right subsystem (see Figures 5.11(a) and (b)). These deviations may be caused due to the following reasons: (1) the finite-size effect. The more simulation runtime and larger system size should be used to confirm this effect in future work; (2) neglecting the cross-correlation between the particles in channels; and (3) errors in the exact positioning this phase boundary. With the increase of α (accordingly increasing β) in the (LD, HD) phase, the slopes of density profiles decrease. In the left subsystem, the slope decreases from 0.19 to 0.01) when α increases from 0.2 to 0.8 (see Figures 5.11(a) and (b)). One can predict that the slope will finally reduce to 0 when α is increased to 1.0. In the right subsystem, the slope decreases from 0.594 to 0.512 when α increases from 0.2 to 0.8 (see Figures 5.11(a) and (b)). Further increasing α to 1.0, the slope is equal to 0.5.

Finally, current profiles in these five phases with $m = 2$ and $n = 4$ are investigated. For simplicity, I assume that α is fixed while β changes from 0 to 1. Figure 5.12 shows stationary current obtained from theoretical calculations and computer simulations for $\alpha = 0.5$ and 1.0, respectively. It can be seen that theoretical predictions are in good agreement with computer simulations. $\alpha = 0.5$, $\beta_1 = 0.2$ correspond to the (LD, HD) phase. When $\beta < \beta_1$, the system is in the (HD, HD) phase (see Figures 5.3(a) and 5.12(a)). In this phase, the current increases with the

increase of β as the current is determined by β. When $\beta > \beta_1$, the system transfers to the (LD, LD) phase in which α dominates the system with $J = \alpha/(1+\alpha) = 1/3$. When $\alpha = 1.0$ and $\beta_2 = 1/3$, the (MC, LD/HD) phase is reached (see Figure 3.6(b)). $\beta < \beta_2$ corresponds to the (HD, HD) phase, which is similar as $\beta < \beta_1$ in Figure 5.12(a). When $\beta > \beta_2$, a phase transition from the (MC, LD/HD) to the (MC, LD) occurs in which the maximal current $J = 0.5$ is maintained.

5.4   Summary and conclusions

Synchronous totally asymmetric exclusion processes (TASEPs) with a multiple-input single-output MISO junction are investigated by using a rule of current conservation, a domain wall approach and extensive computer simulations in this Chapter. Junctions may be relevant to many biological processes as well as vehicular and pedestrian traffic flow. The theoretical solutions, mean-field approximation, domain wall theory are developed. Extensive computer simulations are conducted. The theoretical analysis suggests that there are five possible stationary phases ((LD, LD), (LD, HD), (LD/HD, MC), (HD, HD) and (HD, MC)).

The MISO junction is then extended to a m-input n-output junction. A general theoretical solution for TASEPs with MINO junctions is obtained. More interestingly, it is shown that TASEPs with a *group* of MINO junctions (not only a specific one) can possess the same phase diagram, stationary current, and density profiles when the systems are with the same λ ($\lambda = m/n$). Using Eqs. (5.34) and (5.35), the areas of the (LD, LD) and (HD, HD) phases can be calculated directly. The current and density profiles are calculated, which show good agreement with computer simulations.

For a better understanding of the general dynamics of TASEPs with MINO junctions, it is necessary to investigate TASEPs with MINO junction in *random*

update and compare results with those reported in this paper. It is also interesting to extend this model by considering large particles or lane-changing rules.

This Chapter is based on two published papers. They are: (1) Theoretical investigation of synchronous totally asymmetric exclusion processes on lattices with multiple-input single-output junctions, Physical Review E: Statistical, Nonlinear, and Soft Matter Physics 77 (2008) 051108. This paper has been selected for the Issue of the Virtual Journal of Biological Physics Research (Vir. J. Bio. Phys. Res. Volume 15, Issue 10, Statistical and Nonlinear Physics); and (2) Asymmetric exclusion processes on m-input n-output junctions with parallel update, Physica A: Statistical Mechanics and its Applications 388 (2009) 4068.
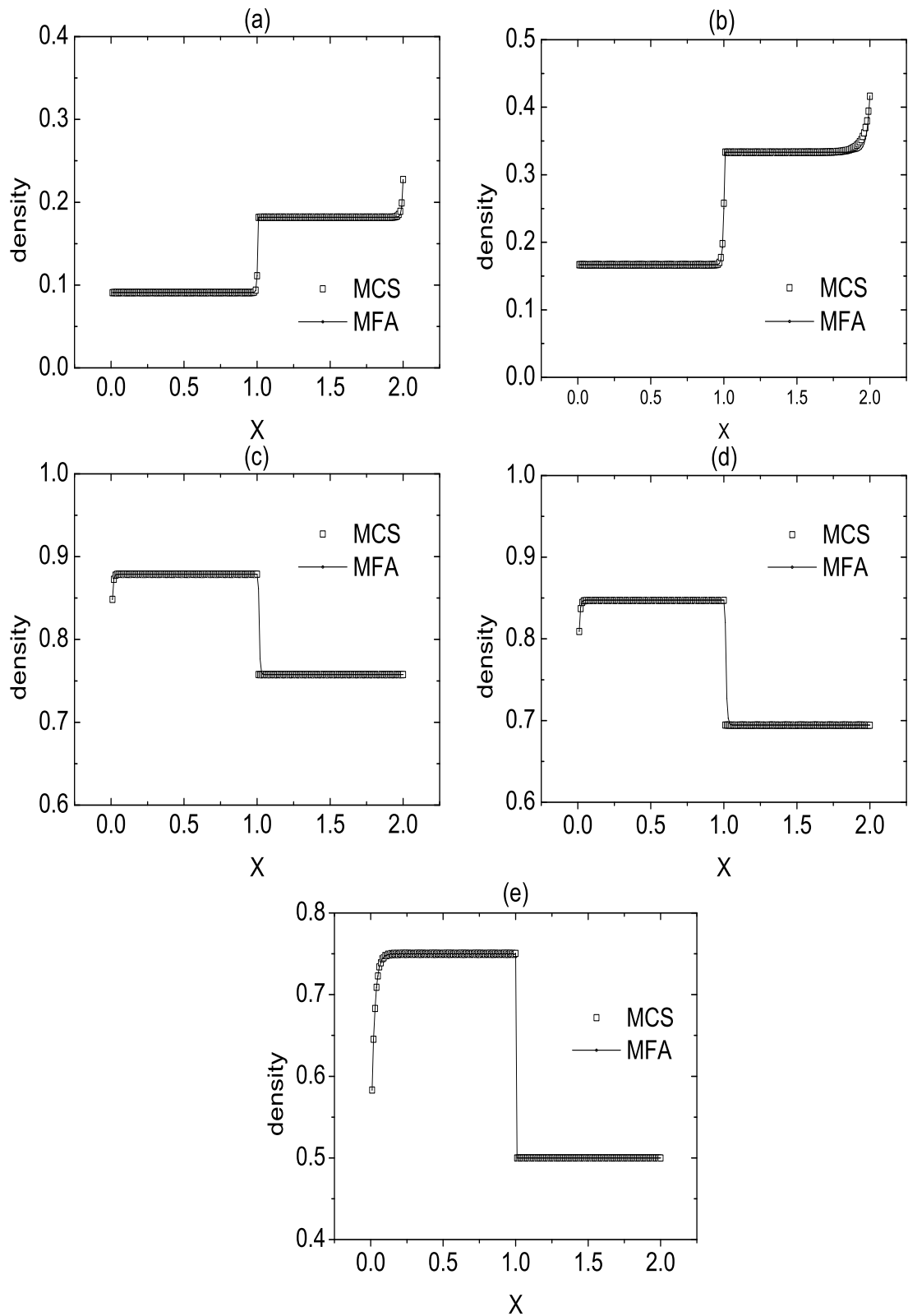
Figure 5.3: Density profiles obtained from mean-field analysis (MFA) and Monte Carlo simulations (MCS) when $m = 2$: (a) and (b) are for the (LD, LD) phase, (c) and (d) are for the (HD, HD) phase, and (e) for the (HD, MC) phase. The parameters are set to: (a) $\alpha = 0.1$ and $\beta = 0.8$, (b) $\alpha = 0.2$ and $\beta = 0.8$, (c) $\alpha = 0.8$ and $\beta = 0.32$, (d) $\alpha = 0.8$ and $\beta = 0.44$, and (e) $\alpha = 0.6$ and $\beta = 1.0$.
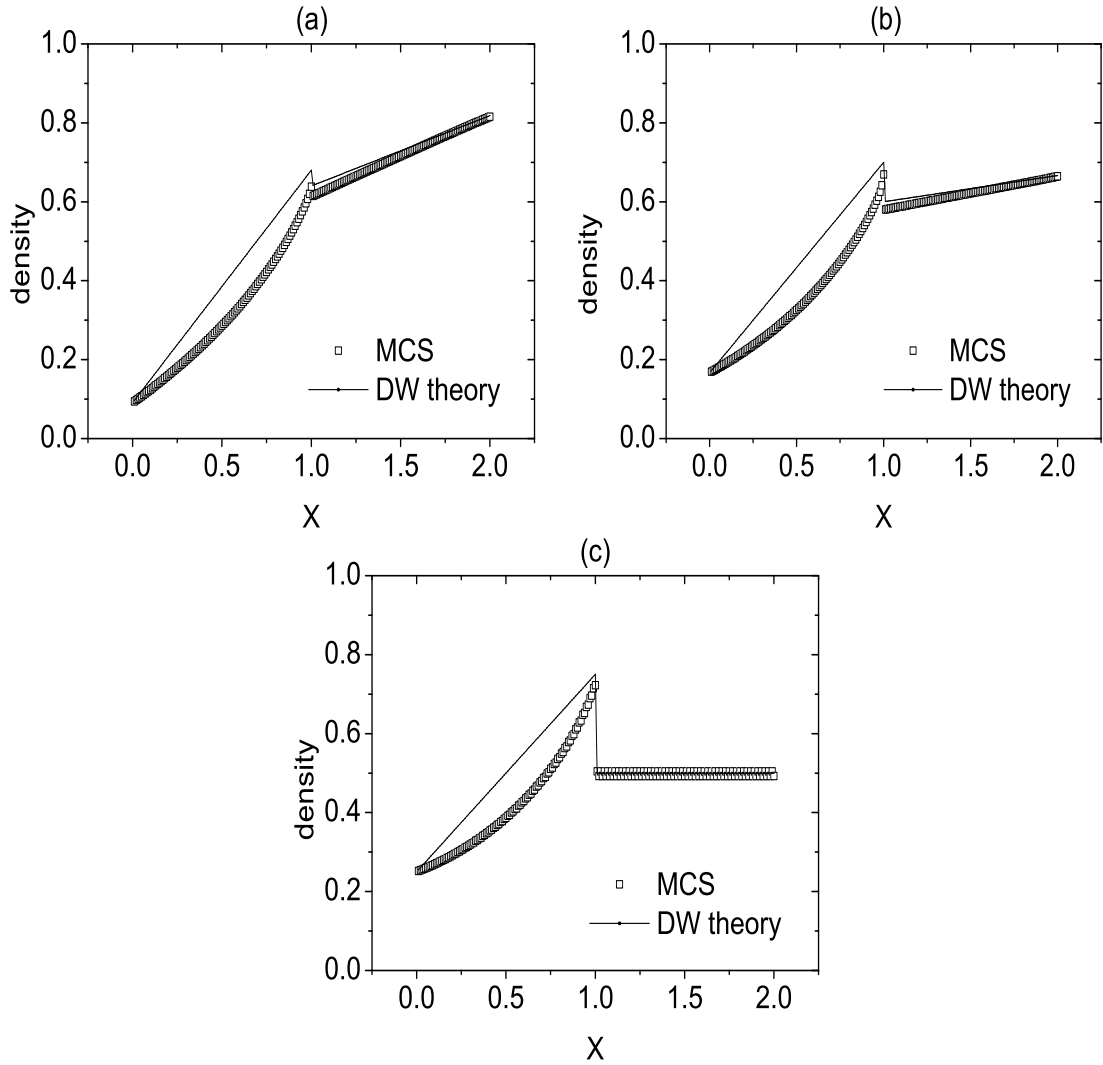
Figure 5.4: Density profiles obtained by the domain wall (DW) theory and Monte Carlo simulations (MCS) when $m = 2$: (a) and (b) for the phase coexistence line between the (LD, LD) and (HD, HD) phases, (c) is for the coexistence phases between the (LD, LD), (LD, HD),(HD,HD)and (HD, MC) phases. The parameters are: (a) $\alpha = 0.1$ and $\beta = 0.222$, (b) $\alpha = 0.2$ and $\beta = 0.5$, and (c) $\alpha = 1/3$ and $\beta = 1.0$.
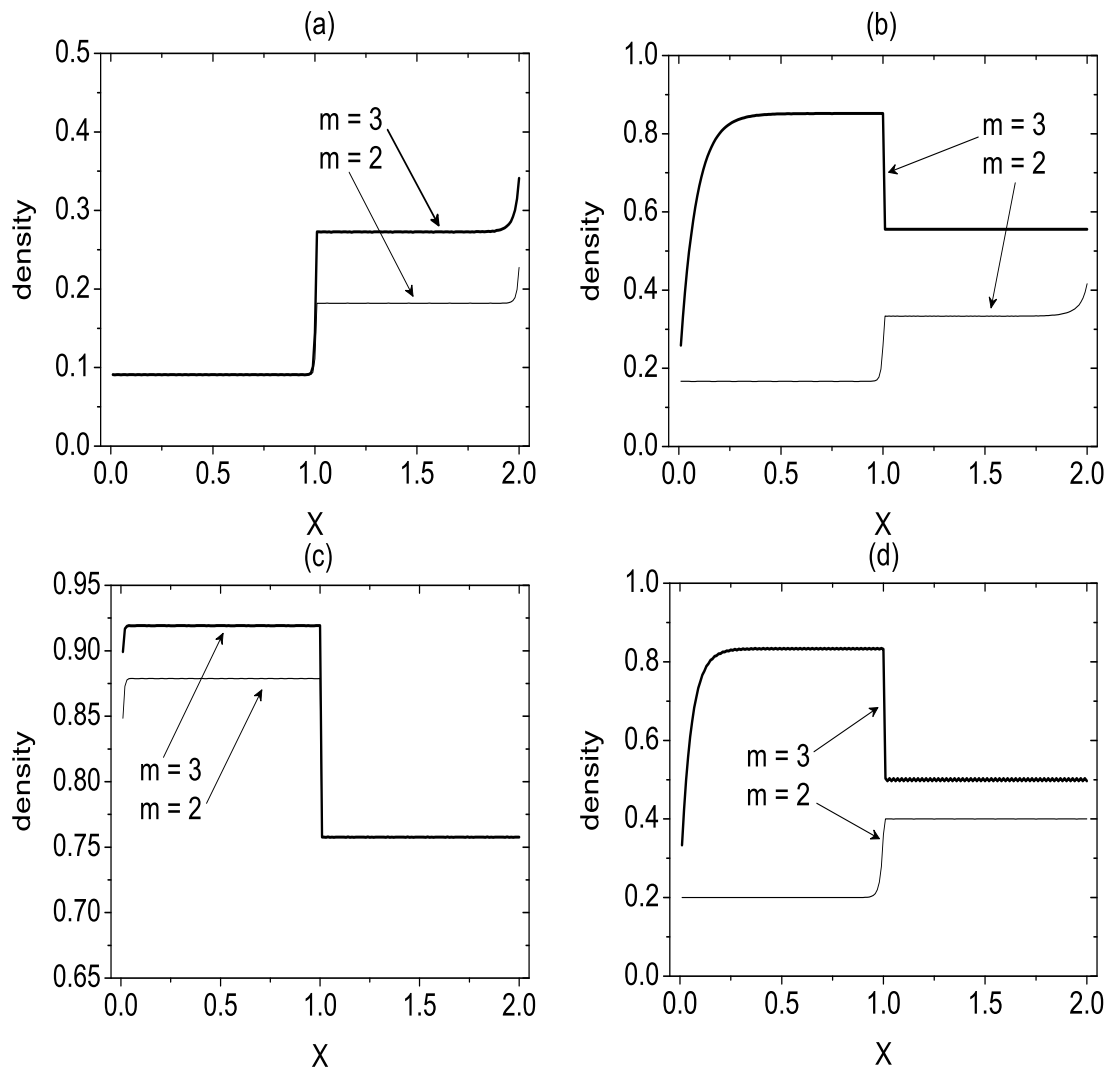
Figure 5.5: Density profiles in Monte Carlo simulations when $m = 2$ and $m = 3$. The parameters are: (a) $\alpha = 0.1$ and $\beta = 0.8$, (b) $\alpha = 0.2$ and $\beta = 0.8$, (c) $\alpha = 0.8$ and $\beta = 0.32$, and (d) $\alpha = 0.25$ and $\beta = 1.0$.
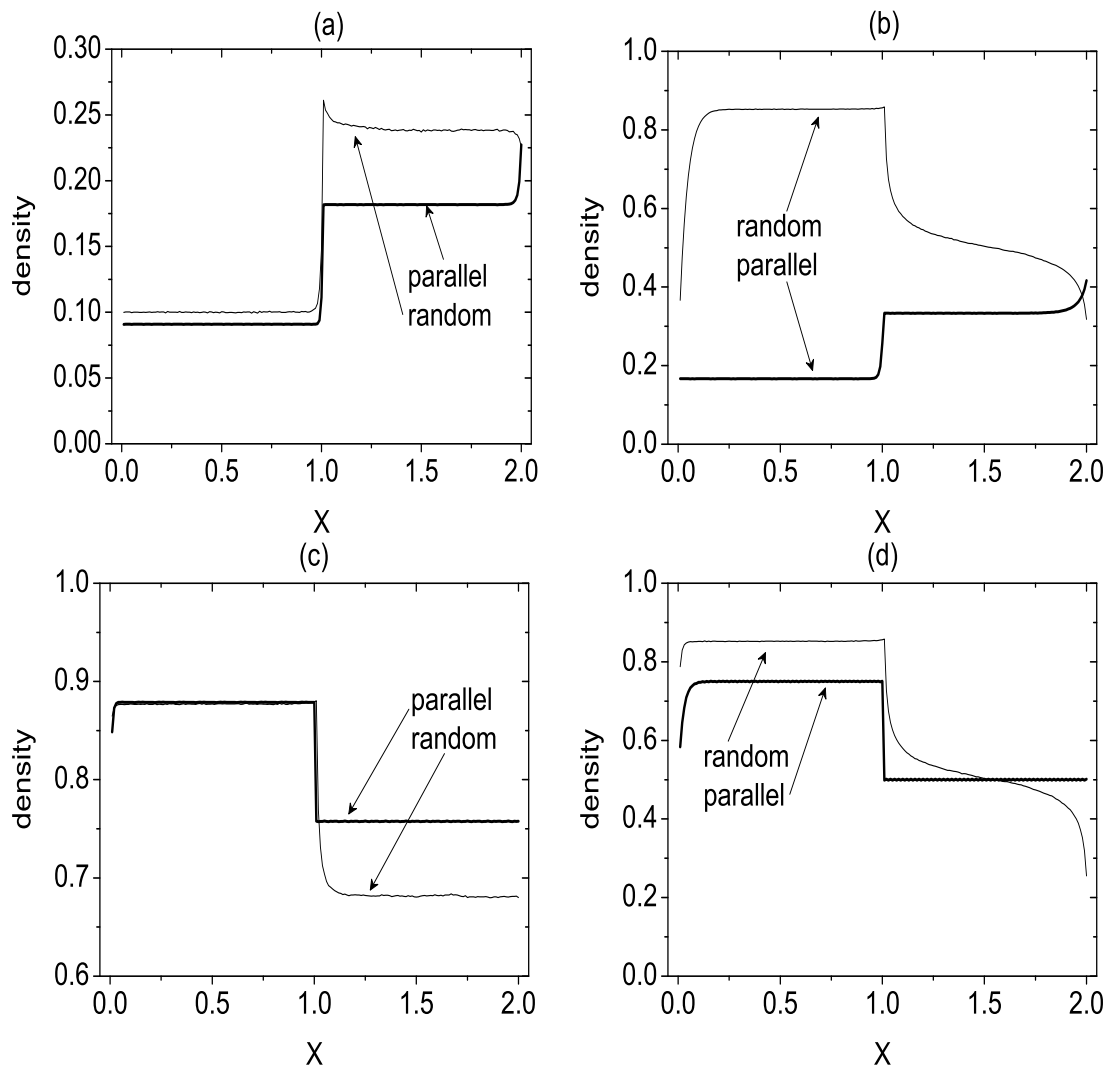
Figure 5.6: Density profiles in Monte Carlo simulations when $m = 2$ in random and parallel updates. The parameters are: (a) $\alpha = 0.1$ and $\beta = 0.8$, (b) $\alpha = 0.2$ and $\beta = 0.8$, (c) $\alpha = 0.8$ and $\beta = 0.32$, and (d) $\alpha = 0.8$ and $\beta = 0.8$.
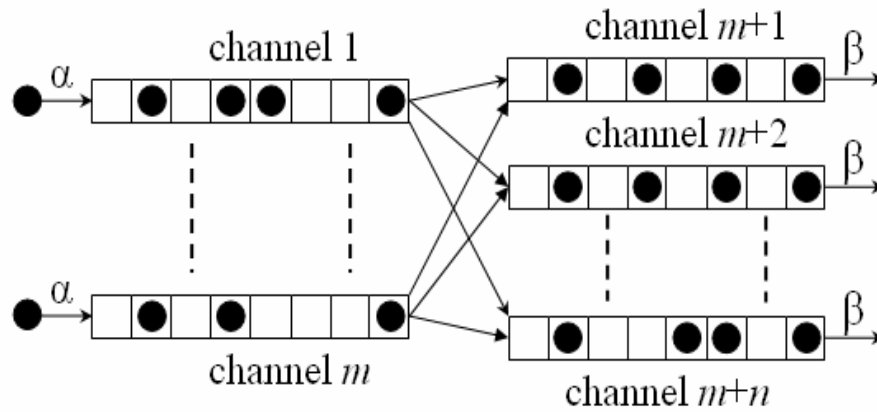
Figure 5.7: Schematic diagram of a m-input n-output (MINO) junction. Particles move from the left to the right with hard-core exclusion. There are m inputs and n outputs in the system.
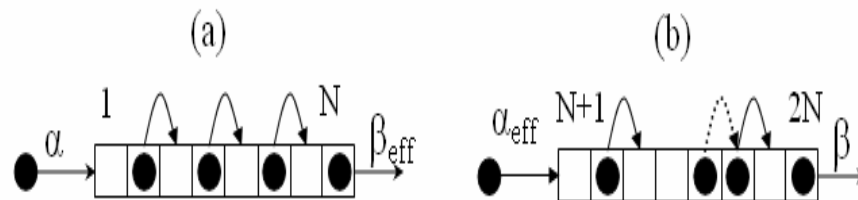
Figure 5.8: (a) The left subsystem. Entrance probability at site 1 and exit probability at site N are denoted as α and β_{eff}, respectively. (b) The right subsystem. Entrance probability at site $N+1$ and exit probability at site $2N$ are denoted as α_{eff} and β, respectively. Solid arrows indicate the allowed hopping with probability one in the bulk, while dashed arrows correspond to the prohibited movement.
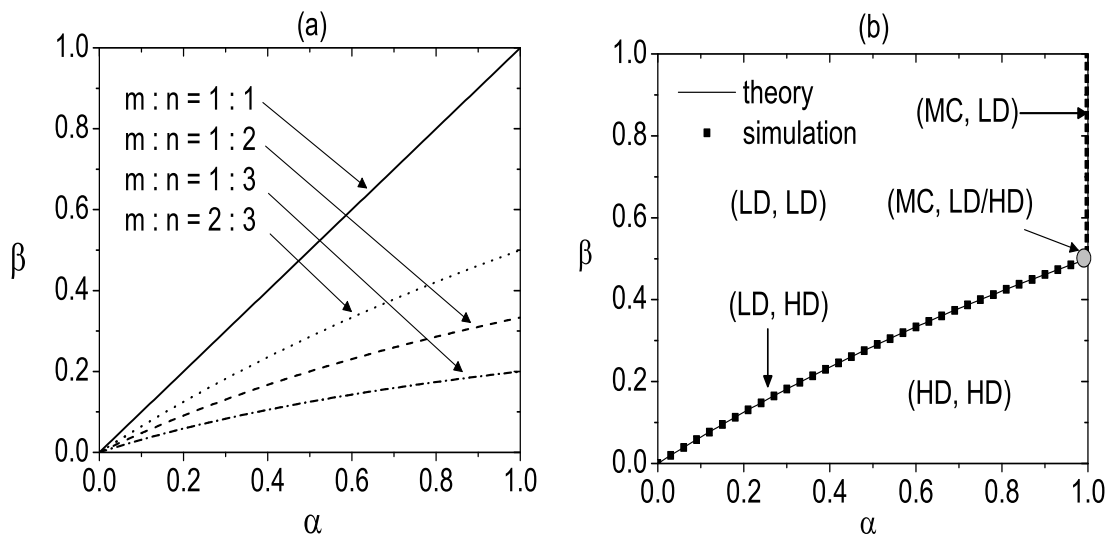
Figure 5.9: (a) Phase boundaries for $m = n$, $m = n/2$, $m = n/3$ and $m = 2n/3$ in TASEPs with a MINO junction in parallel update. (b) Phase diagram for $m = 2n/3$. There are five phases: (LD, LD), (HD, HD), (LD, HD), (MC, LD) and (MC, LD/HD) in the system. The lines are for theoretical prediction, while the symbols are for computer simulations.
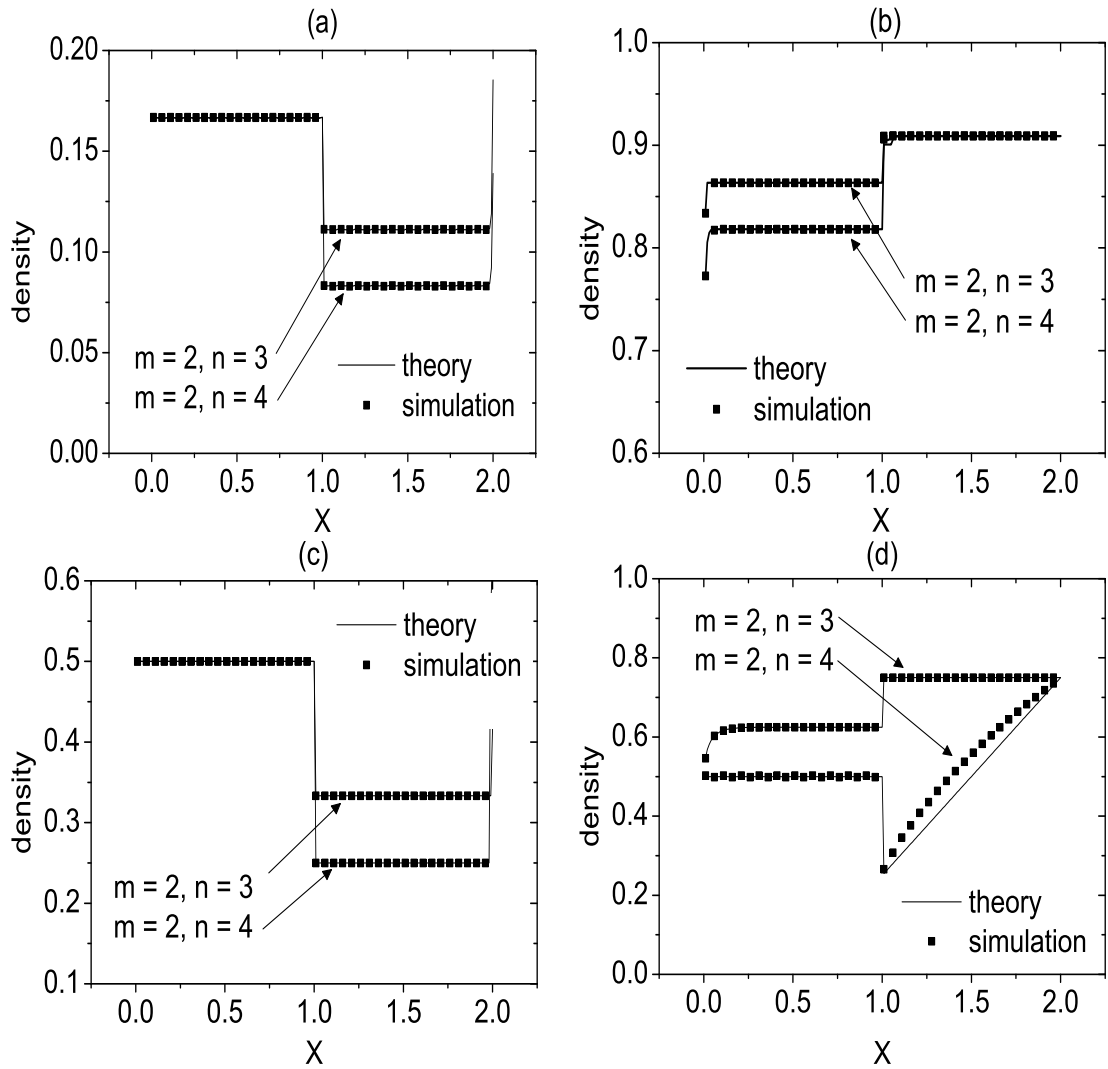
Figure 5.10: Density profiles of theoretical calculations and computer simulations with $m = 2$ and $n = 3, 4$: (a) the (LD, LD) phase, (b) the (HD, HD) phase, (c) the (MC, LD) phase, and (d) the (HD, HD) and (MC, LD/HD) phases. The parameters are: (a) $\alpha = 0.2$ and $\beta = 0.6$, (b) $\alpha = 0.8$ and $\beta = 0.1$, (c) $\alpha = 1.0$ and $\beta = 0.6$, and (d) $\alpha = 1$ and $\beta = 1/3$.
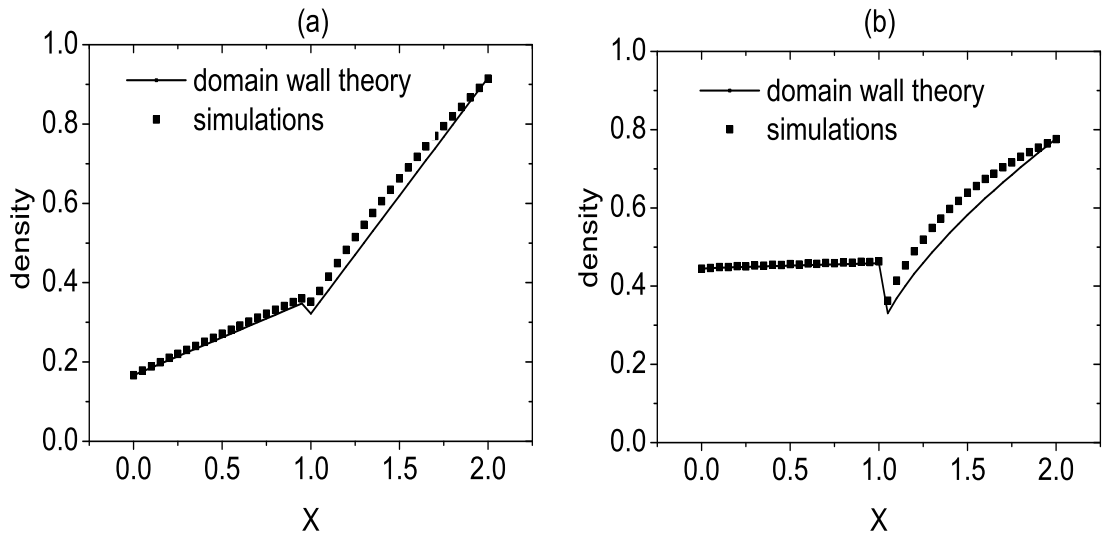
Figure 5.11: Density profiles of the domain wall approach and computer simulations in the (LD, HD) phase with $m = 2$ and $n = 4$. The parameters are: (a) $\alpha = 0.2$ and $\beta = 0.091$, and (b) $\alpha = 0.8$ and $\beta = 0.2857$.
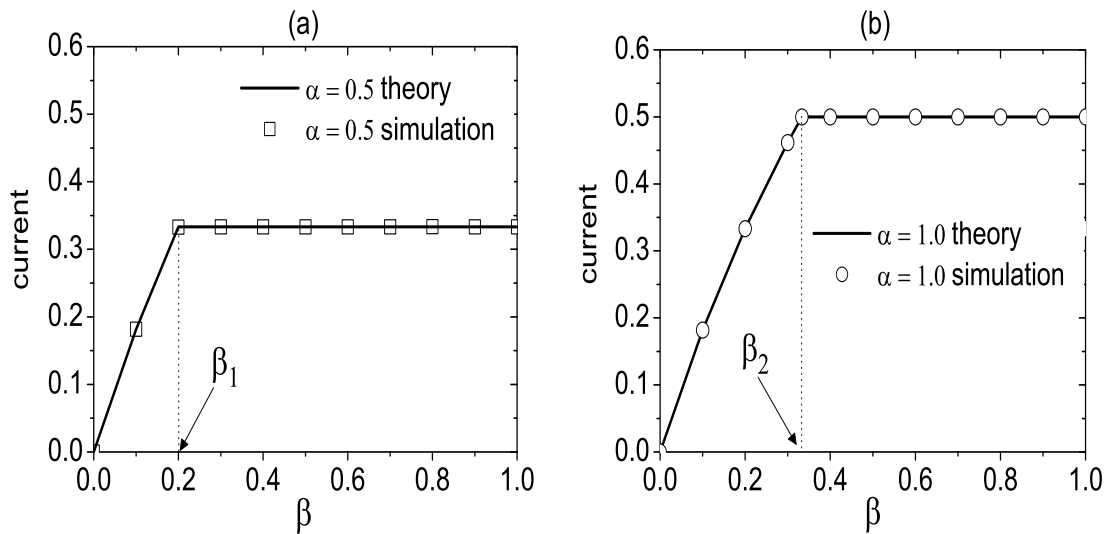
Figure 5.12: Currents are obtained from theoretical calculations and computer simulations with $m = 2$ and $n = 4$. The parameters are: (a) $\alpha = 0.5$, and (b) $\alpha = 1.0$.

Chapter 6

Two-species TASEPs with Site Sharing and Relaxed Boundaries

6.1 Introduction

The totally asymmetric simple exclusion process (TASEP) is a one-dimensional lattice model where particles move unidirectionally with hard-core exclusion (that is, each site can be occupied by at most one particle at any given time). The original TASEP was introduced in 1968 as a model of biopolymersation of ribosomes [7]. Recently, a great number of variants have been developed to model biological transport, such as in [1, 31, 43, 84, 53, 85, 125]. The model also finds applications in traffic simulations and other transport systems e.g., in [16, 126, 127]. Meanwhile, as a paradigm of driven diffusive systems, TASEPs have been investigated theoretically in their own right [8, 9, 27, 28, 30, 33, 39, 47, 54, 56, 71, 89, 97].

In these TASEP models, either single species of particles or multiple species, particles follow the *site-exclusion mechanism*, i.e., hard-core rule, on one channel or multiple channels of movement. The TASEP with *site-sharing mechanism* has not been well studied so far. It is believed that the study on the TASEPs with site sharing is interesting and worthwhile theoretically and practically. In many realistic models component entities such as different species of particles do indeed share the

same sites simultaneously and this multiple occupancy likely plays an important role in system properties. In fact, it is possible that different species particles can share the same site. For instance, when pedestrians walk along a narrow one-channel pathway in opposite directions and meet together, they may share a space, and then pass each other.

The proposed two-species TASEP model is based on the site-sharing mechanism. There is also a substantial literature on two-species ASEP models with a *site-exchanging* mechanism, e.g., under periodic boundary conditions [113, 114, 115] and open boundary conditions [56, 60, 82, 116, 118]. Evans et al. [56] firstly investigated two-species TASEP with a particle-exchange mechanism and open boundaries. Their model is known as the Bridge model. Jafarpour [118] studied an interesting case in which two-species of particles can be converted each other with a certain probability at boundaries. Popkov et al. [82] introduced the Bridge model with two junctions. More recently, Gupta et al. [116] extended the Bridge model to the relaxed case, that is, the particle-exchange mechanism is also applied to the boundaries. The basic stationary and dynamic properties of non-equilibrium systems with two-species of particles are reviewed in [105]. The spontaneous symmetry breaking (SSB) is observed and exhibited as high-density/low-density phase and/or asymmetric low-density/low-density phase in [56, 60, 82, 113, 116]. Physically one would expect that these models show a similar phase diagram and general behaviour since the details of the exchange mechanism (with or without site-sharing) are expected to be irrelevant.

In this Chapter, a one-dimensional lattice model under open boundary conditions is investigated. In the model, two species of particles move in opposite directions and are allowed to share a site with a certain probability when they meet. Note that there are two major differences between the proposed model and previous two-species TASEP models: (1) In the bulk, two species of particles may share the

same site in the present model, rather than exchanging each other in other models; (2) In the boundaries, the model allows two species of particles to share the same site as well, rather than excluding each other like in the Bridge model and its variants. Interestingly, when the boundary conditions of the model are the same as that of the Bridge model, the spontaneous symmetry breaking is observed. This work is now in progress and will be reported later.

This Chapter is organized as follows. In section 6.2, the model is described and mean-field theoretical analysis is conducted. In section 6.3, the results of theoretical calculations and Monte-Carlo simulations are discussed. A comparison is also made between the proposed model and the Bridge model. Conclusions and areas for further investigation are given in section 6.4.

6.2   Model formation and theoretical analysis

An illustration of a one-dimensional TASEP with two species of particles is shown in Figure 6.1. The system includes N sites. Each site can be occupied by a (+) particle and/or a (-) particle, or empty. The (+) particles move from the left to the right, represented by filled circles, while the (-) particles (denoted by open circles) move in the opposite direction (see Figure 6.1). In each time step, a site i is picked. At this site, a (+) particle or a (-) particle may be chosen. If a (+) particle is chosen, one of the following rules is applied:

- In the bulk. (1) A (+) particle at site i can hop to site $i + 1$ with probability 1 if the target site is empty; (2) If the target site is occupied by a (-) particle, the (+) particle can share the site with probability q ($0 \leq q \leq 1$); (3) If the target site is occupied by another (+) particle, the (+) particle stays at site i.

- In the boundaries. (1) A (+) particle enters the left boundary with rate α_+ if the first site is empty, or with probability $q\alpha_+$ if the site is occupied by a (-)

particle; (2) A (+) particle can exit the system from the last site at the right boundary with rate β_+.

If a (-) particle is chosen, the similar rules are performed by (-) particles from the right to the left. For simplicity, this Chapter just discusses the case of $\alpha_+ = \alpha_- = \alpha$ and $\beta_+ = \beta_- = \beta$.
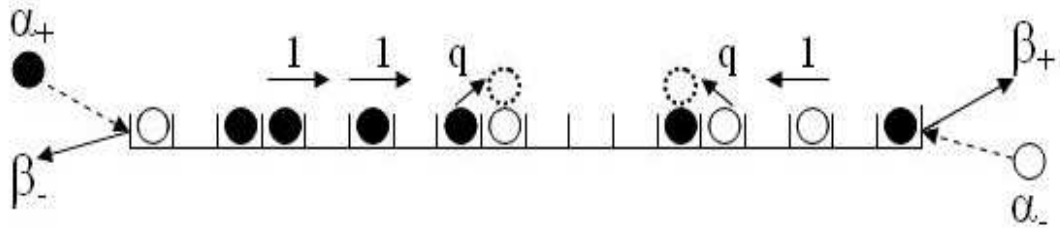
Figure 6.1: Diagrammatical representation of a one dimensional TASEP with two species of particles. The (+) particles move from the left to the right, represented by filled circles, while the (-) particles do the opposite movement, denoted by open circles. A site can be shared with probability q by two species of particles when they meet on the same lattice.
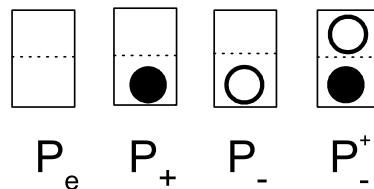
Figure 6.2: Four possible states on each site. P_e, P_+, P_-, and $P_\pm$ denote corresponding probabilities.

Since a site can be shared by two species of particles in the present model, there are four possible states for each site: (1) occupied by a (+) particle; (2) occupied by a (-) particle; (3) occupied by both a (+) and a (-) particle; (4) empty. According to these states, four corresponding probabilities: $P_+(i), P_-(i), P_\pm(i)$, and $P_e(i)$ are

defined, as shown in Figure 6.2. Clearly, these probabilities can be normalised as:

$$P_+(i) + P_-(i) + P_\pm(i) + P_e(i) = 1. \tag{6.1}$$

The evolution equation of $P_\pm(i)$ over time can be given by

$$
\begin{aligned}
\frac{dP_\pm(i)}{dt} &= qP_\pm(i-1)P_-(i) + qP_+(i)P_\pm(i+1) + qP_+(i-1)P_-(i) + \\
&\quad qP_+(i)P_-(i+1) - P_\pm(i)P_e(i+1) - P_\pm(i)P_e(i-1) - \\
&\quad qP_\pm(i)P_+(i-1) - qP_\pm(i)P_-(i+1), \tag{6.2}
\end{aligned}
$$

where the four positive terms represent the possible inflow for the formation of $P_\pm$ from site $i-1$ to site i for a (+) particle and from site $i+1$ to site i for a (-) particle. The four negative terms correspond to the possible outflow from site i. Similarly, the evolution of P_+ and P_- can be written as

$$\frac{dP_+(i)}{dt} = P_+(i-1)P_e(i) + P_\pm(i-1)P_e(i) - qP_+(i)P_-(i+1) - P_+(i)P_e(i+1), \tag{6.3}$$

$$\frac{dP_-(i)}{dt} = P_-(i+1)P_e(i) + P_\pm(i+1)P_e(i) - qP_-(i)P_+(i-1) - P_-(i)P_e(i-1). \tag{6.4}$$

Note that Eqs. (6.2-6.4) are not exact, but mean-field approximations. In steady state, these probabilities are expected to be independent of positions of sites. Thus, it is reasonable to neglect i indices in above equations. The above equations will tend to be zero in a stationary state. That is, $dP_\pm/dt = dP_+/dt = dP_-/dt = 0$, which leads to

$$qP_+P_- = P_\pm P_e. \tag{6.5}$$

The currents and bulk densities for (+) particles and (-) particles can be written as follows

$$J_+ = (P_\pm + P_+)(P_e + qP_-), \quad \rho_+ = P_\pm + P_+, \tag{6.6}$$

$$J_- = (P_\pm + P_-)(P_e + qP_+), \quad \rho_- = P_\pm + P_-, \tag{6.7}$$

where J_+ and J_- represent currents of $(+)$ particles and $(-)$ particles in the system, respectively. ρ_+ and ρ_- denote the corresponding bulk densities. The first term multiplier in the current expression in Eq. (6.6) represents the probability of finding a $(+)$ particle at a site, while the second term corresponds to the probability that the next site is available. The system is in left-right symmetry, and the dynamical rules are identical. Under the conditions where the symmetry of the system is retained, one expects that the currents of $(+)$ particles and $(-)$ particles should be equal.

When $J_+ = J_-$, one obtains $P_+ = P_-$ by comparing Eq. (6.6) with Eq. (6.7). Then by using Eq. (6.1), Eq. (6.5) can be rewritten as

$$qP_+^2 = P_\pm(1 - 2P_+ - P_\pm), \tag{6.8}$$

so that

$$P_+ = \frac{-P_\pm + \sqrt{(1 - q)P_\pm^2 + qP_\pm}}{q}. \tag{6.9}$$

According Eqs. (6.1) and (6.9), Eq. (6.6) is given by

$$J_+ = \frac{1}{q^2}((q-1)P_\pm + \sqrt{(1 - q)P_\pm^2 + qP_\pm})(q + 2P_\pm - 2qP_\pm - (2-q)\sqrt{(1 - q)P_\pm^2 + qP_\pm}). \tag{6.10}$$

In the low-density (LD) phase, the current of $(+)$ particles at the entrance of the left boundary is equal to

$$J_{LD}^+ = \alpha(P_e + qP_-). \tag{6.11}$$

According to the rule of current conservation in a steady state and comparing Eq. (6.11) with Eq. (6.6), one has

$$\alpha = P_\pm + P_+. \tag{6.12}$$

Eq. (6.12) means that the bulk density of (+) particles $\rho_+ = P_\pm + P_+ = \alpha$. Then according to Eqs. (6.9) and (6.12), one obtains

$$P_+ = \frac{1 - \sqrt{1 - 4\alpha(1 - q)(1 - \alpha)}}{2(1 - q)}, \quad P_\pm = \frac{2\alpha(1 - q) - 1 + \sqrt{1 - 4\alpha(1 - q)(1 - \alpha)}}{2(1 - q)}.$$

(6.13)

Substituting Eq. (6.13) into Eq. (6.10), the system current in the LD phase reads,

$$J_{LD}^+ = \frac{\alpha}{2}(1 - 2\alpha + \sqrt{1 - 4\alpha(1 - q)(1 - \alpha)}).$$

(6.14)

In the high-density (HD) phase, the system dynamics is determined by exit rate β. The current for (+) particles at the right boundary is given by

$$J_{HD}^+ = \beta(P_\pm + P_+).$$

(6.15)

Applying the rule of current conservation, the following equation is derived from Eqs. (6.6) and (6.15)

$$\beta = P_e + qP_-.$$

(6.16)

As $P_+ = P_-$, according to Eq. (6.9), then

$$q(1 - q)P_\pm^2 + (q^2 + 4\beta - 4q\beta)P_\pm - q(1 - \beta)^2 = 0,$$

(6.17)

The above equation has a solution

$$P_\pm = \frac{-(q^2 + 4\beta - 4q\beta) + \sqrt{q^4 + 4(1 - q)[q^2 + \beta^2(2 - q)^2]}}{2q(1 - q)}.$$

(6.18)

P_+ can be obtained from Eq. (6.9)

$$P_+ = \frac{2q + 2q^2\beta + 4\beta - 6q\beta - q^2 - \sqrt{q^4 + 4(1 - q)[q^2 + \beta^2(2 - q)^2]}}{2q(1 - q)(2 - q)}.$$

(6.19)

Thus, the bulk density and current in the HD phase can be calculated

$$\rho_{HD}^+ = \frac{q - 2\beta}{2q} + \frac{\sqrt{q^4 + 4(1 - q)[q^2 + \beta^2(2 - q)^2]}}{2q(2 - q)}, \quad J_{HD}^+ = \beta\rho_{HD}^+.$$

(6.20)

In the maximal-current (MC) phase, the current, J_{MC}, is independent of α and β, but is only determined by q. When J is maximal, Eq. (6.10) corresponds to $\frac{\partial J_+}{\partial P_\pm} = 0$ which leads to

$$
\begin{aligned}
[3q - 2q^2 + (8 - 14q + 6q^2)P_\pm]\sqrt{(1-q)P_\pm^2 + qP_\pm} \ = \ & (2 - 5q + 4q^2 - q^3)P_\pm^2 + \\
& (1 + \frac{1}{2}q - \frac{5}{2}q^2 + q^3)P_\pm - \\
& \frac{1}{2}q + 1.
\end{aligned}
\tag{6.21}
$$

When q is known, $P_\pm$ can be solved exactly. Then P_+, ρ_+ and J_{MC} can be calculated using Eqs. (6.9) and (6.10).

Two extreme cases: $q = 0$ and $q = 1$ are examined. With regard to $q = 0$, a $(+)$ particle cannot share a site with a $(-)$ particle, i.e., $P_\pm = 0$. Obviously, the system is blocked and system current $J = 0$. Theoretically, $P_+ = 0.5$ and $P_- = 0.5$, which leads to $P_e = 0$ and $J_+ = 0$. As to $q = 1$, a $(+)$ particle does not distinguish between a $(-)$ particle and a hole. And similarly for a $(-)$ particle. The system is therefore decoupled into two independent TASEPs. Thus, system current J and density ρ satisfy: $J = \rho(1 - \rho)$. According to Eq. (6.9), $P_+ = \sqrt{P_\pm} - P_\pm$. Then Eq. (6.6) is rewritten as

$$
J_+ = \sqrt{P_\pm}(1 - \sqrt{P_\pm}).
\tag{6.22}
$$

When the system is in the LD phase, comparing Eq. (6.22) with Eq. (6.11), one obtains $\sqrt{P_\pm} = \alpha$. The corresponding current in this phase can be read as $J = \alpha(1 - \alpha)$. For the HD phase, comparing Eq. (6.22) with Eq. (6.15), one has $\sqrt{P_\pm} = 1 - \beta$. Thus the current in the HD phase is equal to $J = \beta(1 - \beta)$. In the MC phase, $P_\pm = 1/4$ can be derived from Eq. (6.21) when $q = 1$. Then according to Eq. (6.9), one obtains $P_+ = 1/4$. Substituting values of $P_\pm$ and P_+ into Eq. (6.6), one obtains $J_+ = 1/4$ and $\rho_+ = 1/2$. It can be seen that the system for $q = 1$ is reduced to the usual one-dimensional TASEP with random update [8].

For another limiting case $\alpha_- = 0$, Eq. (6.1) is simplified as $P_+(i) + P_e(i) = 1$ (i.e., $P_\pm(i) = P_-(i) = 0$). The corresponding stationary current and bulk density for (+) particles can be represented as $J_+ = P_+ P_e$ and $\rho_+ = P_+$ (see Eq. (6.6)). Thus, the model reduces to the usual TASEP. A proper mean-field theory for this case has been developed by Derrida et al. [8].

The possibility of observing spontaneous symmetry breaking in the system is discussed. Spontaneous symmetry breaking is characterized by unequal bulk densities of (+) particles and (-) particles under the symmetric structure and updating rules. There are six possibly asymmetric phases in the system, i.e., the (LD, LD), (HD, HD), (MC, MC), (LD, HD), (LD, MC), and (HD, MC) phases. The (LD, HD) phase means that (+) particles are in the LD phase, while (-) particles are in the HD phase.

In the (LD, LD) phase, J_{LD}^- at the entrance of the right boundary is given by

$$J_{LD}^- = \alpha(P_e + qP_+). \tag{6.23}$$

Comparing the equation with Eq. (6.7), one obtains $\alpha = P_\pm + P_-$. Similarly, one has $\alpha = P_\pm + P_+$ for (+) particles. One then derives $P_+ = P_-$, which contracts the assumption $P_+ \neq P_-$. Thus, the (LD, LD) phase does not exist in the system. Similarly, one can confirm nonexistence of the (HD, HD) phase.

For the (LD, HD) phase, according to Eqs. (6.6) and (6.7), $J_{LD}^+ - J_{HD}^- = qP_\pm(P_- - P_+) + P_e(P_+ - P_-) \neq 0$. If $J_{LD}^+ - J_{HD}^- > 0$, one has $qP_\pm > P_e$ as $P_- > P_+$. Then according to Eq. (6.16), $\beta = P_e + qP_+ < qP_\pm + qP_+ = q\alpha$. However, as (+) particles are in the LD phase, one has $\alpha < \beta$, which means $q\alpha < q\beta$. Thus, it leads to $\beta < q\alpha < q\beta$. This is impossible for $0 < q < 1$. In the similar way, one disconfirms the assumption $J_{LD}^+ - J_{HD}^- < 0$. Therefore, the (LD, HD) phase does not exist in the system.

As mentioned above, the MC phase is determined by $P_\pm$. The values of $P_\pm$ are the same for (+) particles and (-) particles in the system. Thus, the (MC, MC) phase reduces to the MC phase. If the (LD, MC) phase could exist in the system, $P_\pm$ in the LD phase should equal to that in the MC phase. However, $P_\pm$ only depends on q in the MC phase (see Eq. (6.21)), while it depends on q and α in the LD phase. Therefore, it is impossible that the (LD, MC) and (HD, MC) phases exist in the system. Therefore, only three stationary phases: LD, HD and MC are identified in this system, which are similar to the standard TASEP [8], but with shifted boundaries according to different sharing probability q.

6.3   Results and discussion

To verify the theoretical analysis above, Monte Carlo simulations were carried out. Open boundary conditions and random update were used with the system size $N = 1000$. For larger size N, thesimulations show little deviations from those presented here. The first 1×10^9 time steps were discarded to let the transient out. The system current and density profiles were obtained by averaging 5×10^9 time steps. The system current J is defined as $J = J_+ = J_-$ and bulk density as $\rho = \rho_+ = \rho_-$, unless stated otherwise.

Phase diagrams obtained from theoretical predictions and computer simulations are presented in Figure 6.3(a). By comparing the simulation results with theoretical calculations one can conclude that the simple mean-field approach agrees well with simulations. However, there are still deviations from simulations for some values of q (see Figure 6.3(b)). The simulations were repeated ten times with different random number seeds and the resulting critical points (α^*, β^*) are shown in Figure 6.3(b). $\alpha^* and \beta^*$ in Figure 6.3(b) are intersection points of the LD, HD, and MC phases. Thus, a phase diagram can be determined once a (α^*, β^*) pair is obtained.
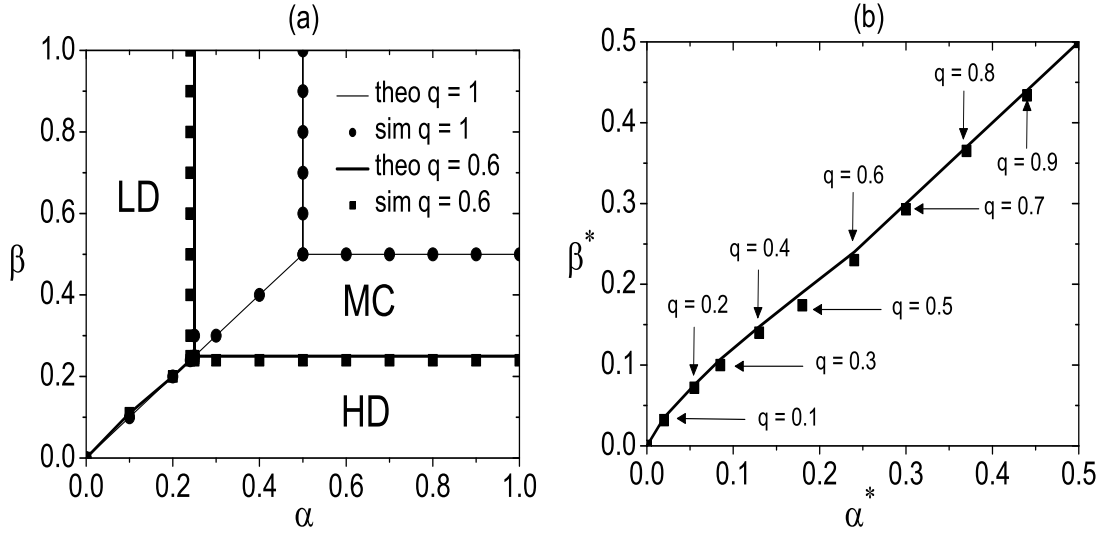
Figure 6.3: (a) Phase diagram of the TASEP with two species of particles and sharing probabilities $q = 0.6$ and 1. (b) The critical points (α^*, β^*) with different q in the $\alpha - \beta$ plane. The solid line is for theoretical results, while the filled symbols correspond to simulation results. These figures are averaged over 10 runs.

For example, the MC phase is specified by $\alpha \geq \alpha^*$ and $\beta \geq \beta^*$. Theoretical analysis of the model indicates that the phase diagram is similar to the normal TASEP [8], however, the phase boundaries are shifted according to different values of sharing probability q.

Current profiles in these phases with different q are investigated. For simplicity, one assumes that α is fixed while β changes from 0 to 1. Figure 6.4(a) shows the stationary current obtained from theoretical calculations and computer simulations for $\alpha = 1.0$. With the increase of β, a phase transition from the HD phase to the MC phase is observed in which the maximal current J_{max} is maintained and its value is determined by q. In Figure 6.4(b), J_{max} versus different q is shown with $\alpha = 0.9$ and $\beta = 0.9$. It can be seen that the theoretical predictions are in agreement with computer simulations for $q = 1$, while they have slight deviations from simulation
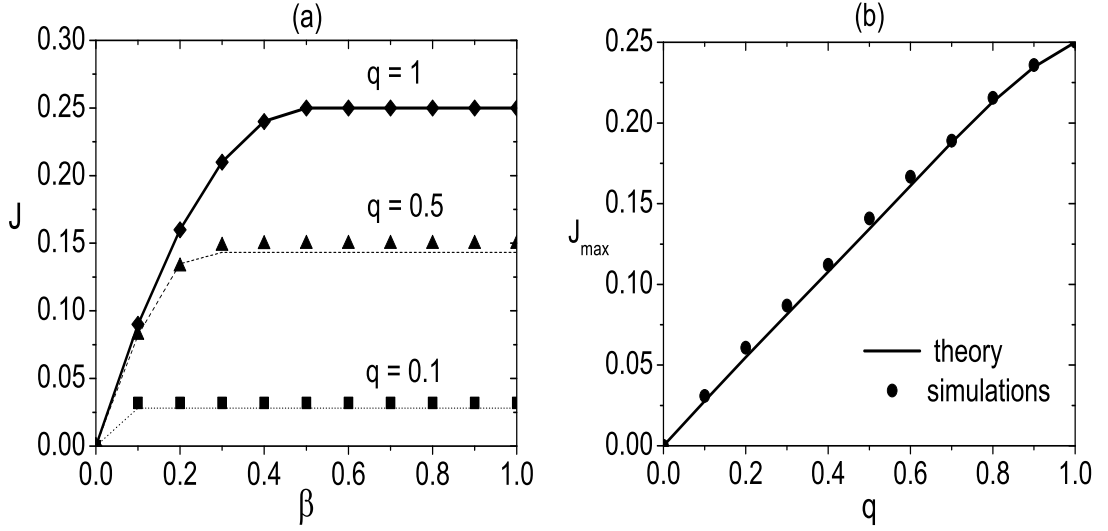
Figure 6.4: (a) Currents obtained from theoretical calculations and computer simulations with $\alpha = 1$. (b) J_{max} versus q with $\alpha = 0.9$ and $\beta = 0.9$. The lines are for theoretical predictions, while the symbols correspond to simulation results. Data are collected by averaging 10 independent configurations.

results (e.g., $q = 0.1$ and $q = 0.5$). The reason for this is probably due to neglecting the correlations between the two species of particles.

An interesting quantity in this study is P_-^+ which is the quantity that is new compared to previous one-dimensional two-species TASEP models. Thus, density profiles (denoted by $P_+, P_-, P_\pm, P_e$) in the LD, HD and MC phases can be obtained from theoretical predictions and computer simulations and are shown in Figure. 6.5. It is seen that theoretical results of $P_+, P_-, P_\pm, P_e$ agree well with computer simulations when the system is in the LD or HD phase (see Figures. 6.5(a-b)). However, when the system is in the MC phase, only P_+ and P_- show a good agreement with simulation results. Large deviations can be found in $P_\pm$ and P_e (see Figure. 6.5(c)). For a better understanding of the MC phase, Figure. 6.5(d) shows the bulk density of (+) particles in the MC phase, i.e., $\rho_+ = P_+ + P_\pm$. One can see that the theoret-

ical results of the bulk density agree qualitatively with simulation results when the system is in the MC phase.
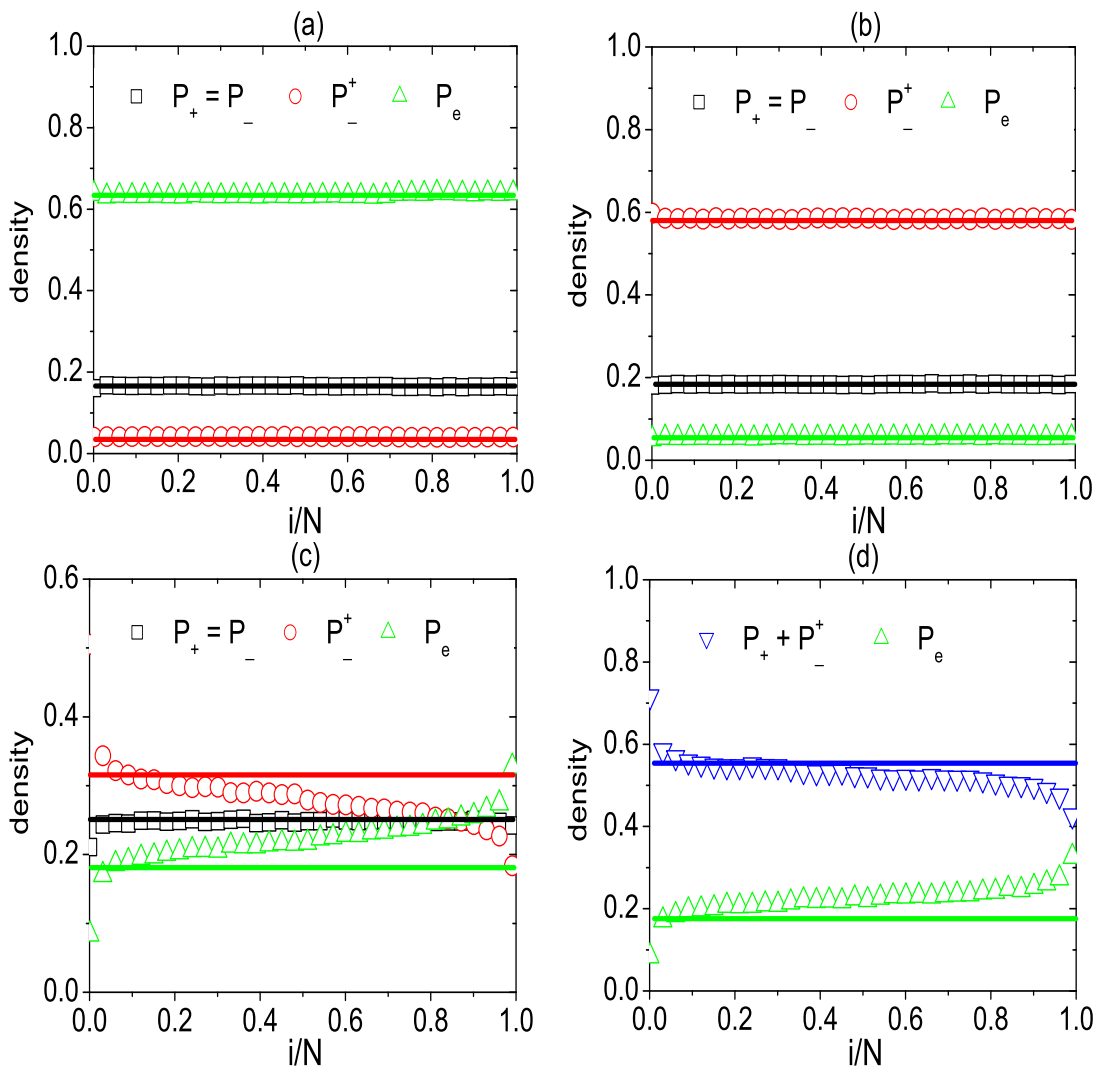
Figure 6.5: Density profiles $(P_+, P_-, P_\pm, P_e)$ in the LD, HD and MC phases obtained from theoretical predictions and computer simulations. Symbols represent the simulation results, while the corresponding thick lines are for the theoretical calculations. (a) LD phase with $\alpha = 0.2$, $\beta = 0.8$ and $q = 0.8$. (b) HD phase with $\alpha = 0.8$, $\beta = 0.2$ and $q = 0.8$. (c) and (d) MC phase with $\alpha = 0.8$, $\beta = 0.8$ and $q = 0.8$. (d) Bulk density of $(+)$ particles in the MC phase, i.e., $\rho_+ = P_+ + P_\pm$.

The relationship among P_+, P_-, P_-^+, P_e and α is simulated and shown in Figure. 6.6. For simplicity, I arbitrarily set $\beta = 1$ and α changing from 0 to 1. In this case, the phase transition from the LD phase to the MC phase is observed. In the MC phase, P_-^+ is determined by sharing probability q, independent of α and β. With the increase of q, P_e increases in the MC phase. Upon increasing to $q = 1$, $P_+ = P_- = P_-^+ = P_e = 0.25$ (see Figure. 6.6(d)). On the other hand, when increasing q, the region of the MC phase shrinks while the region of the LD phase expands (see Figure 3(a) and Figures. 6.6(a-d)).

A comparison of the average currents is also made between the present model and the Bridge model under the same parameters in Monte Carlo simulations. Taking the flipping phenomenon into account in the Bridge model, the average current of (+) and (-) particles is used here, i.e., $J_{ave} = (J_+ + J_-)/2$, where J_+ and J_- are currents of (+) and (-) particles, respectively. It is assumed that $\alpha = 0.2, 1$, $q = 0.3, 0.6, 0.9$ while β changes within [0,1] so that one can observe the average current in all possible phases. It is shown that the proposed model can enhance the average current than that in the Bridge model (see Figure. 6.7). The reason for this is probably due to the relaxed boundary conditions and the site-sharing mechanism used in the present model.

6.4   Summary and conclusions

This chapter studied the dynamics of two-species TASEP with site sharing under random update and open boundary conditions. Hard-core exclusion is only applied to the particles of the same species, while different species of particles may break the hard-core exclusion, that is, they can share the same site with a certain probability q. This kind of sharing mechanism has been little studied in previous TASEP models, to the best of our knowledge. The steady-state phase diagrams, currents and
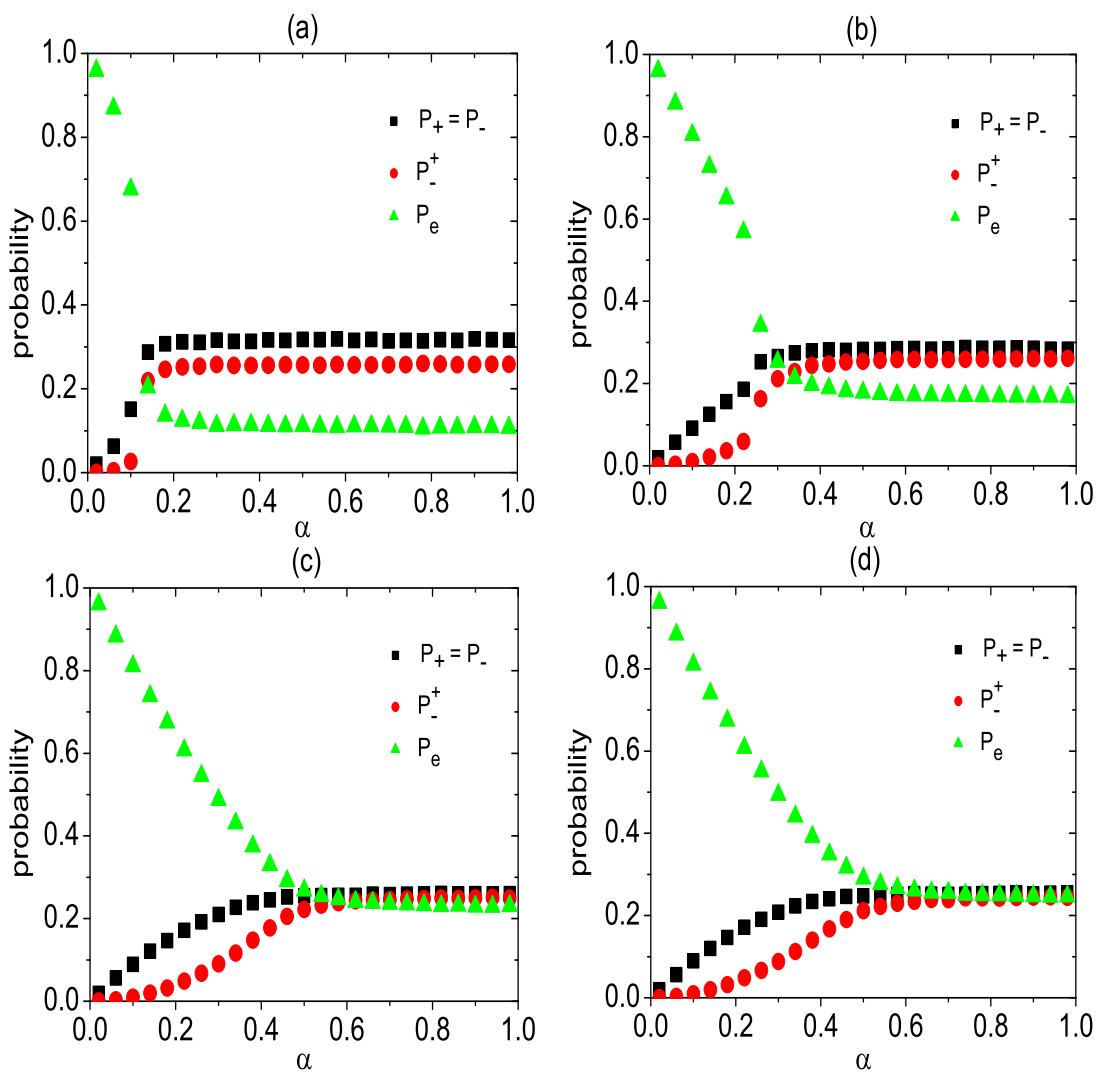
Figure 6.6: P_+, P_-, P_-^+ and P_e versus α with $\beta = 1$ and different q. (a) $q = 0.3$. (b) $q = 0.6$. (c) $q = 0.9$ and (d) $q = 1$.

bulk densities are obtained using a simple mean-field approximation and extensive Monte Carlo simulations. Histograms of two species of particle densities are simulated. Three stationary phases (LD, HD, and MC) are identified with shifted phase boundaries, compared to the normal TASEP. In the MC phase, currents and density
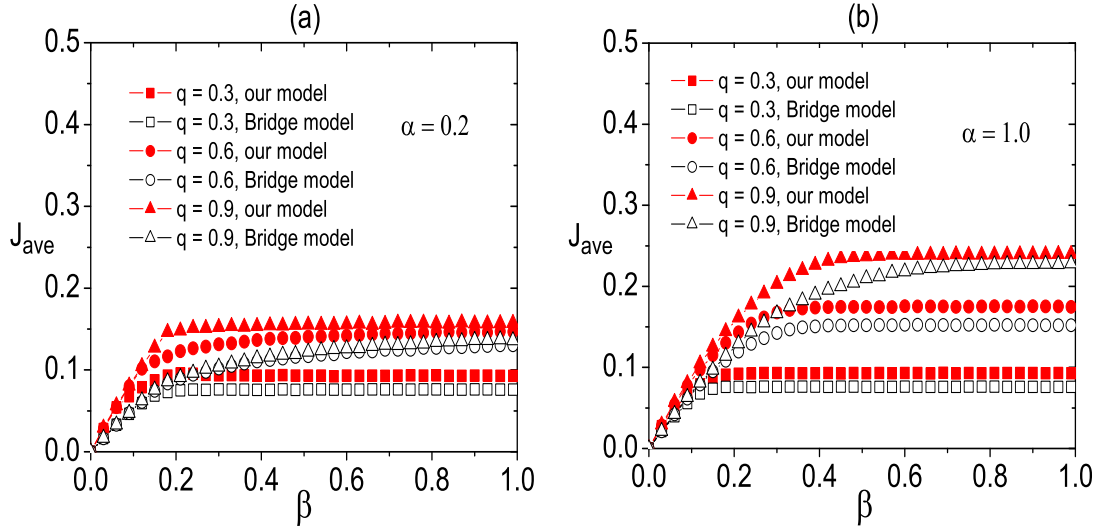
Figure 6.7: A comparison on the stationary currents between the proposed model and the Bridge model with different β in simulations. J_{ave} is the average current of (+) and (-) particles, i.e., $J_{ave} = (J_+ + J_-)/2$. The red filled symbols correspond to the present model, while the black open symbols are for the Bridge model. (a) $\alpha = 0.2$ and (b) $\alpha = 1.0$.

profiles are dictated by the sharing probability q. The theoretical predictions are supported by computer simulations.

This work shows that the sharing mechanism of two species of particles is an interesting issue and needs to be further investigated. The present model can be extended to a more general case where particles can randomly attach to or detach from the lattice. It would be interesting to study the present model with parallel updating procedure.

This Chapter is based on the paper "Asymmetric exclusion processes with site sharing in a one-channel transport system". The paper has been published in Physics Letters A 374 (2010) 516-521.

Chapter 7

Spontaneous Symmetry Breaking in TASEP with Site Sharing and constrained boundaries

7.1 Introduction

Non-equilibrium systems have attracted the interests of interdisciplinary researchers because a variety of interesting phenomena such as boundary-induced phase transitions, phase separations, and spontaneous symmetry breaking are observed. Originally introduced in the description of ribosome motion along mRNA in 1968 [7], totally asymmetric simple exclusion process (TASEP) and its variants have exhibited properties believed to be characteristics of many real-world non-equilibrium processes such as molecular motor traffic [53], protein synthesis [43], fungal hyphal growth [123]. On the other hand, the TASEP has also been extensively studied in its own right in the context of different particle properties (e.g., large particles [39, 41, 42], two species of particles [56, 62] and different lattice geometries (e.g., multiple channels [68, 78], junctions [27, 79]) as well as different updating procedures (e.g., random update [30], parallel update [33]). These investigations enhanced a

broader understanding of non-equilibrium systems.

Recently, the study on spontaneous symmetry breaking (SSB) in non-equilibrium systems has received much attention using TASEP with two species of particles. The SSB in this way is characterised by unequal densies of two species of particles. Evans et al. [56] firstly observed the SSB in one-dimensional two-species TASEP with open boundary conditions. In their model, two-species of particles can exchange their positions with a certain probability when they meet together. As the shape of the model in [56] looks like a bridge, the model is known as the "Bridge model". In the Bridge model, it was shown that a high-density-low-density (HD/LD) phase and an asymmetric LD/LD phase could exist and both of them exhibit broken symmetry. Erickson et al. [61] also revisited the Bridge model via high-precision Monte Carlo data and associated their work with the study of traffic on a narrow bridge. Their simulation results show that the LD/LD phase will disappear if the system size is sufficiently large and/or the exchange probability is sufficiently low. Levine and Willmann [60] extended the Bridge model by considering Langmuir Kinetics (LK) on a lattice. Two-species of particles are assumed to have the same attachment rate and detachment rate. They found that the SSB could exist and the localized shocks appear in some conditions.

The SSB has also been investigated in multiple-channel TASEPs with random update [63] and parallel update [64, 65]. More recently, Popkov et al. introduced the Bridge model fed by two junctions [82]. The SSB is observed as well. In addition, a co-existence region between the symmetry-broken phase and the low-density symmetric phase exists in their system.

In this Chapter, the site-sharing mechanism is still adopted, but with constrained boundaries to study the dynamics of two-species TASEP using extensive Monte Carlo simulations. The constrained boundaries mean that particles cannot enter the system if the corresponding sites at boundaries are not empty. The spon-

taneous symmetry breaking is observed. Phase diagram, bulk density and particle currents are computed. For comparison, the Bridge model is also revisited. It is shown that the model exhibits higher current than the Bridge model in the high-density phase. This Chapter is organized as follows. In section 7.2, the model is formed, followed by simulation results in section 7.3. Conclusions are given in section 7.4.

7.2 Model description

An illustration of a one-dimensional TASEP with two-species of particles is shown in Figure 7.1. The system size is assumed to be N. Each site can be occupied by a (+) particle and/or a (-) particle, or empty. The (+) particles move from the left to the right, represented by filled circles, while the (-) particles denoted by open circles move oppositely (see Figure 7.1). The model is symmetric with regard to the rules and two species of particles. Therefore, the rules of (+) particles are defined. The (-) particles perform the similar rules from the right to the left. For simplicity, I assume $\alpha_+ = \alpha_- = \alpha$ and $\beta_+ = \beta_- = \beta$ in simulations. In each time step, a site i is randomly chosen. A probability for choosing a (+) or (-) particle at site i is equal, i.e., 0.5.

- When i is in the bulk $(1 < i < N)$,

    1. A (+) particle at site i can hop to site $i + 1$ with probability 1 if the target site is empty;

    2. If the target site is occupied by a (-) particle, the (+) particle can share the site with probability q $(0 \leq q \leq 1)$;

    3. If the target site is occupied by the same species particle, the (+) particle stays at site i.

- When i is in the boundaries,

  1. $i = 1$. A (+) particles can enter the left boundary with rate α_+ only if the first site is empty. If the site is occupied by the other (+) particle, the (+) particle already at site 1 can hop to site 2 with probability 1 if site 2 is empty or with probability q if site 2 is occupied by a (-) particle;

  2. $i = N$. A (+) particle can exit the system from the last site with rate β_+.
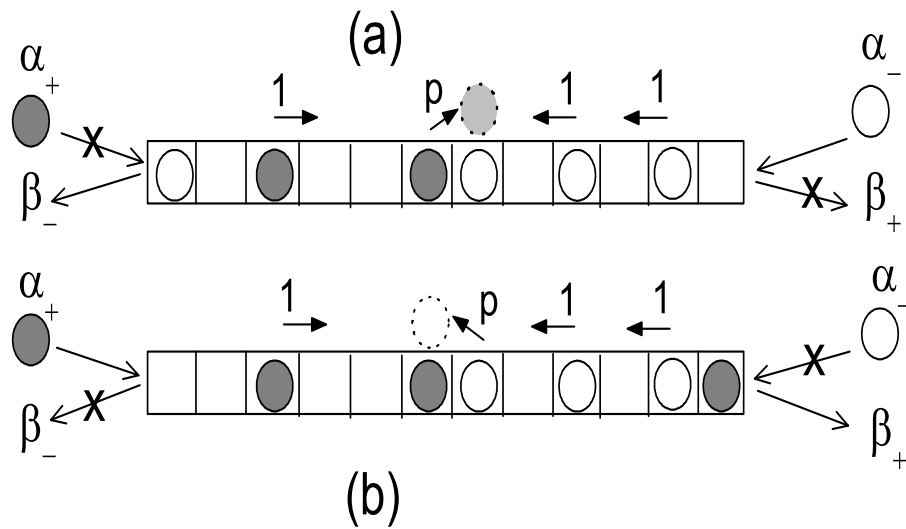
Figure 7.1: Diagrammatical representation of a one dimensional TASEP with two-species of particles. The (+) particles move from the left to the right, represented by filled circles, while the (-) particles (denoted by open circles) move from the right to the left. Arrows mean the possible movements. Symbols over the arrows indicate the corresponding hopping probabilities. A site can be shared with probability q by two-species of particles when they meet each other. (a): prohibited entrance for (+) particles, (b): prohibited entrance for (-) particles.

7.3   Simulation results and discussion

To investigate the dynamics of the system, Monte Carlo simulations are carried out. Open boundary conditions and random update are used with the system size $N = 1000$. The first 1×10^9 time steps are discarded to let the transient out. The phase diagram, stationary current and density profiles are obtained by averaging 2×10^9 time steps.
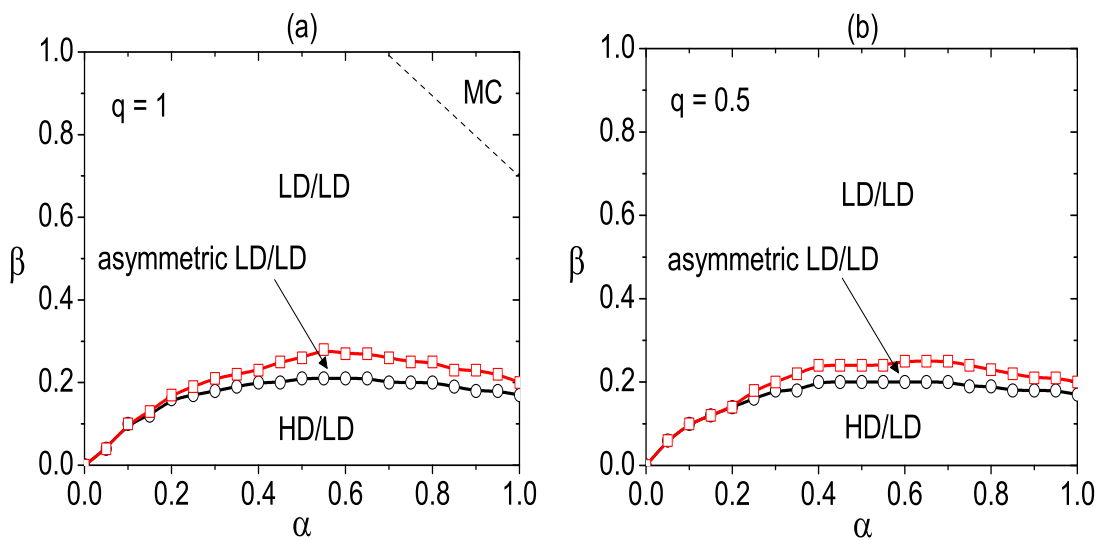
Figure 7.2: Phase diagram of the TASEP with two species of particles and site sharing for different sharing probabilities q. The red open squares correspond to the boundary between the symmetric LD/LD and asymmetric LD/LD phases, while the black open circles denotes the boundary between the asymmetric LD/LD and HD/LD phases. The lines are guided for eyes. (a) $q = 1$ and (b) $q = 0.5$.

The phase diagram is simulated for $q = 0.5, 1$ and shown in Figure 7.2. The red open squares correspond to the boundary between the LD/LD and asymmetric LD/LD phases, while the black open circles denotes the boundary between the asymmetric LD/LD and HD/LD phases. When $q = 1$, a (+) particle does not distinguish between a (-) particle and a hole. Similarly, a (-) particle does not

distinguish between a (+) particle and a hole. In this case, four stationary phases exist in the system, that is, symmetric LD/LD, asymmetric LD/LD, HD/LD and MC phases (see Figure 7.2(a)). Note that the MC phase covers a small region in the site-sharing model, while it is reduced to a point ($\alpha = 1, \beta = 1$) in the Bridge model. The simulation results show that the MC phase will disappear when q is approximately $q < 0.97$. In other words, there are only three phases in the system for $q < 0.97$ (see Figure 7.2(b)). Furthermore, as q decreases approximately to $q \leq 0.3$, the asymmetric LD/LD phase disappears as well. In such conditions, there is only one symmetry-breaking transition from the LD/LD to the HD/LD in this model.

The histograms $P(\rho_+, \rho_-)$ of particle densities is investigated, where ρ_+ and ρ_- are instantaneous densities of (+) and (-) particles, respectively. Figure 7.3 shows four typical particle density histograms in the HD/LD, asymmetric LD/LD, LD/LD and MC phases, respectively. One can see that in the HD/LD phase, a double peak with two off-diagonal maxima appears, while in the symmetric LD/LD and MC phases, a single peak exists on the diagonal.

The flipping process is shown in Figure 7.4. The density difference $\rho_+ - \rho_-$ has been measured as functions of time. The flipping processes of the HD/LD and asymmetric LD/LD phases are observed clearly in Figures 7.4(a) and (b). The system flips between positive net values and negative net values. The positive (negative) net values imply that the bulk density of positive (negative) particles are larger than that of negative (positive) particles. This means the existence of the SSB in the system.

Computer simulations with different system length (up to L = 10,000) are performed in order to study the finite-size effect in the present model (see Figure 7.5). It is shown that the phase boundary between the asymmetric LD/LD and symmetric LD phases little depend on the system size, while the region of the asymmetric
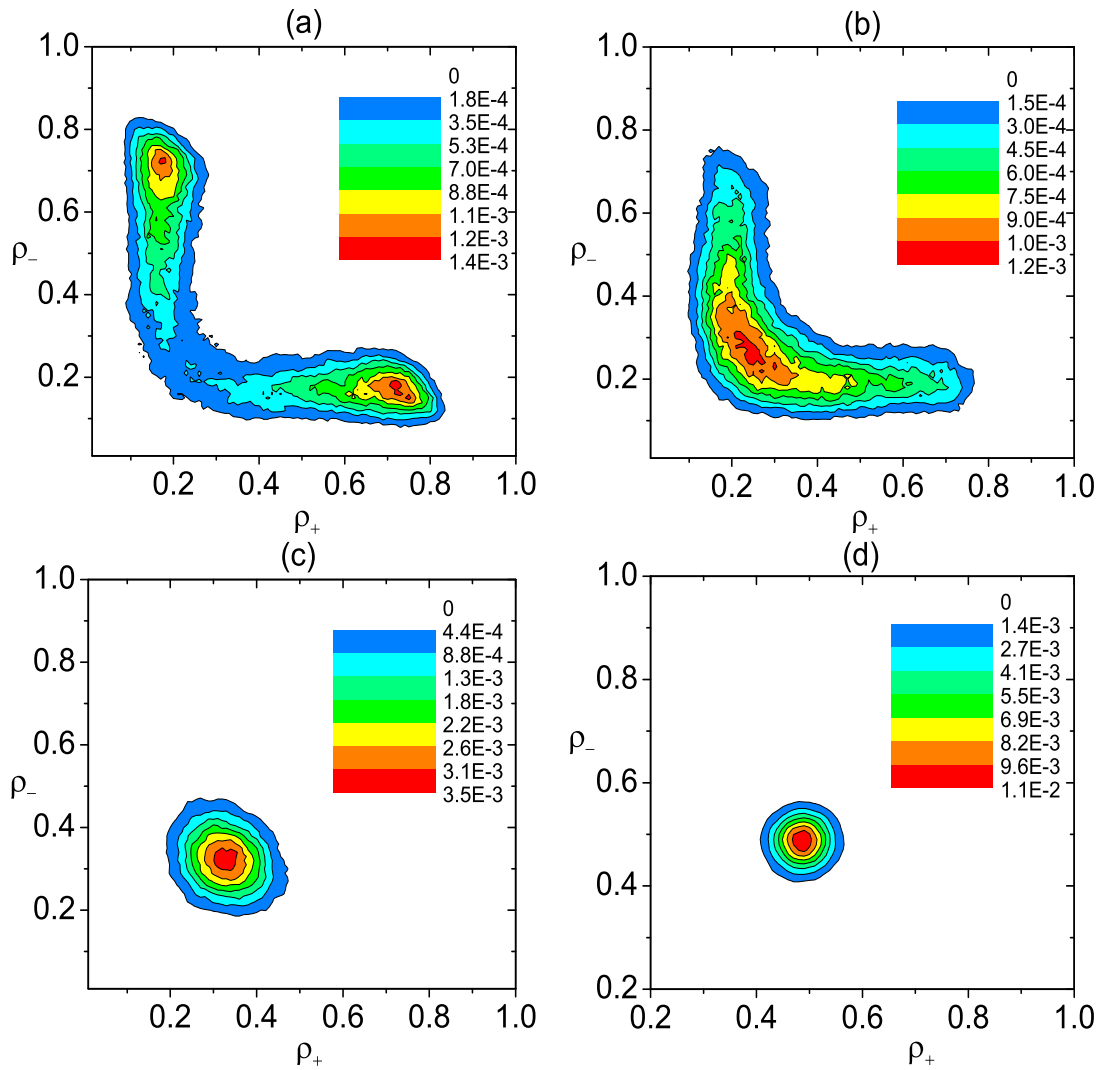
Figure 7.3: The simulation results of densities with (a) HD/LD phase: $\alpha = 0.8$, $\beta = 0.16$ and $q = 0.8$; (b)Asymmetric LD/LD phase: $\alpha = 0.8$, $\beta = 0.26$ and $q = 0.8$; (c) LD phase: $\alpha = 0.8$, $\beta = 0.4$ and $q = 0.8$; (d) MC phase: $\alpha = 1$, $\beta = 1$ and $q = 1$.

LD/LD phase seems to shrink and then keep unchanged with the increase of the system size. This suggests that the asymmetric LD/LD phase probably exists in the thermodynamic limit (L).
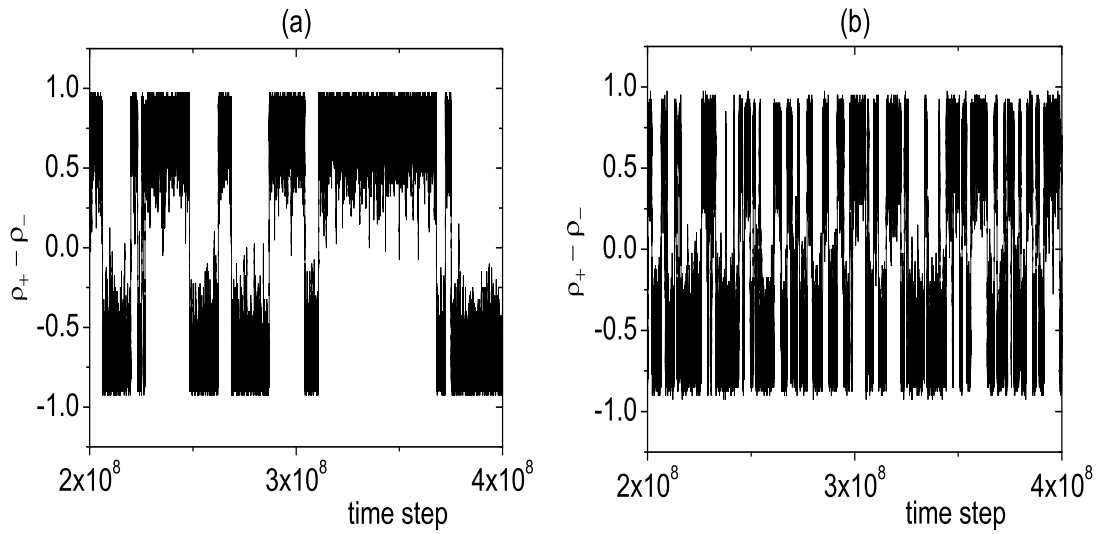
Figure 7.4: Illustration of flipping processes of spontaneous densities in two breaking phases with $q = 0.5$ and $N = 40$. (a) HD/LD phase: $\alpha = 0.4$ and $\beta = 0.1$; (b) Asymmetric LD/LD phase: $\alpha = 0.4$ and $\beta = 0.16$.
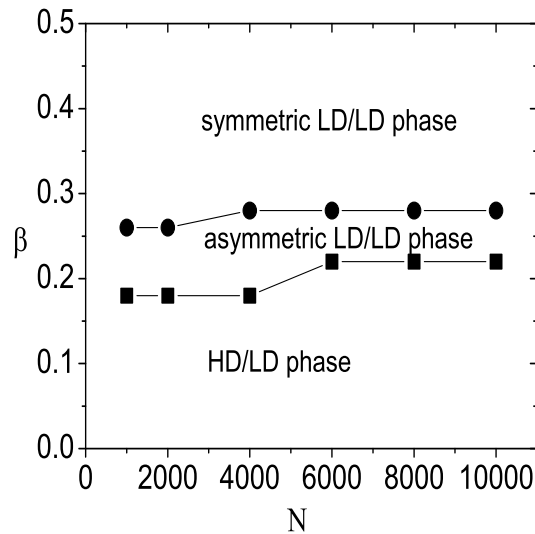
Figure 7.5: The size effect with $q = 1$, $\alpha = 0.6$ and different system sizes.

Stationary currents in the present model are investigated. Due to the flipping phenomenon in the model, the average current of (+) and (-) particles is used as the

system current, i.e., $J_{ave} = (J_+ + J_-)/2$, where J_+ and J_- are currents of (+) and (-) particles, respectively. For simplicity, I assume that $q = 0.5, 1$, $\beta = 0.3, 0.6, 0.9$ while α changes from 0 to 1. Figure 7.6(a) shows the stationary current obtained from computer simulations for $q = 1$. With the increase of β, the average current increases as well. However, when $q \neq 1$ (e.g., $q = 0.5$), an unexpected phenomenon appears. The average current first increases upon increasing β, and then reaches the maximal current (see Figure 7.6(b)). In other words, J_{ave} is maintained and its value is dictated by q rather than α or β even the system is in the symmetric LD phase. It is also observed that the maximal current region shrinks with the increase of q.
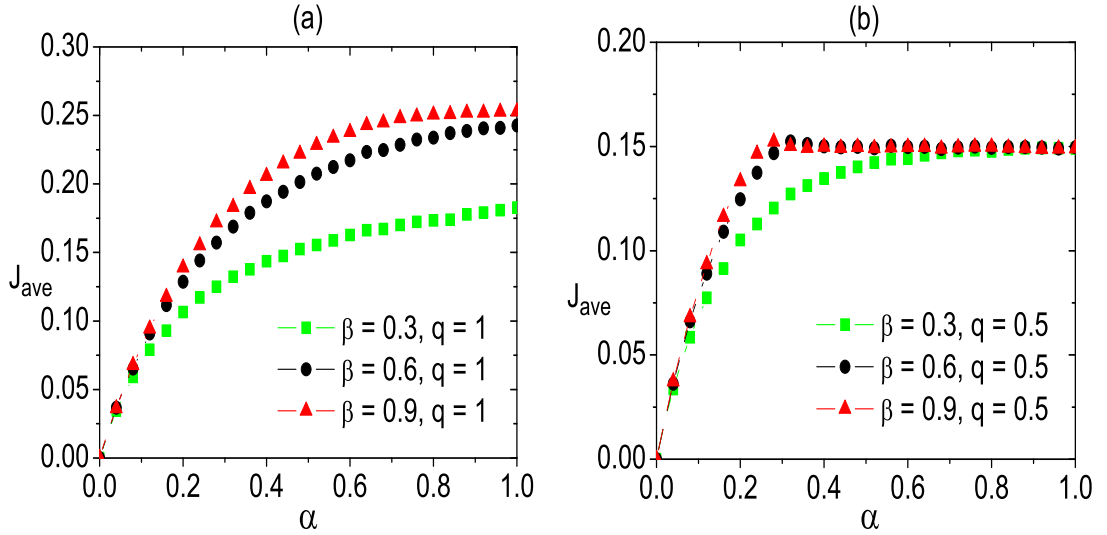
Figure 7.6: The stationary current with different β. J_{ave} is the average current of (+) and (-) particles, i.e., $J_{ave} = (J_+ + J_-)/2$. (a) $q = 1$ and (b) $q = 0.5$.

The average currents between the proposed model and the Bridge model are compared under the same α, β and q. It is assumed that $\alpha = 0.4, 1$, $q = 0.3, 0.6, 0.9$ while β changes from 0 to 1 so that one can observe the current in all possible phases. It is shown that the present model can lead to a higher current than that in

the Bridge model (see Figure 7.7(a)). The reason for this is due to the site-sharing mechanism in the present model rather than the site-exchanging mechanism in the Bridge model.
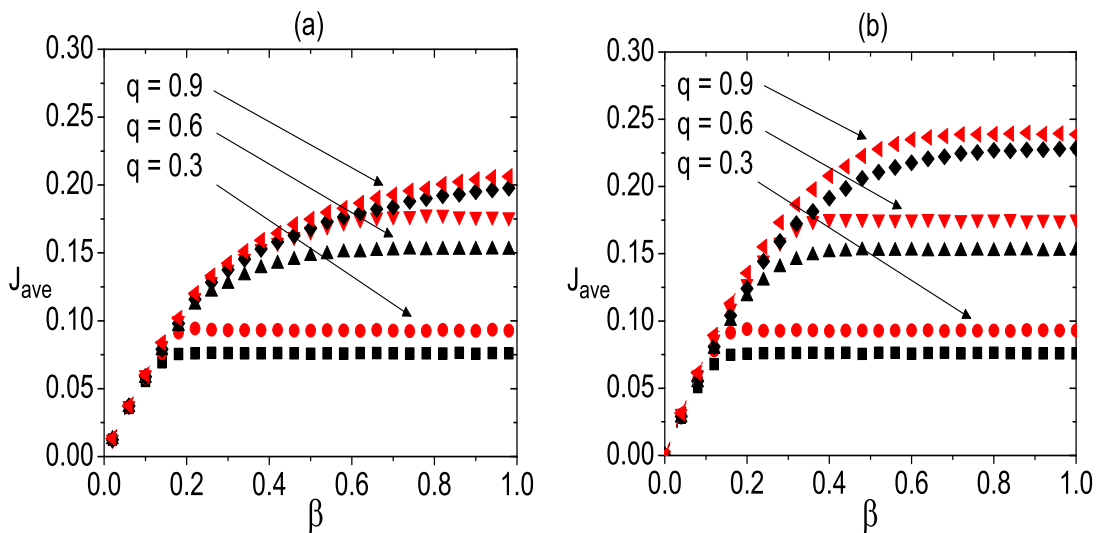
Figure 7.7: The stationary current with different q in the present model and the Bridge model. The red symbols correspond to the present model, while the black symbols are for the Bridge model. (a) $\alpha = 0.4$ and (b) $\alpha = 1$.

7.4 Summary and conclusions

The totally asymmetric simple exclusion process (TASEP) with two species of particles in a one-lane system is studied. The model is reminiscent of pedestrian traffic crossing a narrow pathway in both directions. Two species of particles move oppositely and can enter the system only if the corresponding sites are empty. Hard-core exclusion is applied to the same species of particles while different species of particles are allowed to share the same site at a certain probability q. This kind of sharing effect has not been investigated in previous TASEP models, to the best of our knowledge. There are four possible phases in the system, i.e., MC, symmet-

ric LD/LD, asymmetric LD/LD and HD/LD. The spontaneous symmetry breaking (SSB) is observed in the two phases: HD/LD and asymmetric LD/LD. With the decrease of q, the asymmetric phase reduces to the boundary between the symmetric LD/LD and the HD/LD phases. The MC phase will disappear when $q < 0.97$. The histograms of two species of particles and the flipping process are plotted. The proposed model exhibits higher current, compared to the Bridge model, which is due to the site-sharing mechanism in the present model. More interestingly, it is shown that the average current in the symmetric LD/LD phase is determined by q rather than α or β when $q \neq 1$.

This work shows that the sharing effect on the TASEP is an interesting topic and needs to be further investigated. The present model has been investigated using extensive Monte Carlo simulations. However, it has not been conducted by theoretical analysis. This work is now in progress and will be reported later.

This Chapter is based on the paper "Spontaneous Symmetry Breaking in Aasymmetric Exclusion Process with Site Sharing: a Monte Carlo Study". The paper has been submitted for review.

Chapter 8

Conclusions and Outlook

This research is motivated by recent developments in theoretical investigations of non-equilibrium systems and traffic observations in Biology and Physics. The modelling method is based on a paradigmatic model - totally asymmetric simple exclusion process (TASEP). The self-driven many-body systems are characterised by non-zero currents in conjunction with some emergent properties, e.g., phase separation, phase coexistence, or spontaneous symmetry breaking. These collective behaviors cannot be derived from microscopic interactions among individuals. Thus, these systems are regarded as complex systems. Such systems in nature may be involved in, for example, vehicular traffic, protein motor traffic, Internet traffic.

Originally introduced in the description of ribosome motion along mRNA in 1968 [7], TASEP and its extensions have exhibited properties believed to be characteristics of many real-world non-equilibrium processes such as molecular motor traffic [47, 53], protein synthesis [12, 43, 84], fungal hyphal growth [123].

On the other hand, the TASEP has also been extensively studied in its own right in the context of different particle properties (e.g., large particles, two species of particles) and different lattice geometries (e.g., multiple channels, intersections) as well as different updating procedures (e.g., random update, parallel update), see

Chapter 2 for more details.

The focus of this thesis is on investigating inhomogeneity-induced emergent behavior within the framework of TASEP. Local inhomogeneity (or bottleneck) can lead to some kinds of crowding phenomena, which are often seen as a main source of environmental pollution for vehicular traffic and of some molecular motor-related diseases, e.g., Alzheimer's disease [18], for biological transport. It is known that local inhomogeneity induces traffic jams in vehicular traffic. However, these congested phenomena have not been well understood theoretically.

In the following paragraphs, the main results are briefly summarized. Many fundamental issues remain and many new questions have been raised. The last section of this Chapter is focused on these points, providing an outlook for future research.

8.1 Research summary

8.1.1 Local inhomogeneity in a single-channel system

The starting of the research is from the simplest scenario of local inhomogeneity: a single inhomogeneity is located in a one-dimensional system, far away from boundaries. For simplicity, it is assumed that the local inhomogeneity is in the middle site of the lattice. The system can be divided into two subsystems connected by the single inhomogeneity. The phase diagrams, stationary currents and density profiles are obtained using a rule of current conservation through two subsystems and the single inhomogeneity and known results of the normal TASEP in parallel update.

There are four possible stationary phases ((LD, LD), (LD, HD), (HD, LD), and (HD, HD)) in the system. In the (HD, LD) phase, the system reaches a maximal current which is determined by the strength of the inhomogeneity, but independent of boundary conditions. In the (LD, HD) phase, density profiles cannot be obtained

using a simple mean-field approximation. However, a phenomenological domain wall approach is developed to predict density profiles in the (LD, HD) phase. Density and current profiles obtained from theoretical calculations are in good agreement with Monte Carlo simulations.

Note that this study is related to understanding the general properties of traffic flow. Local inhomogeneities in a system can be viewed as blocks (e.g., road reductions or road works) on roads. Although these blocks just cover very short road segments, they can cause congested traffic. When the system changes from the (LD, LD) phase to the (HD, LD) phase, a phase separation between high and low densities occurs at the local inhomogeneity. Experimental data collected on a German highway near Cologne (see Fig. 2 in Ref. [94]) exhibit such a separation in the presence of an on-ramp where the transition from free flow to congested flow is characterized by a sudden fall of the local velocity. This allows us to separate the data set into free-flow and congested regimes.

The model is then extended to the case of a zoned inhomogeneity in parallel update. The zoned inhomogeneity in vehicular traffic can be seen as a speed limit zone. In the language of physics, the zoned inhomogeneity is characterised by a reduced hopping probability which is applied to all sites within this zone. Two cases (i.e., Cases V and W) of lattice geometries are studied. In Case V, the lattice is divided into two segments; the first segment is a normal TASEP, while the second segment has a reduced hopping rate. Case W is an extension of Case V, and it has three segments (segments I, II and III). Segments I and III have the same hopping probability, while the middle segment (segment II) has a reduced hopping probability. The phase diagrams, stationary current, and density profiles are obtained. Case W shows a more complex system behaviour than Case V. The maximal-current regions in systems with different numbers of successive inhomogeneous sites are compared. The region of the maximal-current phase in Case W is larger than that in Case V

under the same parameters. This indicates that the introduction of segment III in Case W can enhance the current in some conditions.

8.1.2 TASEP with m-input n-output junction

The forementioned theoretical studies of TASEP with inhomogeneity involve particles moving along the one-channel lattices. Although the one-channel systems describe many situations in vehicular traffic and biophysical processes, a more realistic description of traffic conditions require an extension of the normal TASEP to a more complex lattice geometry.

Junctions can be seen as connections of several one-channel systems, which are one of the commonly used traffic facilities in nature. Such systems with junctions may be used to describe a wide range of possible applications such as: (i) kinesins moving on a microtubule in which the number of protofilaments may be various [109]; (ii) transport of vesicles in a branching axon or dendrite [110]; (iii) vehicular traffic on intersections or roundabouts [111], and (iv) data traffic through hubs (e.g., switches, routers) on local/wide networks [112]. As a junction can also be viewed as a "local inhomogeneity" in a transport system, it is necessary to study the effects of such "local inhomogeneity" on traffic dynamics.

Inspired by this wide range of possible applications, TASEP with a multiple-input single-output junction is first investigated, then it is extended to TASEP with a m-input n-output junction. In reality, it can be observed that several traffic lanes merge into one lane and multiple protofilaments come together to form one protofilament [109]. However, they have not been understood well from the viewpoint of theoretical analysis.

This investigation produces three interesting but nontrivial results: (1) A general theoretical solution for traffic dynamics of TASEP with junction is developed, for any m and n (m and n are integer numbers); (2) m-input n-output junctions

can be classified by a parameter, $\lambda = m/n$. The junctions with the same λ exhibit the same dynamic properties (e.g., phase diagrams, stationary currents, and density profiles); (3) When the number of m and/or n changes, the low-density and high-density regions can be measured qualitatively and quantitatively.

8.1.3 Two-species TASEP with site sharing and relaxed boundaries

The previous TASEP models obey the same interaction rule, i.e., hard-core exclusion. In other words, each lattice site is not allowed to be shared by more than one particle at the same time. This study presents a one-dimensional TASEP model in which two species of particles move oppositely. In this model, different species of particles are allowed to share a lattice site at probability q ($0 \leq q \leq 1$) when they meet each other. The same species of particles obey hard core exclusion. An obvious difference between the proposed model and previous TASEP models is that different species of particles can occupy the same site in the proposed model, which is prohibited in previous TASEP models. This relaxed exclusion principle is applied to the bulk as well as the boundaries. Such kind of sharing mechanism has not been explored so far, to the best of our knowledge.

This study is motivated by single- or multiple-channel traffic. When pedestrians walk along a single-channel pathway in opposite directions and meet together, they may share a site, and then pass each other. Particles sharing sites in the TASEP models would represent particles that are side by side on different channels. Multiple channels can be motivated in motor traffic because microtubules have several (usually 13) protofilaments which serve as parallel channels [122].

The site-sharing model is studied using both a simple mean-field approach and extensive Monte Carlo simulations. Theoretical calculations and computer simulations show that there are three stationary phases (LD, HD, and MC) in the system. However, the phase boundaries are shifted according to different sharing probability

q. The theoretical analysis can agree well with Monte Carlo simulations.

8.1.4 SSB in TASEP with site sharing and constrained boundaries

This model is also based on the site-sharing mechanism, but with constrained boundaries. The constrained boundaries mean that particles cannot enter the system if the corresponding sites at boundaries are not empty. There are four possible phases in the system, i.e., MC, symmetric LD/LD, asymmetric LD/LD and HD/LD. The spontaneous symmetry breaking (SSB) is observed in the two phases: HD/LD and asymmetric LD/LD. With the decrease of q (q is sharing probability), the asymmetric phase reduces to the boundary between the symmetric LD/LD and the HD/LD phases. The MC phase will appear when q is sufficiently enough. The histograms of two species of particles and the flipping process are plotted. The model exhibits higher current, compared to the Bridge model, which is due to the site-sharing mechanism in the model. More interestingly, it is shown that the average current in the symmetric LD/LD phase is determined by q rather than α or β when $q \neq 1$.

This work shows that the sharing effect on the TASEP is an interesting topic and needs to be further investigated. The present model has been investigated using extensive Monte Carlo simulations. It would be interesting to analyse this site-sharing model or its variants. In fact, this work is now in progress and will be reported later.

8.2 Future Work

The various aspects of TASEP with inhomogeneity investigated in this thesis only cover a rather small part of problems related to non-equilibrium processes. Theoretical methods (e.g., mean-field approximation, domain-wall theory) introduced in the literature review and in this work could be used as a basis for further developments along the following two lines.

The biological experiments and traffic observations could inspire new classes of models. For instance, in neurons, microtubules are abundantly decorated with microtubule-associated proteins such as Tau. It is found that Tau acts like a speed bump to regulate protein traffic [124]. When kinesins and dyneins encounter a Tau on their travels along microtubules, they show different behavior: kinesins detach their cargo while dyneins maneuver around the Tau. It is clear that the existence of Tau influences the motion of the motors as well as their processivity (i.e., the capability of long walk for motors without getting detached from microtubules). However, such a transport mechanism and its effect on the system have not been understood theoretically.

Mixed vehicular traffic (e.g., small cars and large trucks) has been observed everyday. Detailed theoretical analysis of the mixed traffic has not been conducted so far. Cars and trucks can be mapped into normal-size with normal-range hopping particles and large-size with reduced-hopping particles, respectively. In the context of TASEP, the effect of mixed particles in random and parallel updates are still to be clarified. The model could be extended to a two-channel system considering asymmetric/symmetric coupling rules.

On the other hand, from a perspective of mathematical modelling, there are much more investigations could be made. An example is the attachment-detachment kinetics (LK). [47] assumes that LK can take place on any site in a one-dimensional lattice. If only a site associated with the LK is near or far from boundaries, what kind of dynamic properties can the system exhibit? The similar investigations could be extended to TASEP with inhomogeneity in parallel update, in particular, when a single inhomogeneity is located near the left or right boundary (or inhomogeneities are distributed randomly).

Since the spatial correlations in mean-field treatments are neglected, theoretical calculations normally have some deviations from computer simulations, which has

been indicated in this thesis. More recently, using correlation functions to examine the spatially correlated variability has attracted much attention. Remarkable properties of spatial correlations in TASEP with local inhomogeneities have been reported in [89]. It is suggested to pursue this line in future work and expect a rich variety of new phenomena.

In conclusion, how to model and analyze inhomogeneity-related non-equilibrium systems has been highlighted though they are still simplified and far from reality due to the lack of empirical data. Nevertheless it has inspired various TASEP models which revealed many interesting phenomena and gained the attention from interdisciplinary researchers. Hopefully, future studies along these lines will provide deeper insight into fundamental issues as well as real traffic.

Bibliography

[1] D. Chowdhury, A. Schadschneider and K. Nishinari, Physics of Transport and Traffic Phenomena in Biology: from molecular motors and cells to organisms. Phys. of Life Rev. **2**, 318 (2005).

[2] R. Mahnke, J. Kaupužs and I. Lubashevsky, Probabilistic description of traffic flow. Phys. Rep. **408**, 1 (2005).

[3] N. Boccara, Modeling Complex Systems, Springer-verlag (2004).

[4] M.R. Evans, Phase transitions in one-dimensional nonequilibrium systems. Braz. J. Phys. **30**, 42 (2000).

[5] F. Schm$\ddot{u}$ser and W. Just, Non-Equilibrium Behaviour in Unidirectionally Coupled Map Lattices. J. Stat. Phys. **105**, 525 (2001).

[6] F. Mallamace, H.E. Stanley and S. Italiana di Fisica, The physics of complex systems: new advances and perspectives. IOS Press, (2004).

[7] C.T. MacDonald, J.H. Gibbs and A.C. Pipkin, Kinetics of biopolymerization on nucleic acid templates. Biopolymers **6**, 1 (1968).

[8] B. Derrida, E. Domany and D. Mukamel, An exact solution of one dimensional asymmetric exclusion model with open boundaries. J. Stat. Phys. **69**, 667 (1992).

[9] G.M. Schütz, in *Phase Transitions and Critical Phenomena*, Vol. 19, edited by C. Domb and J.L. Lebowitz (Academic Press, San Diego, 2001).

[10] B. Widom, J.L. Viovy and A.D. Defontaines, Repton model of gel electrophoresis and diffusion. J. Phys. I **1**, 1759 (1991).

[11] G.M. Schütz, The Heisenberg chain as a dynamical model for protein synthesis - Some theoretical and experimental results. Int. J. Mod. Phys. B **11**, 197 (1997).

[12] L.B. Shaw, R.K.P. Zia and K.H. Lee, Totally asymmetric exclusion process with extended objects: A model for protein synthesis. Phys. Rev. E **68**, 021910 (2003).

[13] T. Chou, Ribosome recycling, diffusion and mRNA loop formation in translational regulation. Biophys. J. **85**, 755 (2003).

[14] S. Klumpp and R. Lipowsky, Traffic of molecular motors through tube-like compartments. J. Stat. Phys. **113**, 233 (2003).

[15] G.A. Klein, K. Kruse, G. Cuniberti and F. Jülicher, Filament Depolymerization by Motor Molecules. Phys. Rev. Lett. **94**, 108102 (2005).

[16] D. Chowdhury, L. Santen and A. Schadschneider, Statistical physics of vehicular traffic and some related systems. Phys. Rep. **329**, 199 (2000).

[17] D. Helbing, Traffic and related self-driven many-particle systems. Rev. Mod. Phys. **73**, 1067 (2001).

[18] L.S.B. Goldstein, Kinesin molecular motors: transport pathways, receptors and human disease. Proc. Natl. Acad. Sci. USA **98**, 6999 (2001).

[19] M. Aridor and L.A. Hannan, Traffic Jam: A Compendium of Human Diseases that Affect Intracellular Transport Processes. Traffic **1**, 836 (2000).

[20] M. Aridor and L.A. Hannan, Traffic jams II: an update of diseases of intracellular transport. Traffic **3**, 781 (2002).

[21] B. Albert, A. Johnson, J. Lewis, M. Raff, K. Roberts and P. Walter *The Molecular Biology of the Cell*, Fourth Edition (Garland, New York, 2002).

[22] Y. Okada and N. Hirokawa, A Processive Single-Headed Motor: Kinesin Superfamily Protein KIF1A. Science **283**, 1152 (1999).

[23] J. Howard, *Mechanism of Motor Proteins and the Cytoskeleton* (Sunderland, Massachusetts: Sinauer Associates), (2001).

[24] S.P. Gross, Hither and yon: a review of bi-directional microtubule-based transport. Phys. Biol. **1**, R1 (2004).

[25] A. Ashkin, K. Schütze, J.M. Dziedzic, U. Euteneuer and M. Schliwa, Force generation of organelle transport measured in vivo by an infrared laser trap. Nature **348**, 346 (1990).

[26] M.G.L. van den Heuvel and C. Dekker, Motor Proteins at Work for Nanotechnology. Science **317**, 333 (2007).

[27] M. Liu, R. Wang and R. Jiang, M.-B. Hu and Y. Gao, Defect-induced transitions in synchroneous asymmetric exclusion processes. Phys. Lett. A, **373**, 195 (2009).

[28] R. Wang, M. Liu and R. Jiang, Theoretical investigation of synchronous totally asymmetric exclusion processes on lattices with multiple-inputCsingle-output junctions. Phys. Rev. E **77**, 051108 (2008).

[29] M. Liu and R. Wang, Asymmetric exclusion processes on m-input n-output junctions with parallel update. Physica A **388**, 4068 (2009).

[30] N. Rajewsky, L. Santen, A. Schadschneider and M. Schreckenberg, The asymmetric exclusion process: Comparison of update procedures. J. Stat. Phys. **92** 151 (1998).

[31] R. Lipowsky, Y. Chai, S. Klumpp, S. Liepelt and M.J.I. Mller, Molecular motor traffic: From biological nanomachines to macroscopic transport. Physica A **372**, 34 (2006).

[32] L.G. Tilstra and M.H. Ernst, Synchronous asymmetric exclusion processes. J. Phys. A **31**, 5033 (1998).

[33] J. de Gier and B. Nienhuis, Exact stationary state for an asymmetric exclusion process with fully parallel dynamics. Phys. Rev. E **59**, 4899 (1999).

[34] M.E. Fouladvand and H.W. Lee, Exactly solvable two-way traffic model with ordered sequential update. Phys. Rev. E **60**, 6465 (1999).

[35] M.E. Fouladvand and F. Jafarpour, Multi-Species Asymmetric Exclusion Process in Ordered Sequential Update. Turk. J. Phy. **24**, 329 (2000).

[36] F.H. Jafarpour, F.E. Ghafari and S.R. Masharian, Exact shock profile for the ASEP with sublattice-parallel update. J. Phys. A. **38**, 4579 (2005).

[37] A. Schadschneider, Cellular automata models of highway traffic. Physica A **372**, 142 (2006).

[38] S.M. Block, L.S.B. Goldstein and B.J. Schnapp, Bead movement by single kinesin molecules studied with optical tweezers. Nature **348**, 348 (1990).

[39] G. Lakatos and T. Chou, Totally asymmetric exclusion processes with particles of arbitrary size. J. Phys. A **36**, 2027 (2003).

[40] S. Klumpp and R. Lipowsky, Cooperative cargo transport by several molecular motors. Proc. Natl. Acad. Sci. USA **102**, 17284 (2005).

[41] P. Pierobon, E. Frey and T. Franosch, Driven lattice gas of dimers coupled to a bulk reservoir. Phys. Rev. E **74**, 031920 (2006).

[42] L.B. Shaw, A.B. Kolomeisky and K.H. Lee, Local Inhomogeneity in Asymmetric Simple Exclusion Processes with Extended Objects. J. Phys. A **37**, 2105 (2004).

[43] J.J. Dong, B. Schmittmann and R.K.P. Zia, Inhomogeneous exclusion processes with extended objects: The effect of defect locations. Phys. Rev. E **76**, 051113 (2007).

[44] D.W. Huang, Synchronous asymmetric exclusion processes with extended hopping. Phys. Rev. E **63**, 012104 (2000).

[45] A. Kunwar, A. Schadschneider and D. Chowdhury, From aggressive driving to molecular motor traffic. J. Phys. A **39**, 14263 (2006).

[46] J. Szavits-Nossan and K. Uzelac, Totally asymmetric exclusion process with long-range hopping. Phys. Rev. E **74**, 051104 (2006).

[47] A. Parmeggiani, T. Franosch and E. Frey, Phase Coexistence in Driven One-Dimensional Transport. Phys. Rev. Lett. **90**, 086601 (2003).

[48] A. Parmeggiani, T. Franosch and E. Frey, Totally asymmetric simple exclusion process with Langmuir kinetics. Phys. Rev. E **70**, 046101 (2004).

[49] V. Popkov, A. Rákos, R.D. Willmann, A.B. Kolomeisky and G.M. Schütz, Localization of shocks in driven diffusive systems without particle number conservation. Phys. Rev. E **67**, 066117 (2003).

[50] S. Katz, J.L. Lebowitz and H. Spohn, Nonequilibrium steady states of stochastic lattice gas models of fast ionic conductors . J. Stat. Phys. **34**, 497 (1984).

[51] B. Schmittmann and R.K.P. Zia, in *Phase Transitions and Critical Phenomena*, edited by C. Domb and J. Lebowitz (Academic Press, London, 1995).

[52] R.D. Astumian, Thermodynamics and Kinetics of a Brownian Motor. Science **276**, 917 (1997).

[53] K. Nishinari, Y. Okada, A. Schadschneider and D. Chowdhury, Intracellular Transport of Single-Headed Molecular Motors KIF1A. Phys. Rev. Lett. **95**, 118101 (2005).

[54] P. Pierobon, M. Mobilia, R. Kouyos and E. Frey, Bottleneck-induced transitions in a minimal model for intracellular transport. Phys. Rev. E **74**, 031906 (2006).

[55] P. Greulich and A. SchadschneiderDisordered, Driven lattice gases with boundary reservoirs and Langmuir kinetics. Phys. Rev. E **79**, 031107 (2009).

[56] M.R. Evans, D.P. Foster, C. Godreche and D. Mukamel, Spontaneous Symmetry Breaking in a One Dimensional Driven Diffusive System. Phys. Rev. Lett. **74**, 208 (1995).

[57] M.R. Evans, D.P. Foster, C. Godreche and D. Mukamel, Asymmetric exclusion model with two species: spontaneous symmetry breaking. J. Stat. Phys. **80**, 69 (1995).

[58] P.F. Arndt, T. Heinzel and V. Rittenberg, First-order phase transitions in one-dimensional steady states. J. Stat. Phys. **90**, 783, (1998).

[59] V. Popkov and I. Peschel, Symmetry breaking and phase coexistence in a driven diffusive two-channel system. Phys. Rev. E **64**, 026126 (2001).

[60] E. Levine and R. D. Willmann, Sponteneous symmetry breaking and phase coexistence in a non-conserving one-dimensional model. J. Phys. A **37**, 3333 (2004).

[61] D.W. Erickson, G. Pruessner, B. Schmittmann and R.K.P. Zia, Spurious phase in a model for traffic on a bridge. J. Phys. A **38**, L659 (2005).

[62] R.D. Willmann, G.M. Schtz and S. Grosskinsky, Dynamical origin of spontaneous symmetry breaking in a field-driven nonequilibrium system. Europhys. Lett. **71**, 542 (2005).

[63] E. Pronina and A.B. Kolomeisky, Spontaneous symmetry breaking in two-channel asymmetric exclusion processes with narrow entrances. J. Phys. A **40**, 2275 (2007).

[64] R. Jiang, R. Wang, M.B. Hu, B. Jia and Q.S. Wu, Spontaneous symmetry breaking in a two-lane system with parallel update. J. Phys. A **40**, 9213 (2007).

[65] R. Jiang, M.-B. Hu, B. Jia, R. Wang and Q.-S. Wu, Spontaneous symmetry breaking and periodic structure in a multilane system. Phys. Rev. E **76**, 036116 (2007).

[66] Spontaneous symmetry breaking in Wikipedia http://en.wikipedia.org/wiki/Spontaneous_symmetry_breaking, Retrieved on 20 May 2007.

[67] M. Nocodemi and A. Prisco, Symmetry-Breaking Model for X-Chromosome Inactivation. Phys. Rev. Lett. **98**, 108104 (2007).

[68] E. Pronina and A.B. Kolomeisky, Two-Channel Totally Asymmetric Exclusion Processes. J. Phys. A **37**, 9907 (2004).

[69] E. Pronina and A.B. Kolomeisky, Asymmetric Coupling in Two-Channel Simple Exclusion Processes. Physica A **372**, 12 (2006).

[70] K. Tsekouras and A.B. Kolomeisky, Inhomogeneous coupling in two-channel asymmetric simple exclusion processes. J. Phys. A **41**, 095002 (2008).

[71] A.B. Kolomeisky, Asymmetric Simple Exclusion Model with Local Inhomogeneity. J. Phys. A **31**, 1153 (1998).

[72] K. Tsekouras and A.B. Kolomeisky, Parallel coupling of symmetric and asymmetric exclusion processes. J. Phys. A **41**, 465001 (2008).

[73] T. Mitsudo and H. Hayakawa, Synchronization of kinks in the two-lane totally asymmetric simple exclusion process with open boundary conditions. J. Phys. A **38**, 3087 (2005).

[74] R. Jiang, R. Wang and Q.S. Wu, Two-lane Totally Asymmetric Exclusion Processes with Particle Creation and Annihilation. Physica A **375**, 247 (2007).

[75] R. Wang, R. Jiang, M. Liu, J. Liu and Q.-S. Wu, Effects of Langmuir Kinetics on a Two-lane TASEP of Molecular Motor Traffic. Int. J. Mod. Phys. C **18**(9), 1483 (2007).

[76] B. Trpisová and J. A. Tuszynski, Possible link between 5'-triphosphate hydrolysis and solitary waves in microtubules. Phys. Rev. E **55**, 3288 (1997).

[77] R. Wang, M. Liu and R. Jiang, Local inhomogeneity in two-lane asymmetric simple exclusion processes coupled with Langmuir kinetics, Physica A **387**, 457 (2008).

[78] R. Jiang, M.-B. Hu, Y.-H. Wu and Q.-S. Wu, Weak and strong coupling in a two-lane asymmetric exclusion process. Phys. Rev. E **77**, 041128 (2008).

[79] E. Pronina and A.B. Kolomeisky, Theoretical investigation of totally asymmetric exclusion processes on lattices with junctions. J. Stat. Mech. P07010 (2005).

[80] A.B. Kolomeisky, G.M. Schütz, E.B. Kolomeisky and J.P. Straley, Phase diagram of one-dimensional driven lattice gases with open boundaries. J. Phys. A **31**, 6911 (1998).

[81] Z.-P. Cai, Y.-M. Yuan, R. Jiang, K. Nishinari and Q.-S. Wu, The effect of attachment and detachment on totally asymmetric exclusion processes with junctions, J. Stat. Mech. P02050 (2009).

[82] V. Popkov, M.R. Evans and D. Mukamel, Spontaneous symmetry breaking in a bridge model fed by junctions, J. Phys. A **41**, 432002 (2008).

[83] L.B. Shaw, A.B. Kolomeisky and K.H. Lee, Local Inhomogeneity in Asymmetric Simple Exclusion Processes with Extended Objects. J. Phys. A **37**, 2105 (2004).

[84] T. Chou and G. Lakatos, Clustered Bottlenecks in mRNA translation and protein synthesis. Phys. Rev. Lett. **93**, 198101 (2004).

[85] S. Klumpp and R. Lipowsky, Asymmetric simple exclusion processes with diffusive bottlenecks. Phys. Rev. E **70**, 066104 (2004).

[86] G. Lakatos, T. Chou and A.B. Kolomeisky, Phys. Rev. E **71**, 011103 (2005).

[87] K. Qiu, X.-Q. Yang, W. Zhang, D. Sun and Y. Zhao, Density profiles in the totally asymmetric exclusion processes with both local inhomogeneity and Langmuir kinetics. Physica A **373**, 1 (2007)

[88] M.E. Foulaadvand, S. Chaaboki and M. Saalehi, Characteristics of the asymmetric simple exclusion process in the presence of quenched spatial disorder. Phys. Rev. E **75**, 011127 (2007).

[89] M.E. Foulaadvand, A.B. Kolomeisky and H. Teymouri, Investigation of Asymmetric Exclusion Processes with Disorder: Effeect of Correlations. Phys. Rev. E **78**, 061116 (2008).

[90] P. Greulich and A. Schadschneider, Phase diagram and edge effects in the ASEP with bottlenecks. Physica A **387**, 1972 (2008).

[91] S. Huang and D.E. Ingber, The structural and mechanical complexity of cell-growth control. Nature Cell Biol. **1**, E131 (1999).

[92] K. Kullander, Genetics moving to neuronal networks. Trends Neurosci. **28**, 239 (2005).

[93] B. Estrella, R. Estrella, J. Oviedo, X. Narvez, M.T. Reyes, M. Gutirrez and E.N. Naumova, Acute Respiratory Diseases and Carboxyhemoglobin Status in School Children of Quito, Ecuador. Environ. Health Perspect. **113**, 607 (2005).

[94] L. Neubert, L. Santen, A. Schadschneider and M. Schreckenberg, Single-vehicle data of highway traffic: A statistical analysis. Phys. Rev. E **60**, 6480 (1999).

[95] T. Kretz, A. Grünebohm and M. Schreckenberg, Experimental study of pedestrian flow through a bottleneck. J. Stat. Mech. P10014 (2006).

[96] D. Helbing, A. Hennecke and M. Treiber, Phase Diagram of Traffic States in the Presence of Inhomogeneities. Phys. Rev. Lett. **82**, 4360 (1999).

[97] F.H. Jafarpour, Numerical Study of Phase Transition in An Exclusion Model with Parallel Dynamics. Phys. Lett. A, **326**, 14 (2004).

[98] A. Povolotsky and J. Mendes, Bethe Ansatz Solution of Discrete Time Stochastic Processes with Fully Parallel Update. J. Stat. Phys. **123**, 125 (2006).

[99] A.M. Povolotsky and V.B. Priezzhev, Determinant solution for the totally asymmetric exclusion process with parallel update. J. Stat. Mech. p07002 (2006).

[100] D.W. Huang, Analytical results of asymmetric exclusion processes with ramps. Phys. Rev. E **72**, 016102 (2005).

[101] I.M. Sobol', The Monte Carlo Method, The University of Chicago Press, Chicago (1974).

[102] N. Metropolis and S. Ulam, The Monte Carlo method. J. Amer. Stat. Assoc. **44**, 335 (1949).

[103] B. Lapeyre, É. Pardoux and R. Sentis, Introduction to Monte Carlo Methods for Transport and Diffusion Equations, Oxford University Press, (2003).

[104] B.S. Kerner, *The Physics of Traffic: Empirical Freeway Pattern Features, Engineering Applications and Theory (Understanding Complex Systems)*, Springer (2006).

[105] G.M. Schütz, Critical phenomena and universal dynamics in one-dimensional driven diffusive systems with two species of particles. J. Phys. A **36**, R339 (2003).

[106] A.B. Kolomeisky and M.E. Fisher, *Molecular Motors: A Theorists's Perspective*, Annual Reviews of Physical Chemistry **58**, 675 (2007).

[107] D. Chowdhury, A. Basu, A. Garai, P. Greulich, K. Nishinari, A. Schadschneider and T. Tripathi, Intra-cellular traffic: bio-molecular motors on filamentary tracks. Eur. Phys. J. B **64**, 593 (2008).

[108] A. Schadschneider, Cellular automata models of highway traffic. Physica A, **372**, 142 (2006).

[109] D. Chrétien, F. Metoz, F. Verde, E. Karsenti and R.H. Wade, Lattice defects in microtubules: protofilament numbers vary within individual microtubules. J. Cell Biol. **117**, 1031 (1992).

[110] M.A. Burack, M.A. Silverman and G. Banker, The role of selective transport in neuronal protein sorting. Neuron **26**, 465 (2000).

[111] M.E. Fouladvand, Z. Sadjadi and M.R. Shaebani, Characteristics of vehicular traffic flow at a roundabout. Phys. Rev. E **70**, 046132 (2004).

[112] B. Tadić and S. Thurner, Information super-diffusion on structured networks. Physica A **332**, 566 (2004).

[113] P.F. Arndt, T. Heinzel and V. Rittenberg, Spontaneous breaking of translational invariance and spatial condensation in stationary states on a ring. J. Stat. Phys. **97**, 1, (1999).

[114] K. Mallick, S. Mallick and N. Rajewsky, Exact solution of an exclusion process with three classes of particles and vacancies. J. Phys. A **32**, 8399 (1999).

[115] M.R. Evans, Y. Kafri, E. Levine and D. Mukamel, Phase transition in a non-conserving driven diffusive system. J. Phys. A **35**, L433 (2002).

[116] S. Gupta, D. Mukamel, G.M. Schütz, Robustness of spontaneous symmetry breaking in a bridge model. J. Phys. A **42**, 485002 (2009).

[117] S. Klumpp and R. Lipowsky, Phase transitions in systems with two species of molecular motors. Europhys. Lett. **66**, 90 (2004).

[118] F.H. Jafarpour, Multiple shocks in a driven diffusive system with two species of particles. Physica A **358**, 413 (2005).

[119] M. Ebbinghaus and L. Santen, A model for bidirectional traffic of cytoskeletal motors. J. Stat. Mech. P03030 (2009).

[120] M. Hongler and R. Filliger, Mesoscopic derivation of a fundamental diagram of one-lane traffic. Phys. Lett. A **301**, 408 (2002).

[121] R. Jiang, M.-B. Hu, B. Jia, R. Wang and Q.-S. Wu, Spatiotemporal congested traffic patterns in macroscopic version of the Kerner-Klenov speed adaptation model. Phys. Lett. A **365**, 6 (2007).

[122] M. Schliwa (Ed.), Molecular Motors, Wiley-VCH, 2002.

[123] M.R. Evans and K.E.P. Sugden, An exclusion process for modelling fungal hyphal growth. Physica A **384**, 53 (2007).

[124] R. Dixit, J.L. Ross, Y.E. Goldman, and E.L.F. Holzbaur, Differential Regulation of Dynein and Kinesin Motor Proteins by Tau. Science **319**, 1086 (2008).

[125] A. Morozov, E. Pronina, A.B. Kolomeisky and M.N. Artyomov, Solutions of Burnt-Bridge Model for Molecular Motors Transport. Phys. Rev. E **75**, 031910 (2007).

[126] J. Otwinowski and S. Boettcher, A totally asymmetric exclusion process with hierarchical long range connections. J. Stat. Mech. P07010 (2009).

[127] S. Srinivasa, M. Haenggi, TASEPs: A Statistical Mechanics Tool to Analyze the Performance of Wireless Line Networks, IEEE/ACM Transactions on Networking, 2009. Submitted.

Selected publications

Mingzhe Liu, Ruili Wang, Rui Jiang, Mao-Bin Hu and Yang Gao (2009): Defect-induced transitions in synchronous asymmetric exclusion processes, *Physics Letters A*, Vol. 373, Issue 2, pp. 195-200, Elsevier Science [Chapter 3].

Mingzhe Liu, Ruili Wang, Mao-Bin Hu, Rui Jiang and Yang Gao (2010): Synchronous asymmetric exclusion processes with an extended defect, *Physics Letters A*, Vol. 374, Issue 13-14, pp. 1407-1413, Elsevier Science [Chapter 4].

Mingzhe Liu and Ruili Wang (2009): Asymmetric exclusion processes on multiple-input multiple-output junctions with parallel update. *Physica A*, Vol. 388, Issue 19, pp. 4068-4074 [Chapter 5].

Ruili Wang, **Mingzhe Liu**, and Rui Jiang (2008): Theoretical investigation of synchronous totally asymmetric exclusion processes on lattices with multi-input-single-output junctions. *Physical Review E*, Vol. 77, 051108, The American Physical Society (This paper has been selected for the May 15, 2008, Issue of the Virtual Journal of Biological Physics Research) [Chapter 5].

Mingzhe Liu, Ken Hawick and Stephen Marsland (2010): Asymmetric exclusion processes with site sharing in a one-channel transport system, *Physics Letters A*, Vol. 374, Issue 4, pp. 516-521, Elsevier Science [Chapter 6].

Mingzhe Liu, Ken Hawick, Stephen Marsland and Rui Jiang (2010): Spontaneous symmetry breaking in asymmetric exclusion process with site sharing: A Monte Carlo study. Submitted. [Chapter 7].